GEOCHEMISTRY AND PETROLOGY OF THE DRY HILL GNEISS AND RELATED GNEISSES, PELHAM DOME, CENTRAL MASSACHUSETTS

BY CATHERINE E. HODGKINS

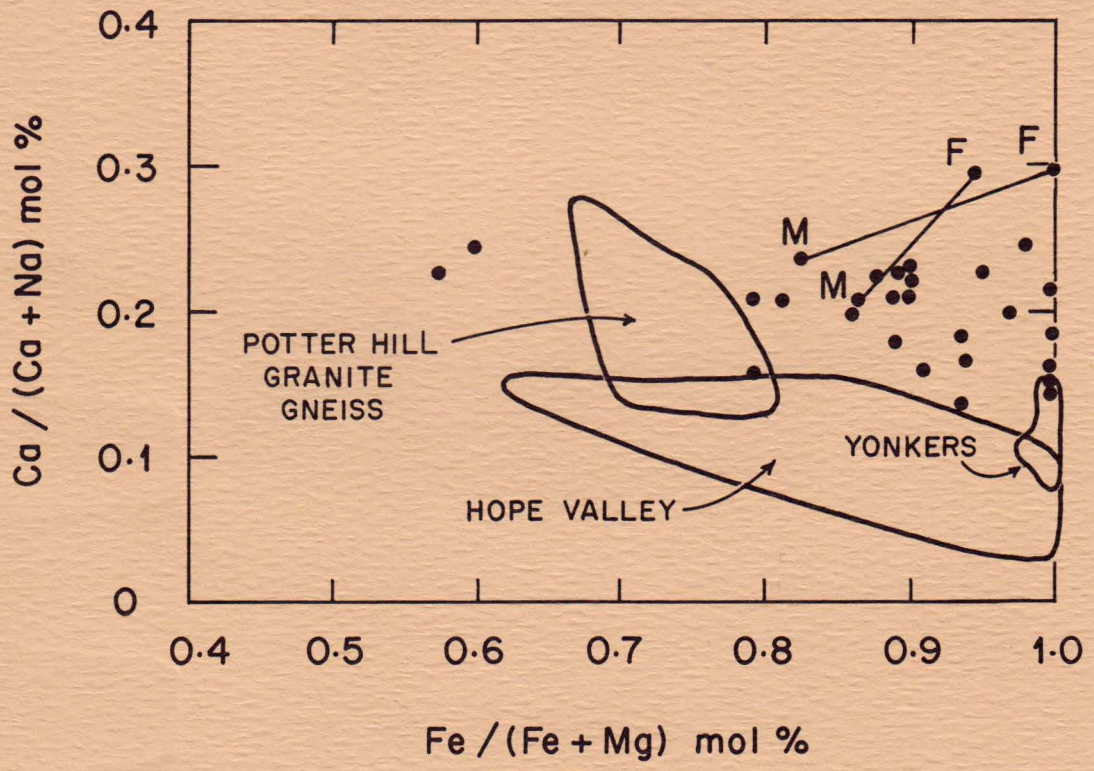

CONTRIBUTION NO. 48
DEPARTMENT OF GEOLOGY & GEOGRAPHY
UNIVERSITY OF MASSACHUSETTS
AMHERST, MASSACHUSETTS

GEOCHEMISTRY AND PETROLOGY OF THE DRY HILL GNEISS AND RELATED GNEISSES, PELHAM DOME, CENTRAL MASSACHUSETTS

(M.S. Thesis)

By

Catherine E. Hodgkins

Contribution No. 48

Department of Geology and Geography

University of Massachusetts

Amherst, Massachusetts

September 1985

TABLE OF CONTENTS

Page

ABSTRACT 1
INTRODUCTION 2
Location 2
Regional Setting 2
Previous Work 2
Structural Geology 5
Metamorphism 5
Purpose of Study 6
Acknowledgements 7
DESCRIPTION OF ROCK UNITS AND PETROGRAPHY 7
Stratigraphy of the Pelham Dome 7
General Description of Sampled Rock Formations 9
Dry Hill Gneiss Hornblende Member 11
Dry Hill Gneiss Biotite Member 20
Granitic Gneiss within the Poplar Mountain Quartzite 20
Felsic Gneiss within the Poplar Mountain Gneiss 22
Poplar Mountain Gneiss 27
Fourmile Gneiss 30
Belchertown Tonalite 31
MINERAL CHEMISTRY OF THE DRY HILL GNEISS 35
Amphibole 35
Biotite 46
Plagioclase 49
Microcline 49
Garnet 49
Chemographic Relations 53
GEOCHEMISTRY AND PETROLOGY 55
Methods of Study 55
Discussion of Paired-sample Statistics 56
Major Element Chemistry of the Dry Hill Gneiss 58
Comparison of Dry Hill Gneiss with Anorogenic Granites ... 72
Trace Element Chemistry of the Dry Hill Gneiss 76
Introduction to Poor Man's Rare Earth Elements 81
Dry Hill Gneiss PMREE 82
Dry Hill Gneiss Biotite Member PMREE 82
Comparison of Dry Hill Gneiss with Average Crustal Rocks . 82
On the Problem of Layering in the Dry Hill Gneiss 85
Granitic Gneiss within the Poplar Mountain Quartzite 93
Felsic Gneiss within the Poplar Mountain Gneiss 93
Poplar Mountain Gneiss 97
Fourmile Gneiss 100
Belchertown Tonalite 100
STRATIGRAPHIC AND CHEMICAL COMPARISONS IN REGIONAL GEOLOGY 104
Introduction 104
Comparisons of Major Element Chemistry: Dry Hill and Other Granitoid Gneisses 108
Trace Element Data 114

Comparisons between Fourmile Gneiss and other Plagioclase Gneisses 118
CONCLUSIONS 123
REFERENCES 127
APPENDIX A 134

ILLUSTRATIONS

Figure

1. Generalized regional geologic map 3
2. Geologic map of study area 4
3. Cross section of the Northfield Mountain Pumped Storage Hydroelectric Project, showing sampled formations .. 8
4. Plot of estimated modes of the Dry Hill Gneiss 21
5. Plot of estimated modes of the granitic gneiss within the Poplar Mountain Quartzite and the felsic gneiss within the Poplar Mountain Gneiss and the Poplar Mountain Gneiss proper 25
6. Plot of estimated modes of the Fourmile Gneiss and the sill of tonalite related to the Belchertown Complex. 34
7. Amphibole discriminant diagrams, adapted from Leake (1978) and Hawthorne (1981) 40
8. Amphibole classification diagram 41
9. Visually estimated 2Vs plotted on a diagram of tetrahedral aluminum vs. a ferrous iron and magnesian ratio 42
10. Amphibole identification diagram, adapted from Hawthorne (1981) 44
11. The ratio of total Fe to total Fe plus Mg (atomic) in amphiboles vs. the same ratio in corresponding whole rocks 45
12. Biotite classification diagram 48
13. Plot of garnet core and rim compositions from Dry Hill Gneiss sample TR 44+50 52
14. AKFm diagram 54
15. Harker diagram for all samples 65
16. Norms plotted in volumetric percent on a modified Streckeisen diagram 69
17. Calc-alkaline/tholeiite discriminant diagram, modified from Miyashiro (1974) 70
18. AFM diagram 71
19. Shand alumina saturation diagram 74
20. Plot of Rb vs. K2O 77
21. Plot of Zr vs. SiO2 78
22. Plot of Nb vs. Zr 79
23. Plot of Ba vs. Zr 80
24. Plot of Poor Man's Rare Earth Element Analyses for Dry Hill Gneiss 83
25. Plot of PMREE for Dry Hill Gneiss Biotite Member 84

26. PMREE diagram of leucogneiss layers and biotite gneiss layers of Dry Hill Gneiss 87
27A-D. The granite system at various pressures 89
28. A plot of normative orthoclase vs. Ba 94
29. PMREE diagram of granitic gneiss within the Poplar Mountain Quartzite 96
30. PMREE diagram of felsic gneiss within the Poplar Mountain Gneiss 98
31. PMREE diagram of Poplar Mountain Gneiss 101
32. PMREE diagram of Fourmile Gneiss 103
33. PMREE diagram of Belchertown Tonalite 105
34. Clustering of norms of Dry Hill Gneiss, Yonkers Gneiss, Potter Hill Gneiss, and Hope Valley Alaskite Gneiss plotted on a modified Streckeisen diagram 109
35. Harker diagram comparing Dry Hill Gneiss to other Connecticut and New York Gneisses 110
36. Shand alumina saturation diagram 111
37. Plot of albite-anorthite-orthoclase for Dry Hill Gneiss and other Connecticut and New York Gneisses 112
38. Harker diagram of mafics 113
39. Felsic vs. mafic components of Dry Hill Gneiss vs. other Connecticut and New York Gneisses 115
40. AFM diagram 116
41. A comparison of selected trace element data for Dry Hill Gneiss and Yonkers Gneiss 117
42. Norms of Fourmile Gneiss, the Waterford Group, and Shelburne Falls dome gneiss, plotted on a modified Streckeisen diagram 119
43. Harker diagram comparing Fourmile Gneiss to other Massachusetts and Connecticut gneisses 120
44. Calc-alkaline/tholeiitic discriminant diagram 124
45. AFM diagram 125
46. REE and PMREE diagram for Dry Hill Gneiss 136
47. REE and PMREE diagram for Fourmile Gneiss 137

TABLES

1. Estimated modes of the Dry Hill Gneiss Hornblende and Biotite Members 12
2. Estimated modes of the granitic gneiss within the Poplar Mountain the Quartzite and the felsic gneiss within Poplar Mountain Gneiss 23
3. Estimated modes of the Poplar Mountain Gneiss 28
4. Estimated modes of the Fourmile Gneiss and the Belchertown Tonalite 32
5. Electron microprobe analyses of fifteen amphiboles from the Dry Hill Gneiss and three from the felsic gneiss within the Poplar Mountain Gneiss 36
6. Electron microprobe analyses of a biotite from Dry Hill Gneiss Hornblende Member sample TR 44+50 47

7. Electron microprobe analyses of feldspars from Dry Hill Gneiss sample TR 44+50 50
8. Representative electron microprobe analyses of garnet from Dry Hill Gneiss sample TR 44+50 51
9. Standard deviation of sample pairs 57
10. Standards 59
11. X-ray fluorescence analyses and CIPW norms of Dry Hill Gneiss Hornblende and Biotite Members 60
12. Average crustal values of selected trace elements 85
13. X-ray fluorescence analyses and CIPW norms of three samples of granitic gneiss with in Poplar Mountain Quartzite and five samples of felsic gneiss within the Poplar Mountain Gneiss 95
14. X-ray fluorescence analyses and CIPW norms of Poplar Mountain Gneiss 99
15. X-ray fluorescence analyses and CIPW norms of Fourmile Gneiss and Belchertown Tonalite 102
16. REE data for Dry Hill Gneiss and Fourmile Gneiss 135

ABSTRACT

Thirty samples of Dry Hill Gneiss, three samples of granitic gneiss within the Poplar Mountain Quartzite, five samples of felsic gneiss within the Poplar Mountain Gneiss, eight samples of Poplar Mountain Gneiss, four samples of Fourmile Gneiss, and two samples of a tonalite sill associated with the Belchertown Complex were analysed for major and trace element chemistry by X-ray fluorescence analyses at the University of Massachusetts. The samples were collected by Robinson and Ashenden in 1968-1970 in the tunnels of the Northfield Mountain Pumped Storage Hydroelectric Project, in the towns of Erving and Northfield, Massachusetts.

The gneisses crop out in the Pelham Dome, a mantled gneiss dome which is part of the Bronson Hill Anticlinorium. The Dry Hill Gneiss is the oldest of the dome gneisses and has a U/Pb zircon age date of approximately 600 million years (Zartman and Naylor, 1984; Naylor, et al., 1973, corrected according to Steiger and Jager, 1977.)

The Dry Hill Gneiss is chemically a granite, and is interpreted to be a metamorphosed rhyolite, based on field evidence. It has high K2O, K2O/Na2O, BaO, FeOT/MgO and low CaO, Al2O3, and MgO. The gneiss fits well into the classification of anorogenic granite of Loiselle and Wones (1979).

In outcrop, the Dry Hill Gneiss has striking, pink microcline- and hastingsite-rich leucogneiss layers alternating with gray biotite gneiss layers. Two split samples were prepared of the layers and were analysed separately. The leucogneiss layers are greatly enriched in K as K2O, Ba, Ce, and Zr and moderately enriched in Y and Nb, relative to the biotite gneiss layers. The biotite gneiss layers contain more Na2O and Al2O3. SiO2 values are the same for each layer. The layering is interpreted to be the result of crystal settling by density during subaerial eruption of tuffs of the Dry Hill Gneiss protolith. Crystals of orthoclase, quartz, allanite, hornblende, zircon, and perhaps sphene, settled out into crystal accumulations, which became the leucogneiss layers, as the glass was winnowed away and deposited elsewhere to become the biotite gneiss layers. Because the melt was on the quartz-orthoclase eutectic surface, the silica values in the liquid did not change as orthoclase and quartz crystallized.

The granite gneiss within the Poplar Mountain Quartzite is chemically similar to the Dry Hill Gneiss and only slightly younger. It probably represents a reactivation of the Dry Hill magma source after a short hiatus. The felsic gneiss within the Poplar Mountain Gneiss is also chemically similar to the Dry Hill Gneiss, but is slightly more primitive. It may have tapped a slightly lower level in the magma chamber. The Poplar Mountain Gneiss is a sedimentary formation, with a trace element signature similar to the Dry Hill Gneiss. It probably represents reworked ash deposits of a slightly

more primitive layer in the magma chamber.

The Fourmile Gneiss is chemically a dacite, and has fractionation trends similar to Chilean andesites of Thorp et al. (1976). It is interpreted to be of orogenic origin, perhaps forming under similar conditions to those which occur today in the Andes of South America.

INTRODUCTION

Location

The study area is located in the Millers Falls quadrangle, in the towns of Northfield and Erving, Massachusetts, between the Connecticut River and Northfield Mountain. Samples were collected by Peter Robinson and David Ashenden and assistants in the tailrace and access tunnel excavations during the construction of the Northfield Mountain Pumped Storage Hydroelectric Project, from 1968 to 1970.

Regional Setting

The rocks studied are part of the Pelham Dome, a mantled gneiss dome, which is part of the Bronson Hill Anticlinorium (Figure 1). The Bronson Hill Anticlinorium trends from southern Connecticut to northern New Hampshire and is formed by a series of such domes (Eskola, 1948; Thompson, et al., 1968). Extending from Belchertown, Massachusetts, to Northfield, Massachusetts, the Pelham dome is approximately forty-three kilometers long. The late Precambrian and Ordovician rocks in the core are mantled by younger Paleozoic strata (Figure 2). The origin of the core rocks has been disputed for the past eighty years (Emerson, 1898, 1917; Balk, 1956a; Robinson, 1963, 1967, 1979; Naylor, 1969; Hall and Robinson, 1982).

Previous Work

The area was mapped in 1898 by B. K. Emerson, who briefly described the rocks and assigned them to the Becket Gneiss (Emerson, 1898). In the southern part of the Pelham Dome, he described an actinolite quartzite, which he named the Pelham Quartzite. In 1917, Emerson renamed the dome rocks the Pelham Granite. Robert Balk mapped the Millers Falls quadrangle and the adjacent Northfield quadrangle, naming the Dry Hill Granite Gneiss and the Poplar Mountain Gneiss (Balk, 1956a, 1956b). Robinson (1963, 1967) did reconnaissance mapping in the area. Ashenden (1973) subdivided the Dry Hill Gneiss in the Northfield area into the Hornblende Member and the Biotite Member, and recognized a large recumbent anticline, with an inverted stratigraphy below a normal stratigraphy. Balk placed the Dry Hill Gneiss above the Poplar Mountain Gneiss in his stratigraphic column, but the work of Ashenden suggested that the Dry Hill Gneiss is stratigraphically lower than the Poplar Mountain Gneiss. Onasch (1973) mapped biotite schist and amphibolite units in the Quartzite Member of the Poplar Mountain

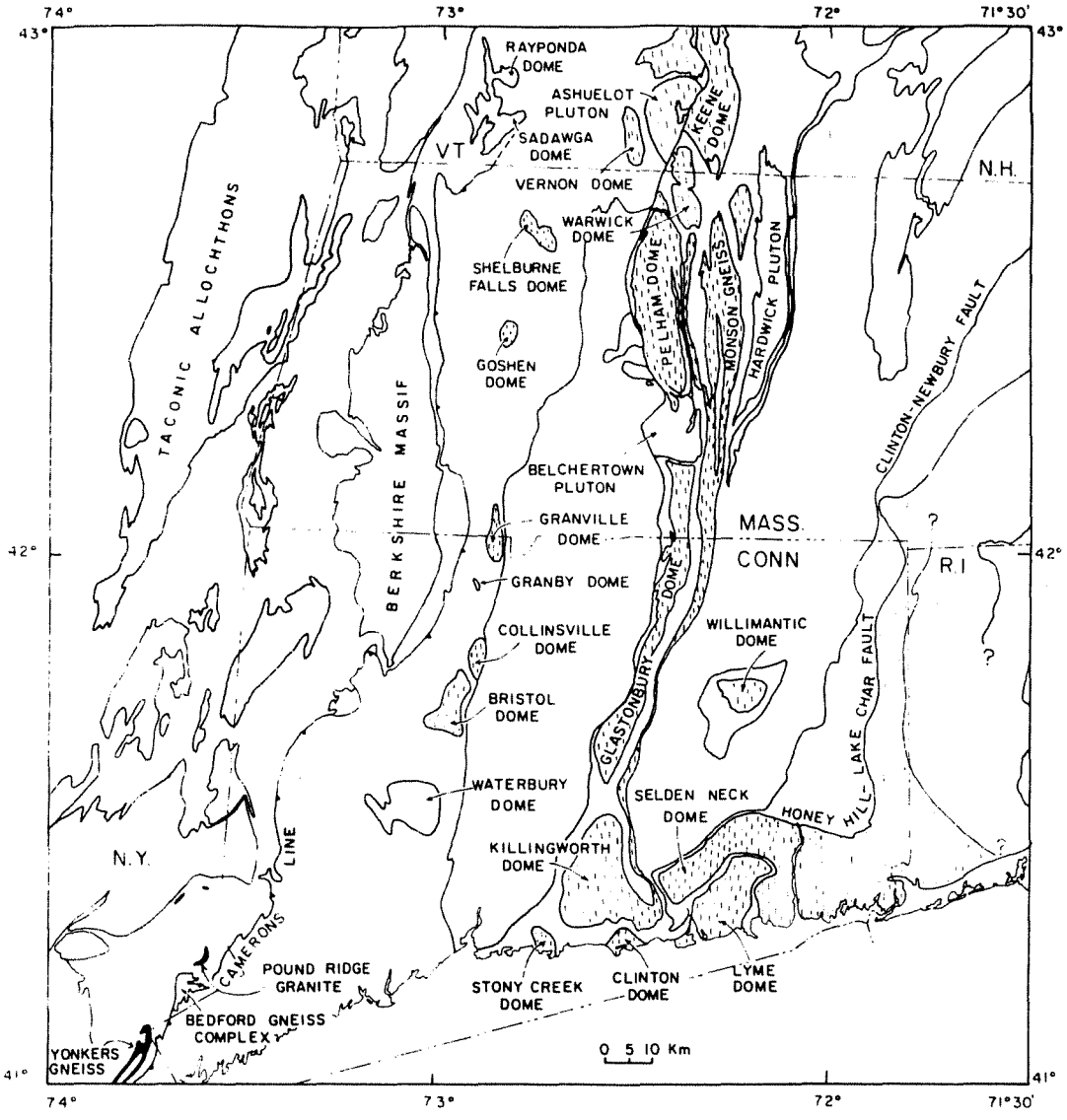

Figure 1. Map of the gneiss domes in southern New England and eastern New York, adapted from Hall and Robinson (1982). Domes are dashed.

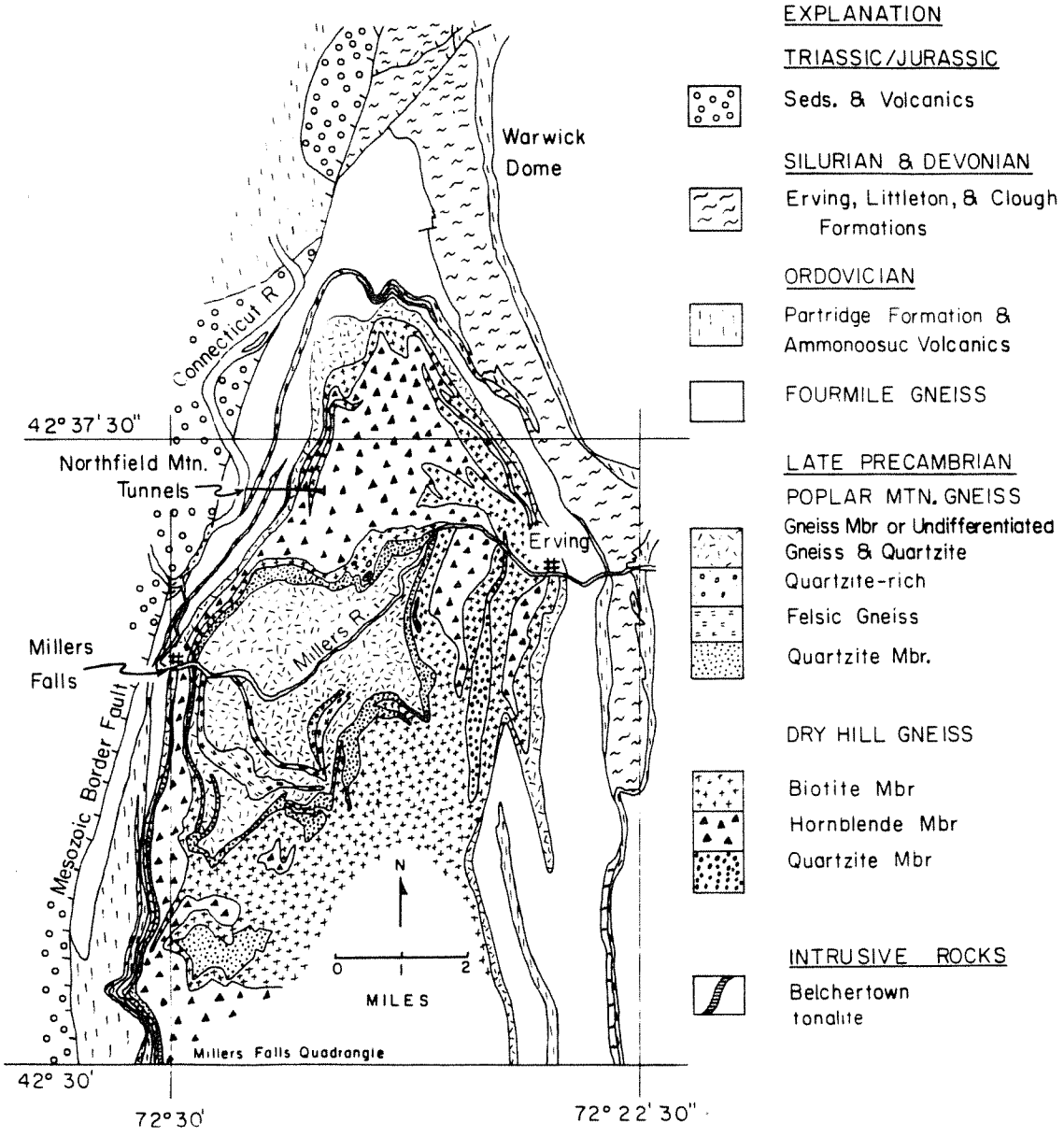

Figure 2. Map of the north part of the Pelham Dome, showing the location of the Northfield Mountain Tunnels. From Robinson (1979), based on an original map of Onasch (1973), modified to include Laird (1974) and Robinson, Ashenden and Onasch (unpublished). Earlier work by Ashenden (1973), Robinson (1963, 1967), and Onasch (1973). Also includes Michener (1983).

Gneiss and recognized lenses of a quartzite-rich gneiss and a felsic gneiss on Jerusalem Hill in the Gneiss Member of the Poplar Mountain Gneiss. Laird (1974) mapped bedrock geology of the dome on the west side, in the vicinity of Montague.

Structural Geology

In central Massachusetts, rocks of lower Devonian age and older were subject to three stages of folding and deformation, during the Acadian orogeny (Robinson, 1979). The earliest stage was one of recumbent folding, in which huge nappes were folded to the west. That stage resulted in stratigraphic repetitions common in the central Massachusetts area. Local nappes, folded to the east or to the southeast have been mapped in the Pelham Dome and are thought to be part of the nappe stage, although relative timing is uncertain (Ashenden, 1973).

The second stage was one of major eastward backfolding which deformed the first stage recumbent folds. No indisputable evidence of the backfolding stage has been found in the Pelham Dome area, although there is evidence in other gneiss domes (Robinson, personal communication, 1983).

Differential densities between the core rocks and the more dense Paleozoic mantling rocks may have caused the third and final stage, to form the Pelham dome. The main phase of the doming was accompanied by the development of a gently plunging, northward-trending lineation in the Pelham dome that was first mapped by Balk (1956a) and by the development of upright isoclinal folds. Late asymmetric folds, also of the dome stage, deformed the north-south lineation (Onasch, 1973).

In the late Triassic and early Jurassic, the dome strata were truncated by a normal fault on the west side and north end of the Pelham dome. The western side was downthrown about 5 km with respect to the eastern side (Robinson, 1979).

Metamorphism

The dome stage of Acadian deformation was accompanied by kyanite-staurolite grade regional metamorphism (Robinson, 1979) under conditions of approximately 580°C and a minimum pressure of 6.2 kilobars (Tracy, Robinson, and Thompson, 1976). Relict sillimanite and orthoclase, discovered in the Mount Mineral Formation, within late Precambrian rocks in the southern part of the dome, indicate a pre-Acadian metamorphism of much higher grade (Robinson, Tracy, and Ashwal, 1975) which may have had a major influence on mineralogy and rock textures in the Northfield Mountain area.

Purpose of Study

The goals of this study were four-fold. First, petrographic analysis has been done on thin sections of the Dry Hill Gneiss, the Poplar Mountain Gneiss, and the Fourmile Gneiss of the Pelham dome, as well as a small sill of tonalite related to the Belchertown Complex, to determine mineralogy, modes, and textural evidence for metamorphic reactions. The thin sections correspond to samples selected for bulk chemical analysis. Also, the mineral chemistry of a typical thin section of the Dry Hill Gneiss Hornblende Member has been analysed using an electron microprobe, to explore how the mineral chemistry relates to the whole rock chemistry. Amphibole separates were made of 15 samples of the Dry Hill Gneiss Hornblende Member and the felsic gneiss within the Poplar Mountain Gneiss to examine the amphibole chemistry and to try to relate it to the small 2V. The second goal of this study was to characterize chemically the above-mentioned formations and to use the chemical data to evaluate the nature of the protolith of each rock type, if possible. The third goal was to analyse the leucogneiss layering and the biotite gneiss layering in the Dry Hill Gneiss and to determine whether it is primary or a result of partial melting during high-grade metamorphism. Fourth, an attempt was made, using major and trace element geochemistry, to correlate the Dry Hill Gneiss, Poplar Mountain Gneiss, and Fourmile Gneiss with core and mantle rocks of other gneiss domes in New England and adjacent New York (Figures 1 and 2).

It is not completely clear, at present, whether the basement gneiss of the domes should be correlated with the late Proterozoic "Avalonian" basement to the east or with the earlier Proterozoic "Grenvillian" basement and related rocks to the west. The Dry Hill Gneiss is similar to rocks of the Sterling Granite Gneiss in the Selden Neck dome of southern Connecticut (Ashenden, 1973 and Lundgren, 1966) and the Stony Creek Granite, a pink, granite dated at 616 $\pm$ 78 million years in the Stony Creek dome of southern Connecticut (Hills and Dasch, 1972). Unpublished major element geochemistry, provided by Richard Goldsmith (U. S. Geological Survey), of the Hope Valley Alaskite Gneiss and the Potter Hill Granite Gneiss of the Sterling Plutonic Group in the Selden Neck and Lyme domes of Connecticut were compared to data on the Dry Hill Gneiss. Similar rocks of late Proterozoic or probable late Proterozoic age are also found in the Clinton, Willimantic, and Lyme domes. The Dry Hill Gneiss is quite similar to the Yonkers Gneiss of New York City, a 560 $\pm$ 30 million year old granite gneiss containing hastingsite (Long, 1969; M. Goldstein, unpublished). The Poplar Mountain Gneiss may correlate with the Plainfield Formation, mapped by Lundgren (1966, 1967) in the Selden Neck and Lyme domes. The Fourmile Gneiss was correlated to the Ivoryton Group, now called the Waterford Group, of Connecticut by Ashenden (1973). Rocks of the Shelburne Falls dome, mapped as Monson Gneiss by Emerson (1917), bear a lithic similarity and some chemical similarity to the Fourmile Gneiss (L. M. Hall, unpublished data). The geochemistry of the Fourmile

Gneiss was also compared to analyses of gneiss from the Glastonbury Dome and the main body of the Monson Gneiss (Leo, et al., 1984).

Acknowledgements

This study was done in partial fulfillment of a Masters Degree in Geology at the University of Massachusetts. I would like to thank my advisor, Peter Robinson, for invaluable help and advice. I also wish to thank Howard Jaffe and J. Michael Rhodes for helpful advice and recommendations. Leo M. Hall generously allowed the writer to use unpublished analyses of rocks from the Shelburne Falls dome as did Richard Goldsmith for unpublished analyses of rocks from the Selden Neck and Lyme domes. Others deserving thanks are Joel Sparks for help in the laboratory; Laurie Autio for advice on trace element modelling; Kurt Hollocher for assistance with the electron microprobe and many hours of spirited "discussions"; and John Schumacher for aid with amphibole formulae corrections. Lastly, I would like to thank my husband, William Verts, for assistance with the computer, encouragement, patience, and his font file. Field, laboratory, and publication costs of this study were supported by National Science Foundation Grants EAR-79-11207 and EAR-81-16197 (to Robinson and Rhodes), and EAR-84-10370 (to Robinson).

DESCRIPTION OF ROCK UNITS AND PETROGRAPHY

Stratigraphy of the Pelham Dome

The outcrop pattern of the Pelham Dome reveals a duplication of stratigraphy with an outer ring of Poplar Mountain Gneiss consisting of Poplar Mountain Gneiss overlying Poplar Mountain Quartzite; an intermediate zone of Dry Hill Gneiss; and an inner core of Poplar Mountain Gneiss consisting of Poplar Mountain Quartzite overlying Poplar Mountain Gneiss (Figure 2). Ashenden (1973) showed that the pattern is a normal stratigraphy on top of a reversed stratigraphy, and interpreted it as due to an anticlinal recumbent fold refolded into a dome. Rocks which crop out in the core of the dome (inner Poplar Mountain Gneiss) shown in Figure 2, are actually not the basal unit of the dome stratigraphy, but are part of the inverted limb of the recumbent anticline (Figure 3). Both the recumbent anticline and the dome formed during the Acadian orogeny (Robinson, 1979).

The oldest unit of the Pelham Dome is the Dry Hill Gneiss, divided into the older Hornblende Member and the younger Biotite Member. Slightly younger than the Dry Hill Gneiss is the Poplar Mountain Gneiss, consisting of the Poplar Mountain Quartzite and the Poplar Mountain Gneiss. The Biotite Member of the Dry Hill Gneiss pinches out along the upper limb of the recumbent anticline, so the Poplar Mountain Quartzite locally lies directly on the Dry Hill Hornblende Member (Figure 3). Poplar Mountain Quartzite and Poplar Mountain Gneiss are thinner on the upper limb of the recumbent anticline than on the lower

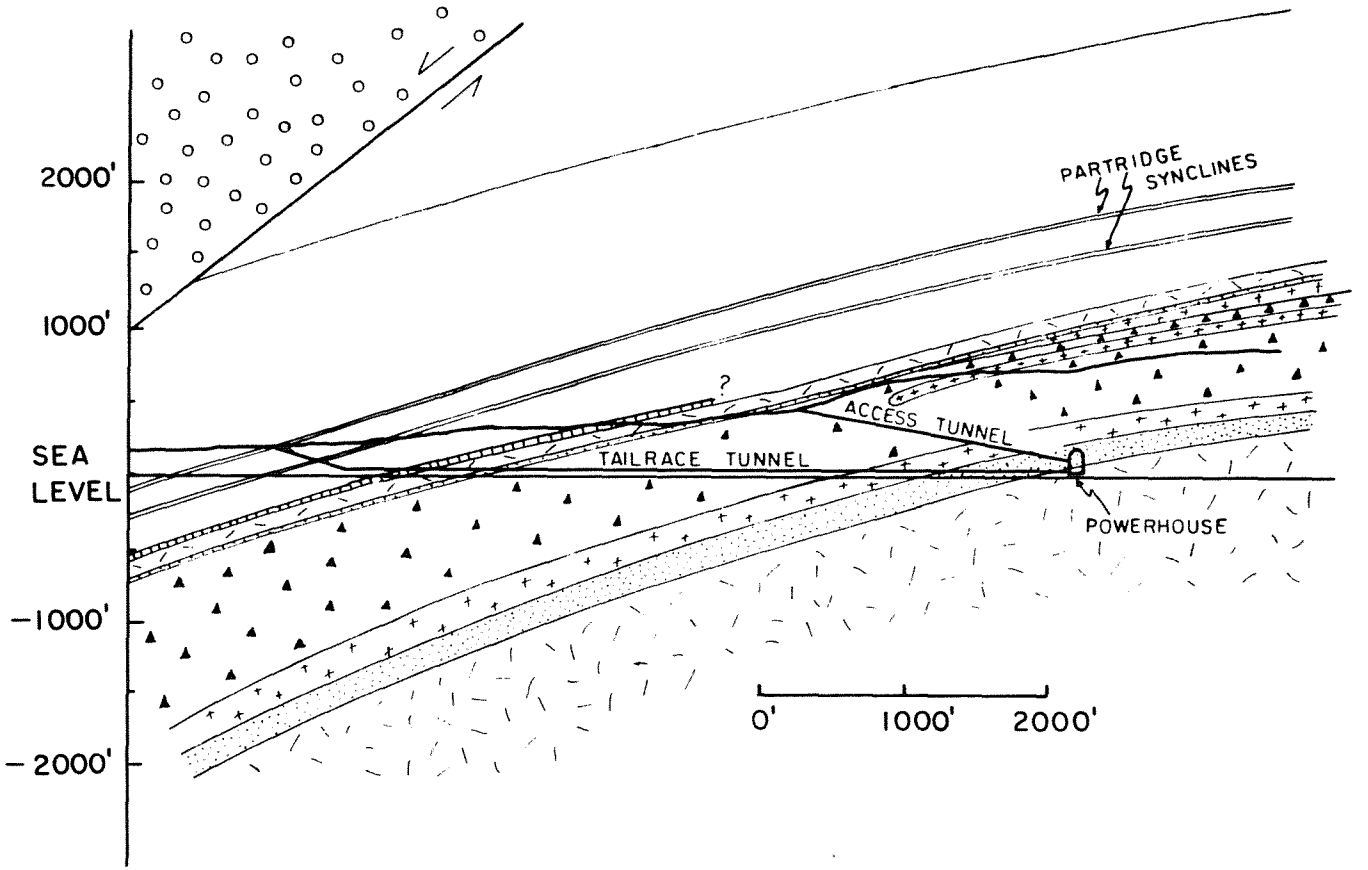

Figure 3. Cross section, looking north, on the west limb of the Pelham gneiss dome, of the Northfield Mountain Pumped Storage Hydroelectric Project tunnels, showing sampled formations. Note repetition of stratigraphy on either side of Dry Hill Gneiss Hornblende Member. Axial trace of overturned anticline is within the Hornblende Member and anticline closes to the east. Width of Partridge synclines is exaggerated. Symbols are the same as those in Figure 2. Adapted from Ashenden (1973).

limb. The youngest of the dome rocks is the Fourmile Gneiss of unknown age. An upper limit on the age of the Fourmile Gneiss is indicated by synclines within it of mid-Ordovician Partridge Formation. A sill of a tonalite, lithologically correlated with the Devonian Belchertown Complex, intrudes along the base of the Fourmile Gneiss.

General Description of Sampled Rock Formations

The Dry Hill Gneiss Hornblende Member is a coarse-grained, well layered granitic gneiss composed of microcline, quartz, plagioclase, hastingsite, biotite, and accessory minerals. Ashenden (1973) mapped the Biotite Member to include rocks similar to the Hornblende Member, but without the hastingsite. Both members contain megacrysts of pink microcline up to 10 cms in diameter. Megacrysts of hastingsite occur, up to one cm in size, in the Hornblende Member. The Dry Hill Gneiss also contains minor quartzite, calc-silicate rocks and white leucogneiss layers that may be sills of Acadian (Devonian) age (Ashenden, 1973 and Robinson, unpublished tunnel notes, July 1968 to March 1970).

The Dry Hill Gneiss has been dated by the U/Pb method at about 600 million years on a zircon separate (Zartman and Naylor, 1984; Naylor, et al., 1973, corrected according to Steiger and Jäger, 1977). Ashenden (1973) and Robinson (1979) suggest that the formation may be a metamorphosed rhyolite. They theorize that the protolith was a rhyolite rather than a granite based on three lines of evidence: the concordent contacts between the Dry Hill Gneiss and adjacent formations; the interbedded quartzites; and the well layered character of the Dry Hill Gneiss.

Ashenden divided the Poplar Mountain Gneiss into two members. The Quartzite Member of the Poplar Mountain Gneiss rests on the Biotite Member or the Hornblende Member of the Dry Hill Gneiss and is locally interbedded with it (Ashenden, 1973). It contains interbedded biotite schist and gray gneiss and, less commonly, amphibolite and calc-silicate (Onasch, 1973). Of limited thickness, but considerable importance is a granite gneiss within the Quartzite Member that outcrops within the Northfield Tunnels. The granite gneiss, described by Ashenden, strongly resembles the Dry Hill Gneiss, and is probably of similar origin, perhaps a later pulse from the same magma chamber. The Gneiss Member of the Poplar Mountain Gneiss contains striking, large, white feldspar megacrysts in a dark gray microcline-plagioclase-biotite gneiss. Muscovite occurs in minor amounts. In thin section, the biotite is a red-brown color, indicating a high ratio of $Ti^{4+}/(Fe^{3+} + Ti^{4+})$ (Hayama, 1959 cited in Guidotti, 1984). perhaps indicating a reducing environment of deposition and thus a sedimentary origin. Onasch (1973) mapped a felsic gneiss and a quartzite-rich gneiss in the Jerusalem Hill area within the Gneiss Member. A felsic gneiss that is similar to Onasch's felsic gneiss crops out in the Northfield Tunnels. Perhaps the northern exposure is merely an extension of Onasch's unit.

Because the Poplar Mountain Gneiss is locally interbedded with the Dry Hill Gneiss, it is probably of comparable age, albeit slightly younger (Ashenden, 1973). It may be of sedimentary or of volcanoclastic origin, perhaps derived from the same source as the Dry Hill Gneiss (Ashenden, 1973 and Laird, 1974).

Balk (1956a and 1956b) described a border facies of the Dry Hill granite gneiss. Ashenden (1973) recognized that the "border facies" of Balk is actually a different formation, since the Poplar Mountain Gneiss is stratigraphically between the Dry Hill Gneiss and the "border facies", and the composition of the rocks in question is strikingly different from that of the Dry Hill Gneiss. He named the formation the Fourmile Gneiss, and described it as a fine- to medium-grained gneiss dominantly composed of quartz, plagioclase, and red-brown biotite with minor amphibolite layers. The variable composition of the Fourmile Gneiss led Ashenden to suggest a volcanoclastic or pyroclastic origin.

The contact between the Fourmile Gneiss and the Poplar Mountain Gneiss was described by Ashenden (1973) as sharp, with no evidence of interbedding. However, it is now known (Robinson, personal communication, 1981) that the contact described by Ashenden is the intrusive base of the Belchertown sill, a feature discussed later in this report. The Fourmile Gneiss is of unknown age, but must be younger than the Poplar Mountain Gneiss. The fact that the Fourmile Gneiss contains isoclinal synclines of the Middle Ordovician Partridge Formation, suggests that it is older than Middle Ordovician (Ashenden, 1973, and Robinson, unpublished tunnel notes, July 1968 to March 1970).

A large sample of "Fourmile Gneiss" was collected in 1980 on Northfield Mountain six hundred feet north of the access tunnel portal area (Ashenden's sample no. 164). The outcrop is just above the base of the Fourmile Gneiss. G. W. Leo and R. A. Zartman of the U. S. Geological Survey, (personal communication to Robinson, 1980), obtained a concordant age of 370 million years on a zircon separate. That led Robinson (personal communication) to suggest that the sample was actually from a strongly foliated sill of tonalite intruding the Fourmile Gneiss. Robinson suggested that the tonalite may be associated with the Belchertown Complex, which is dominantly composed of quartz monzodiorite, but contains minor zones of tonalite. Comparison with thin sections of rocks collected by Guthrie (1972) of Belchertown Quartz Monzodiorite confirmed Robinson's hypothesis. Although unsuspecting at the time, Robinson had actually mapped the sill in the tailrace tunnel of the Northfield Mountain Hydroelectric Project as a homogeneous hornblende-rich layer at the very base of the Fourmile Gneiss. Calculations from contact data in Robinson's tunnel notes indicate that the sill is 10.5 meters thick.

Dry Hill Gneiss Hornblende Member

As shown in thin section (Table 1), the Dry Hill Gneiss Hornblende Member is typically coarse grained with interlocking and elongate quartz crystals, and large megacrysts of microcline. Quartz is clear and many grains have strained extinction. Some crystals are up to 0.8 mm in diameter. Plagioclase is oligoclase (An 18 to An 24), and is zoned, with a variation in extinction angles between core and rim from 2 to 3 degrees. The rims are more sodic. Many of the plagioclase crystals are altered to some degree by sericite. Some of the clear, untwinned, unzoned plagioclase might have been mistaken for quartz, while visually estimating the modes, because samples were not stained.

Microcline is plentiful and usually twinned. Megacrysts can be up to 3 cm long in thin section and up to 10 cm in hand specimen. Sample TR 42+23 contains a megacryst of microcline which biases the mode.

Hastingsite occurs as anhedral megacrysts up to 14mm in diameter. Most crystals are strongly pleochroic from dark blue-green (Z) to brownish green (Y) to pale yellow green (X). The darker green hastingsites have a 2V close to zero degrees, while the less strongly colored hastingsites have a 2V of 20° to 40°. Small grains of allanite and zircon form pleochroic haloes in the amphiboles. The hastingsite is poikilitic with sphene, quartz, biotite, garnet, and feldspar. Alteration products of the amphibole are biotite and chlorite. Hastingsite usually occurs in clots with biotite and/or sphene and/or garnet.

Dark-greenish-brown (Z=Y) to pale-greenish-yellow (X) pleochroic biotite apparently enriched in Fe3+, occurs as small, 0.5 to 2.0mm, subhedral plates, which define the dominant metamorphic foliation. Biotite also clusters with hastingsite. Traces of iron-rich chlorite occur as an alteration product rimming the biotite, locally accompanied by small, anhedral opaques. The biotite which forms on hastingsite as an alteration product is generally more red brown than biotite not in contact with hastingsite. Three samples of Dry Hill Gneiss Hornblende Member, TR 31+79, TR 33+40, and TR 35+00, have biotite that is pleochroic from red brown (Z=Y) to pale orange yellow (X).

Sphene occurs as subhedral to euhedral crystals 0.3 to 0.7mm in length. Sphene generally occurs with mafic minerals, especially hastingsite and garnet. A few grains of sphene form radioactive haloes against biotite and hastingsite; the majority of crystals do not. Sphene is pale brown and mildly pleochroic.

Minute crystals of zircon appear to be far more radioactive than sphene. They are subhedral to euhedral and may be more numerous in the quartz- and feldspar- rich layers. Apatite occurs in trace amounts in the form of small euhedral crystals.

Table 1. Estimated modes of the Dry Hill Gneiss Hornblende and Biotite Members. Plagioclase composition determined by the Michel-Levy method.

	Hornblende Member							
	0+50	8+45	9+07	9+40F	9+40M	11+83	15+84	15+96
Quartz	32	35	31	34	47	31	39	29
Plagioclase	14	11	21	12	8	15	15	18
Microcline	50	37	42	43	37	50	42	44
Hastingsite	1	tr	3	10		1		2
Biotite	3	7	3	1	7	3	4	5
Garnet	tr	tr	tr	tr			tr	tr
Pistacite	tr	tr	tr	tr	tr	tr		
Allanite	tr	tr	tr	tr	tr	tr	tr	tr
Sphene	tr	tr	tr	tr	tr	tr	tr	tr
Apatite	tr	tr	tr	tr	tr	tr	tr	tr
Zircon	tr	tr	tr	tr	tr	tr	tr	tr
Opaque	tr	tr	tr	tr	tr	tr	tr	tr
Chlorite	tr	tr	tr	tr	tr	tr		tr
Sericite			tr			tr		tr
Calcite		tr	tr	tr	tr	tr		tr
An content:	An_{18}	An_{18}	An_{20}	An_{20}	An_{18}	An_{21}	An_{21}	An_{21}

Table 1, continued.

	Hornblende Member							
	TR 31+79	TR 32+18	TR 33+23	TR 33+40	TR 34+91	TR 35+00	TR 37+82	TR 38+29
Quartz	29	34	26	34	33	32	36	34
Plagioclase	17	14	13	18	13	16	12	14
Microcline	45	47	47	42	49	40	46	43
Hastingsite	2	3	6	3	1	10	tr	4
Biotite	7	2	2	3	4	3	6	5
Garnet		tr	tr				tr	tr
Pistacite		tr	tr	tr	tr		tr	tr
Allanite	tr	tr	tr	tr	tr	tr	tr	tr
Sphene	tr	tr	tr	tr	tr	tr	tr	tr
Apatite	tr	tr	tr	tr	tr	tr	tr	tr
Zircon	tr	tr	tr	tr	tr	tr	tr	tr
Opaque	tr	tr	tr	tr	tr	tr	tr	tr
Chlorite	tr	tr	tr					
Sericite			tr					
Calcite			tr	tr	tr		tr	
An content:	An_{20}	An_{21}	An_{20}	An_{24}	An_{22}	An_{21}	An_{20}	An_{22}

Table 1, continued.

	Hornblende Member							
	TR 39+40	TR 40+85	TR 41+95	TR 42+23	TR 43+46	TR 44+50	TR 44+90F	TR 44+90M
Quartz	37	30	38	26	36	34	31	40
Plagioclase	14	15	15	5	16	13	10	17
Microcline	45	44	41	62	39	35	50	33
Hastingsite	2	7	1	4	tr	10	5	tr
Biotite	2	4	5	3	9	8	3	10
Garnet		tr				tr	1	
Pistacite	tr	tr	tr	tr	tr	tr	tr	tr
Allanite	tr	tr	tr	tr	tr	tr	tr	tr
Sphene	tr	tr	tr	tr	tr	tr	tr	tr
Apatite	tr	tr	tr	tr	tr		tr	tr
Zircon	tr	tr	tr	tr	tr	tr	tr	tr
Opaque	tr	tr	tr	tr	tr	tr	tr	tr
Chlorite	tr		tr	tr		tr	tr	tr
Sericite	tr						tr	tr
Calcite	tr		tr		tr	tr	tr	tr
An content:	An_{19}	An_{20}	An_{19}	An_{22}	An_{24}	An_{19}	An_{22}	An_{23}

Sample TR 42+23 contains a microcline megacryst.
Sample TR 44+50 contains a trace amount of tourmaline.

Table 1, continued.

	-Hbd Member-		------Biotite Member------			
	TR 47+75	TR 56+88	17+82	18+43	18+72	TR 57+88
Quartz	35	38	38	36	31	38
Plagioclase	18	14	19	12	11	16
Microcline	39	42	38	47	48	30
Hastingsite	2	1	tr			
Biotite	6	5	3	5	10	16
Garnet	tr	tr	tr		tr	tr
Pistacite	tr	tr	tr			tr
Allanite	tr	tr	tr	tr	tr	tr
Sphene	tr	tr	tr	tr	tr	tr
Apatite	tr	tr	tr	tr	tr	tr
Zircon	tr	tr	tr	tr	tr	tr
Opaques	tr	tr	2	tr	tr	tr
Chlorite			tr			
Sericite			tr	tr		
Calcite		tr	tr	tr	tr	tr
An content:	An_{19}	An_{20}	An_{22}	An_{21}	An_{23}	An_{21}

A note on sampling:

Most of the sampling was done on the north wall of the access tunnel and the south wall of the tailrace tunnel (Robinson, personal communication, 1984). Sample numbers are engineering marks, in feet, measured due east from a survey position on the east bank of the Connecticut River for the tailrace tunnel, and measured from the portal for the access tunnel. Thus, sample 0+50 was collected in the access tunnel 50 feet east of the portal. Samples collected in the tailrace tunnel are prefixed by "TR", whereas those from the access tunnel have no prefix.

Specimens in Table 1

Hornblende Member

0+50 - Light-pink feldspar-quartz-biotite leucogneiss with indistinct pink feldspar layers 2-3 mm thick. Rare hastingsite megacrysts up to 4 mm across. Northfield Mountain Project Access Tunnel, 50 feet from portal.

8+45 - Light-pinkish-gray biotite-feldspar gneiss with pink and white feldspar augen 6 mm in diameter. Rare hastingsite crystals. Northfield Mountain Project, Access Tunnel, 845 feet from portal.

9+07 - Well layered pink feldspar-biotite gneiss with scattered hastingsite megacrysts and pink feldspar layers 2 mm thick. Northfield Mountain Project, Access Tunnel, 907 feet from portal.

9+40F - Split sample. Pink feldspar-quartz leucogneiss layer with numerous hastingsite megacrysts. Northfield Mountain Project, Access Tunnel, 940 feet from portal.

9+40M - Split sample. Light-gray fine-grained feldspar-biotite gneiss. Northfield Mountain Project, Access Tunnel, 940 feet from portal.

11+83 - Pink feldspar-quartz-biotite gneiss with pink feldspar augen 1 cm in diameter. Scattered hastingsite megacrysts up to 6 mm in size. Concentrated layers of pink feldspar and hastingsite 2-3 cm thick. Northfield Mountain Project, Access Tunnel, 1183 feet from portal.

15+84 - Pink feldspar-biotite gneiss with pink feldspar augen 1 cm diameter and sparse hastingsite megacrysts. Indistinct pink feldspar layering. Northfield Mountain Project, Access

Tunnel, 1584 feet from the portal.

15+96 - Pink feldspar-biotite gneiss with elongate white and pink feldspar augen concentrated in layers 5 mm thick. Scattered hastingsite megacrysts. Northfield Mountain Project, Access Tunnel, 1596 feet from portal.

TR31+79 - Light-gray feldspar-biotite gneiss with white feldspar layering 4 mm thick. Scattered hastingsite megacrysts. Northfield Mountain Project, Tailrace Tunnel, 3179 feet from west end.

TR32+18 - Light-gray feldspar-quartz-biotite gneiss with some some hastingsite megacrysts up to 7 mm long. One layer of concentrated pink and white feldspar is 1 cm across. Northfield Mountain Tunnel, Tailrace Tunnel, 3218 feet from west end.

TR33+23 - Light-gray feldspar-quartz leucogneiss with one biotite-feldspar zone of 2 cm thick. Scattered hastingsite megacrysts up to 7 mm across. Northfield Mountain Project, Tailrace Tunnel, 3323 feet from west end.

TR33+40 - Light-gray feldspar-biotite gneiss with concentrated layers of biotite 1 mm thick. Scattered hastingsite megacrysts. Northfield Mountain Project, Tailrace Tunnel, 3440 feet from west end.

TR34+91 - Light pink and gray feldspar-biotite gneiss with 2.5 cm thick layers of slightly more concentrated feldspar. Hastingsite crystals are mostly in the feldspar zones. Northfield Mountain Project, Tailrace Tunnel, 3491 feet from west end.

TR35+00 - Light-gray feldspar-biotite leucogneiss with indistinct layers slightly more rich in biotite. Numerous hastingsite megacrysts concentrated in the more felsic layers. Northfield Mountain Project, Tailrace Tunnel, 3500 feet from west end.

TR37+82 - Pink feldspar-quartz-biotite gneiss with hastingsite megacrysts up tp 1.2 cm long. Elongated pink feldspar augen 1 cm wide. Northfield Mountain Project, Tailrace Tunnel, 3782 feet from west end.

TR38+29 - Pink feldspar-biotite gneiss with pink feldspar augen 2 cm long. Divided into thin pink feldspar and biotite layers 2-3 mm thick. Northfield Mountain Project, Tailrace Tunnel, 3829 feet from west end.

TR39+40 - Pink feldspar-quartz-biotite gneiss with numerous hastingsite megacrysts. Northfield Mountain Project, Tailrace Tunnel, 3940 feet from west end.

TR40+85 - Pink feldspar-quartz-biotite gneiss with scattered pink feldspar augen 1 cm long and some hastingsite megacrysts 1 cm long. Northfield Mountain Project, Tailrace Tunnel, 4085 feet from west end.

TR41+95 - Pink feldspar-quartz-biotite gneiss with scattered hastingsite megacrysts. Indistinct layering of felsic components and biotite 0.5 cm thick. Northfield Mountain Project, Tailrace Tunnel, 4195 feet from west end.

TR42+23 - Pink feldspar-quartz-biotite gneiss with pink feldspar augen 0.8 cm thick. Scattered hastingsite. Northfield Mountain Project, Tailrace Tunnel, 4223 feet from west end.

TR43+46 - Medium-gray biotite-feldspar gneiss with large scattered pink feldspar megacrysts up to 1.5 cm across, otherwise fairly homogeneous. Northfield Mountain Project, Tailrace Tunnel, 4346 feet from west end.

TR44+50 - Pink feldspar-quartz-biotite gneiss with scattered biotite-rich layers 1 cm thick. A few pink feldspar augen 1.5 cm in diameter. Scattered hastingsite. Northfield Mountain Project, Tailrace Tunnel, 4450 feet from west end.

TR44+90F - Split sample. Taken from a pink feldspar-rich layer 8 cm thick. Zone contains abundant hastingsite megacrysts up to 5 mm thick. Northfield Mountain Project, Tailrace Tunnel, 4490 feet from west end.

TR44+90M - Split sample. Biotite-feldspar gneiss with scattered hastingsite megacrysts. Indistinct pink feldspar layers 1-2 cm thick. Northfield Mountain Project, Tailrace Tunnel, 4490 feet from west end.

TR47+75 - Medium-gray biotite-feldspar gneiss with scattered pink and white feldspar augen up to 1 cm in diameter. Some pink feldspar-rich layers up to 3mm thick. Northfield Mountain Project, Tailrace Tunnel, 4775 feet from west end.

TR56+88 - Pink feldspar-quartz-biotite gneiss with layers of pink feldspar and hastingsite together up to 1 cm thick. Northfield Mountain Project, Tailrace Tunnel, 5688 feet from west end.

Biotite Member

17+82 - Pale pink and gray, feldspar-biotite gneiss, medium grained, with fine gneissic layering. Northfield Mountain Project, Access Tunnel, 1782 feet from portal.

18+43 - Light-gray feldspar-biotite gneiss, medium-grained, with biotite-rich layers up to 1.5 cm thick, alternating with 1-2 mm thick pink feldspar layers. Northfield Mountain Project, Access Tunnel, 1843 feet from portal.

18+72 - Light-gray fine-grained biotite-feldspar gneiss with prominent layers of pink feldspar 1-3 mm thick. Northfield Mountain Project, Access Tunnel, 1872 feet from portal.

TR57+88 - Light-gray fine-grained biotite-feldspar gneiss with scattered light pink and white feldspar augen up to 2.5 cm long. Northfield Mountain Project, Tailrace Tunnel, 5788 feet from west end.

Allanite is probably strongly radioactive, because most grains are isotropic and cause large dark haloes in adjacent biotite and hastingsite. A few crystals of allanite have a murky dark brown to dark orangish brown pleochroism, and exhibit zoning in concentric rings. The allanite is subhedral, up to 2.6mm in length and is generally overgrown with pistacite. Pistacite occurs alone or in crystallographic continuity rimming allanite. The solitary grains are interstitial, poikilitic, and locally skeletal, and are therefore probably of metamorphic origin. Calcite, ranging in size from 0.2 mm to 2 mm, is interstitial and may be retrograde. Calcite is anhedral and occurs with biotite, hastingsite, sphene, and garnet.

Garnet is small, subhedral to anhedral and a pale salmon pink color. It is fairly free of inclusions and unaltered. Commonly, it occurs with hastingsite.

In all of the Dry Hill Gneiss thin sections studied, only two grains of tourmaline were observed, both in sample TR 44+90F. The tourmaline exhibits spectacular pleochroism from plum brown (E) to a very deep, almost black, purple (O). The crystals are in contact with a grain of pistacite which touches a grain of hastingsite.

Dry Hill Gneiss Biotite Member

The Dry Hill Gneiss Biotite Member as mapped by Ashenden has a similar mineralogy to the Hornblende Member, but typical specimens have either no hastingsite or almost no hastingsite compared to the Hornblende Member. Some of the samples of the Biotite member are also free of pistacite, but do have large, zoned allanites. In general, the Biotite Member is finer grained than the Hornblende Member. Modal biotite ranges from 3% to 16%. Most of the calcite occurs in parallel intergrowths with the dominant biotite foliation. The Biotite Member has more opaque minerals than the Hornblende Member.

The modes of both members of the Dry Hill Gneiss plot in the granite field of a modified Streckeisen diagram (Figure 4), although one sample of the Hornblende Member plots in the alkali granite field of the diagram because it contains a microcline megacryst. The biotite-rich layers of the split samples, marked "M" on the diagram, contain less potassium feldspar, so they plot further away from the Or corner of the triangle. The variation in felsic mineralogy in the split samples is almost as large as the variation in the Dry Hill Gneiss as a whole. The Biotite Member has a similar felsic mineralogy to the Hornblende Member except for having more modal biotite and less modal hastingsite.

Granitic Gneiss within the Poplar Mountain Quartzite

The granitic gneiss layers within the Poplar Mountain Quartzite bear a striking resemblance in thin section to the Dry Hill Gneiss

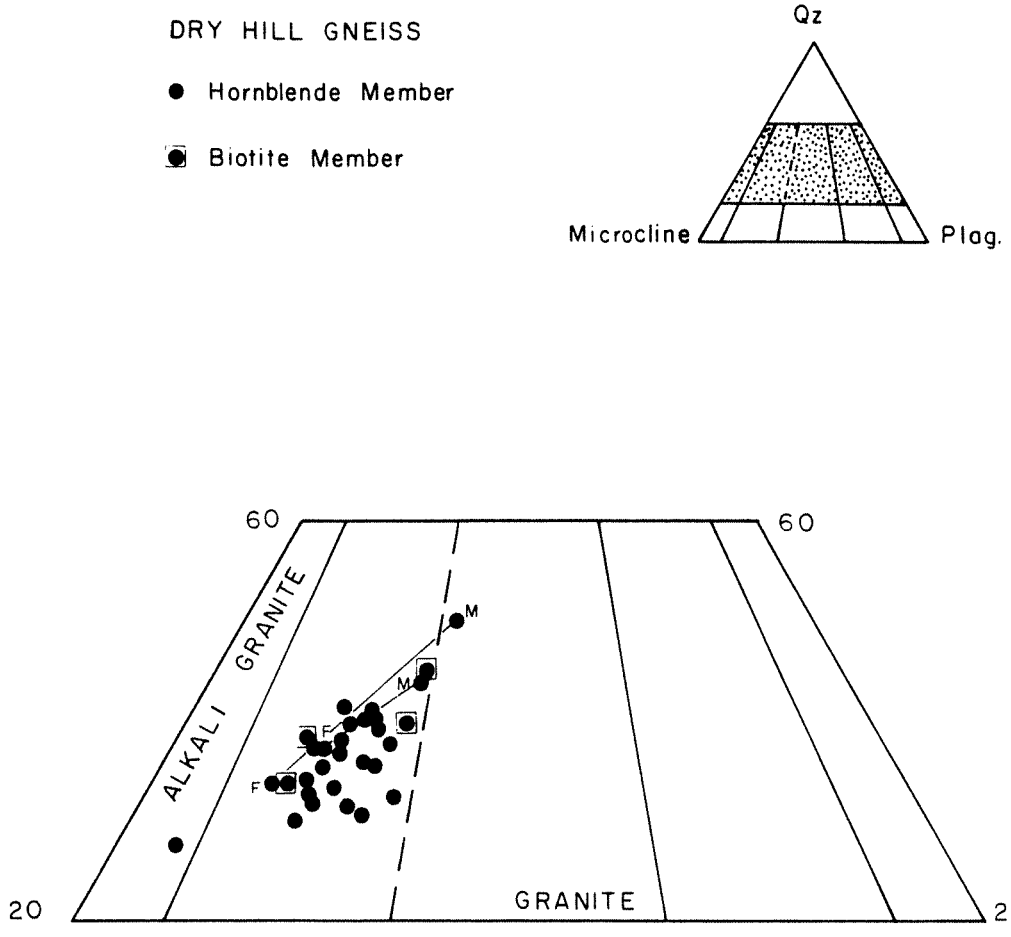

Figure 4. Plot of estimated modes of the Dry Hill Gneiss in volume percent on a modified Streckeisen diagram. One sample plots in the field of alkali granite due to a megacryst of microcline in the thin section. Split samples marked with "F" or "M".

(Table 2). This is not surprising, because the Poplar Mountain Quartzite directly overlies the Dry Hill Gneiss and is probably only slightly younger. In thin section, the quartz is clear and unaltered, and has some serrated grain boundaries. Microcline occurs in large megacrysts up to 4 mm and has "scotch-plaid" twinning. Plagioclase is smaller, less abundant and has a composition of An 14 to An 18. The plagioclase is very slightly zoned and the rims are more sodic.

Biotite, in long thin plates, defines the metamorphic foliation. It is pleochroic from brown (Z=Y) to slightly greenish yellow (X) and has small, dark, radioactive haloes from inclusions of zircon. The biotite is unaltered.

Hastingsite is scarce or absent. It has strong pleochroism from dark blue-green(Z) to brownish green(Y) to pale yellow green(X). The 2V is small, and ranges from 10 to 20 degrees.

Garnet is subhedral to euhedral and not very large, ranging in size from 0.2mm to 0.4mm. It is a uniform salmon pink in color and unaltered.

Sphene is subhedral and a slightly pleochroic golden color. It does not appear to be radioactive. Apatite occurs as small subhedral to euhedral colorless grains. Zircon ranges from minute to 0.16mm. It is subhedral, occurs in stubby prisms, and has rounded ends. Zircon, in stubby prisms, generally indicates origin in alkalic igneous rocks (Jaffe, personal communication, 1985).

Allanite is up to 1.8mm in length, and zoned. The crystals are brown in the center and golden on the edges and are pleochroic. Radioactive haloes are visible in ferromagnesian minerals in contact with allanite, such as biotite. Interference colors are quite low, due to the partially metamict character of the mineral. Allanite is rimmed sparingly by epidote. The epidote is pistacite, because it is colorless and has a moderate birefringence and a negative 2V of about 70-80^{o}. Since it occurs rimming allanite, it is probably prograde metamorphic. Calcite is retrograde metamorphic and usually occurs with hastingsite and biotite.

The modes of the granite gneiss within the Poplar Mountain Quartzite plot in the granite field of a modified Streckeisen diagram and are indistinguishable from Dry Hill Gneiss (Figure 5). The granite gneiss is quite uniform in composition and texture.

Felsic Gneiss within the Poplar Mountain Gneiss

The felsic gneiss within the Poplar Mountain Gneiss strongly resembles Dry Hill Gneiss in hand specimen, but some differences are visible in thin section, especially among the mafic minerals (Table 2),

Table 2. Estimated modes of granitic gneiss within Poplar Mountain Quartzite and felsic gneiss within Poplar Mountain Gneiss. Plagioclase feldspar composition by the Michel-Levy method.

	--Granitic Gneiss--			----------Felsic Gneiss----------				
	20+00	20+23	21+60	TR 28+44	TR 28+66	TR 29+47	TR 29+64	TR 29+99
Quartz	39	34	37	58	32	34	35	41
Plagioclase	12	20	18	17	24	39	17	36
Microcline	44	41	43	23	37	18	32	15
Hornblende				tr		2	13	2
Hastingsite	1	tr			4			
Biotite	4	5	2	2	3	7	3	6
Garnet	tr	tr	tr					
Pistacite	tr	tr	tr	tr	tr	tr	tr	tr
Allanite	tr	tr	tr	tr	tr	tr	tr	tr
Sphene	tr	tr	tr	tr	tr	tr	tr	tr
Apatite	tr	tr	tr	tr	tr	tr	tr	tr
Zircon	tr	tr	tr		tr	tr		tr
Opaque	tr	tr	tr	tr	tr	tr	tr	tr
Chlorite				tr	tr		tr	tr
Muscovite					tr		tr	
Calcite	tr	tr	tr			tr	tr	tr
An content:	An_{14}	An_{18}	An_{16}	An_{32}	An_{24}	An_{27}	An_{31}	An_{22}

Specimens in Table 2

Granitic gneiss in Poplar Mountain Quartzite

20+00 - Light-gray feldspar-biotite gneiss with one layer of pink feldspar 4 mm thick. Scattered hastingsite megacrysts up to 3 mm in diameter. Northfield Mountain Project, Access Tunnel, 2000 feet from portal.

20+23 - Light-gray feldspar-biotite gneiss with pink and white feldspar augen up to 1.8 cm long. Northfield Mountain Project, Access Tunnel, 2023 feet from portal.

21+60 - Light-gray feldspar-biotite gneiss with rare pink feldspar augen up to 1 cm long. Northfield Mountain Project, Access Tunnel, 2160 feet from portal.

Felsic gneiss in Poplar Mountain Gneiss

TR28+44 - Light-gray feldspar-biotite gneiss with scattered feldspar augen up to 1.4 cm long. Northfield Mountain Project, Tailrace Tunnel, 2844 feet from west end.

TR28+66 - Light-gray feldspar-biotite gneiss with scattered hornblende megacrysts and indistinct layering of feldspar 3 mm thick. One white feldspar augen 1.2 cm across. Resembles Dry Hill Gneiss. Northfield Mountain Project, Tailrace Tunnel, 2866 feet from west end.

TR29+47 - Gray biotite-feldspar gneiss with 5 mm thick layering of white feldspar. White feldspar augen 2 cm long. Northfield Mountain Project, Tailrace Tunnel, 2947 feet from west end.

TR29+64 - Light-gray feldspar-biotite gneiss with numerous hornblende megacrysts up to 7 mm long. Faint biotite layering 3 mm thick. Northfield Mountain Project, Tailrace Tunnel, 2964 feet from west end.

TR29+99 - Light-gray feldspar-biotite gneiss with indistinct white feldspar layering. Hornblende megacrysts up to 8 mm in diameter. Northfield Mountain Project, Tailrace Tunnel, 2999 feet from west end.

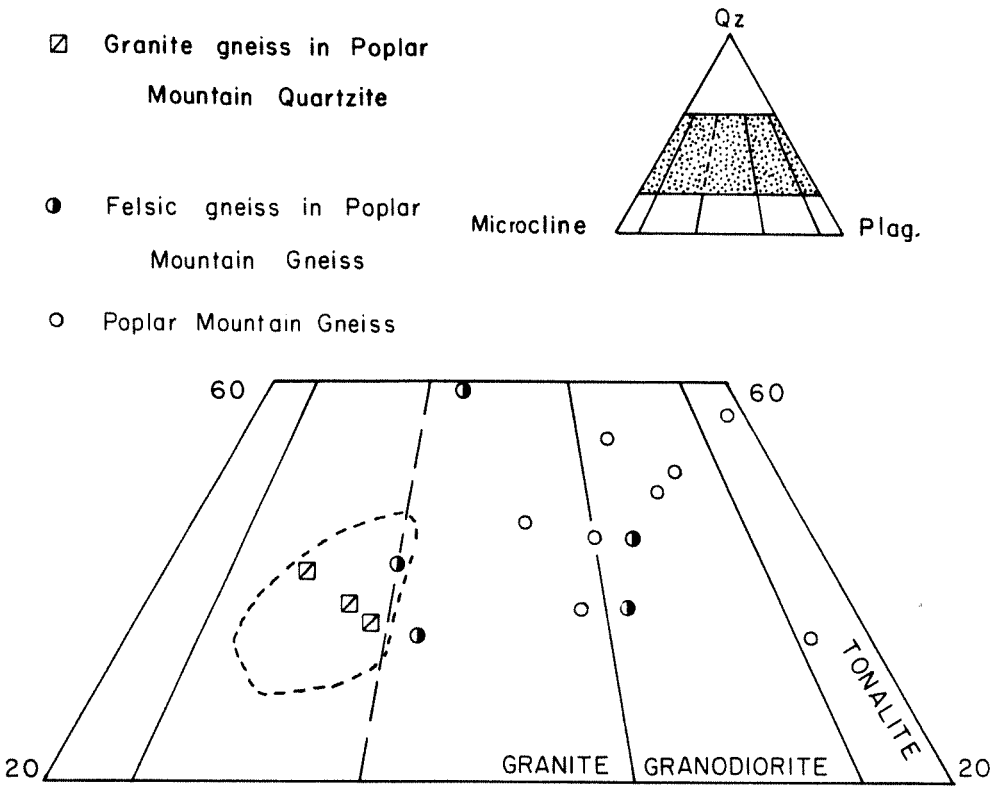

Figure 5. Plot of the estimated modes of the granite gneiss within the Poplar Mountain Quartzite, the felsic gneiss within the Poplar Mountain Gneiss, and the Poplar Mountain Gneiss proper, on a modified Streckeisen diagram. Plotted in volume percent. Field of Dry Hill Gneiss is outlined by a dashed line. Although the Poplar Mountain Gneiss is probably of sedimentary derivation, it is plotted on this diagram for contrast.

and in modal proportions of quartz, plagioclase, and K-feldspar (Figure 5). Quartz is clear and unaltered, but shows strained extinction under crossed polars. The quartz is up to 5 mm in diameter although 0.4 mm is more usual, and forms a mosaic texture with some serrated grain edges. Some crystals are elongate in the direction of foliation. Others are myrmekitic in feldspar. Microcline is plentiful and some grains are as large as 4.5 mm although the average is 0.5 mm. Plagioclase is much smaller and is from An 22 to An 32 in composition. It has some sericite alteration.

The mafic minerals are different from those of the Dry Hill Gneiss. Hastingsite is from 15 mm to 0.2 mm in size and is pleochroic from dark blue green (Z) to brownish green (Y) to pale yellow green(X). The pleochroism is not so strong as in the Dry Hill hastingsites, nor is the 2V so small, ranging from 30° in the hastingsites to 60° in the hornblendes. Some of the amphiboles with larger 2vs could more properly be called hornblende (Table 2). The hastingsite in the felsic gneiss is altered by biotite and iron-rich chlorite and occurs in association with epidote and calcite.

Biotite has pleochroism of red brown(Z=Y) to medium yellow(X) in samples TR 29+47, TR 29+64, and TR 29+99; and of dark brown(Z=Y) to yellow(X) in samples TR 28+44 and TR 28+66 rather than the greenish brown of the Dry Hill Gneiss biotites. The color of biotite is diagnostic to separate the Dry Hill Gneiss from the felsic gneiss within the Poplar Mountain Gneiss and from the Poplar Mountain Gneiss proper. The biotite defines the metamorphic foliation and also occurs on hastingsite crystals. Pale green iron-rich chlorite is an alteration product of the biotite. The biotite plates are generally thin and about 0.8 mm long.

The same accessory and secondary minerals occur in the felsic gneiss in the Poplar Mountain Gneiss as in the Dry Hill Gneiss. Pistacite may be metamorphic, for it rims allanite in crystallographic continuity. The allanite formed dark, radioactive haloes on adjacent biotite and hornblende, but the pistacite appears to be slightly radioactive too, based on the same evidence. Allanite is a slightly pleochroic tan color, with very low gray interference colors, suggesting it is partially metamict. The epidote and allanite generally occur in clots with biotite.

Sphene is a golden brown color with slight pleochroism. The crystals are euhedral and in most cases the long axes of the crystals are up to 0.5 mm long, parallel to the biotite foliation. Sphene is very slightly radioactive, and poikilitic with quartz.

Apatite is subhedral to euhedral and 0.2 mm in size. Calcite is interstitial, secondary, and normally occurs on hastingsite. Opaques occur in trace amounts in the form of skeletal anhedral black crystals. Neither garnet, nor tourmaline, was observed in the five thin sections.

The felsic gneiss within the Poplar Mountain Gneiss is extremely variable in composition. The modes plot in the granodiorite field and in the granite field of a modified Streckeisen diagram (Figure 5), due to major variations in the proportions of potassium feldspar and plagioclase. Only one sample plots within the field of Dry Hill Gneiss.

Poplar Mountain Gneiss

In thin section, the Poplar Mountain Gneiss is well foliated, with medium-sized grains of biotite and less commonly hornblende occuring with large megacrysts(Table 3). Some of the large white megacrysts visible in hand specimen are microcline, plagioclase, or a combination of the two. The megacrysts can be up to 15 cm in diameter, although 1 cm is more common.

Quartz is clear, elongate and shows a preferred orientation in the direction of foliation. Most crystals have strained extinction under crossed polars and some have serrated edges. Quartz occurs in some porphyroblasts with feldspar, also. A few specimens contain myrmekite.

Plagioclase is slightly altered by sericite. The composition ranges from An 21 in sample TR 26+01 to An 37 in sample TR 26+6 to An 44 in sample TR 21+07. The formation is extremely variable, in keeping with its proposed sedimentary source. Grain size is up to 3cm, but most are 0.4 mm. Polysynthetic twinning is usually perpendicular to the foliation. Some grains have a myrmekitic texture.

Microcline occurs in big patches up to 1 cm and as small, almost rectangular grains of 0.4 mm in length. Most crystals are twinned.

Hornblende appears in thin section in only some samples. In sample TR 21+07, it is moderately pleochroic: green (Z) to olive green (Y) to yellowish green (X), and has a 2V of about 40°. The crystal habit is elongate, up to 3.8 mm, and some grains are twinned. In TR 26+95, the amphibole is lighter in color, pleochroic with Z>Y>X from green (Z) to olive green (Y) to pale yellow (X) and has a 2V of 70°. It has a stubbier crystal shape and is poikilitic. Biotite and epidote are associated with the amphibole and it is altered by iron-rich chlorite. In TR 27+92, the actinolite is pleochroic with Z>Y>X from pale bluish green (Z) to pale green (Y) to very pale yellow (X) and it has a 2V of 80°.

One sample, TR 30+18, contains a calcic pyroxene. It has moderate birefringence and positive sign with a 2V of about 60°. The pyroxene is colorless, with traces of an orange weathering product, which may be iddingsite. The pyroxene occurs with or within a hornblende that has a 2V of $60\text{-}70^{\circ}$. The hornblende has a moderate pleochroism of dark blue green (Z) to olive green (Y) to pale yellow green (X). In one place, the pyroxene is overgrown by epidote.

Table 3. Estimated modes of Poplar Mountain Gneiss. Plagioclase feldspar composition by the Michel-Levy method.

	TR 21+07	TR 25+86*	TR 26+01	TR 26+40	TR 26+60	TR 26+95	TR 27+92	TR 30+18
Quartz	49	22	35	38	35	47	41	42
Plagioclase	36	68	37	25	29	38	34	25
Microcline	tr	3	22	20	15	11	12	10
Actinolite							5	
Hornblende						2		6
Hastingsite	6							
Ca Pyroxene								tr
Biotite	5	4	4	17	19	4	8	17
Garnet	4		tr	tr	tr	tr		
Pistacite	tr			tr	tr	tr	tr	tr
Allanite	tr			tr	tr	tr	tr	tr
Sphene	tr		tr	tr	tr	tr	tr	tr
Apatite	tr	tr	tr	tr	tr	tr	tr	tr
Zircon	tr	tr	tr	tr	tr	tr	tr	tr
Opaque	tr	tr	tr	tr	tr	tr	tr	tr
Chlorite	tr	tr	tr	tr	tr	tr		tr
Muscovite	tr	3	tr			tr		tr
Calcite	tr	tr	tr	tr	tr	tr		tr
An content:	An_{44}	An_{24}	An_{21}	An_{26}	An_{37}	An_{26}	An_{26}	An_{23}

* Sample contains a large feldspar megacryst with polysynthetic plagioclase twinning.

A note on sampling:

Only the outer layers of the Poplar Mountain Gneiss were sampled. The inner layers were not sampled. Please see Figure 3.

Specimens in Table 3

TR21+07 - Light-gray feldspar-biotite gneiss. Northfield Mountain Project, Tailrace Tunnel, 2107 feet from west end.

TR25+86 - Gray fine-grained feldspar-biotite gneiss with abundant slightly stretched white feldspar augen 1 cm in length. Northfield Mountain Project, Tailrace Tunnel, 2586 feet from west end.

TR26+01 - Light-gray feldspar-biotite gneiss with layers of white feldspar 6 mm thick. Northfield Mountain Project, Tailrace Tunnel, 2601 feet from west end.

TR26+40 - Gray fine-grained biotite-feldspar gneiss with elongate white feldspar megacrysts 1 cm long. One large feldspar augen is 3.5 cm long. Northfield Mountain Project, Tailrace Tunnel, 2640 feet from west end.

TR26+60 - Gray fine-grained biotite-feldspar gneiss with numerous white feldspar augen up to 4 cm in diameter, averaging 8 mm in diameter. Northfield Mountain Project-2660 feet from west end.

TR26+95 - Gray fine-grained biotite-feldspar quartzose gneiss with quartz-rich layers up to 1 cm thick. Rare white feldspar augen 8 mm in diameter. Northfield Mountain Project, Tailrace Tunnel, 2695 feet from west end.

TR27+92 - Gray fine-grained biotite-feldspar gneiss with scattered white feldspar augen up to 5 mm in diameter, averaging 3 mm in diameter. Northfield Mountain Project, Tailrace Tunnel, 2792 feet from west end.

TR30+18 - Gray fine-grained biotite-feldspar gneiss with elongate white feldspar augen up to 2 cm long, averaging 5 mm long. Northfield Mountain Project, Tailrace Tunnel, 3018 feet from west end.

Biotite, in all samples, is pleochroic from reddish brown(Z=Y) to pale yellow(X) and occurs in subhedral, elongate crystals which define the foliation. Pale green iron-rich chlorite with positive elongation and some colorless magnesium-rich chlorite with negative elongation are alteration products of the biotite. Plates of muscovite occur locally in Poplar Mountain Gneiss. Plates are up to 4.0mm in diameter and occur in parallel intergrowths with biotite or rimming large feldspar megacrysts.

Garnet occurs in most samples of Poplar Mountain Gneiss. It is up to 2.7mm in diameter, anhedral and poikilitic with quartz, biotite and opaques. The biotite foliation wraps around the garnet and large crystals of calcite locally occur in the garnet pressure shadows. Based on slight gradations in color, the garnet may have minor zoning.

Sphene is pale golden brown and subhedral. Some grains have an alteration rim of opaques at the edges of the crystals. The crystals are elongate in the direction of foliation and generally occur with epidote and opaques. Sphene is only mildly radioactive, judging from pleochroic haloes. Allanite is a dirty brown color with very low birefringence and occurs in the center of grains of pistacite, which are in crystallographic continuity. Some crystals of the epidote are elongate in the direction of foliation. Pistacite occurs associated with biotite and calcite. Both apatite and zircon occur in small euhedral to subhedral grains. The apatite is up to 0.5 mm long. The zircon is radioactive.

Opaques are anhedral and black, and most occur in association with biotite, chlorite,and sphene. A few, minute, dark red, translucent hematite crystals occur in some samples.

Modes of the Poplar Mountain Gneiss plot in the granodiorite, granite, and tonalite fields of a modified Streckeisen diagram (Figure 5). Although the Poplar Mountain Gneiss is of probable sedimentary derivation, the modes were plotted on a Streckeisen diagram for contrast with the other rocks studied. The formation is extremely variable and contains feldspar megacrysts which may bias the mode. A much larger thin section of each sample would be necessary to be confident of properly estimated modes.

Fourmile Gneiss

Fourmile Gneiss is medium grained. In thin section, quartz is colorless and unaltered and elongated in the direction of foliation. The grains have strained extinction and serrated boundaries. Plagioclase ranges in composition from An 23 to An 26 (Table 4). It has both pericline twinning and albite twinning. Most grains are altered to varying degrees by sericite. Microcline contains only subordinate gridiron twinning but has lower relief than the plagioclase and is much less altered.

Biotite is fresh, with only a trace of iron-rich chlorite alteration. Elongate plates from 0.3 to 1.0 mm long define the foliation. Most of the biotite has strong pleochroism from red brown(Z=Y) to light yellow(X). Sample TR 17+90 has biotite that is pleochroic from brown (Z=Y) to slightly greenish yellow (X). It is altered by magnesian chlorite and opaques rather than iron chlorite.

Garnet occurs in two out of the four samples studied. It is pinkish orange and slightly fractured. It is poikilitic with quartz and has biotite in embayments in the crystals. Traces of chlorite also occur with garnet.

Epidote is from 0.6 to 1.8 mm in diameter and is elongate in the plane of foliation. It is clear, unaltered and well crystallized. A few grains are slightly poikilitic with quartz. The moderate birefringence under crossed polars, the negative sign, and the 2V of 70-80^{o}, show it is pistacite. A few faint, radioactive haloes form in adjacent mafic minerals, such as biotite, indicating the pistacite is mildly radioactive. Allanite occurs in the centers of a few grains. It is pleochroic dirty brown and has a low birefringence, masked by the color in some crystals. It has produced pleochroic haloes in adjacent minerals, indicating it is radioactive.

Apatite is subhedral, colorless and up to 0.3 mm in length. Zircon forms pleochroic, dark haloes in the biotite. Sample TR 17+90 contains some calcite in the pressure shadow of a pistacite crystal.

Fourmile Gneiss plots in the granodiorite field of a modified Streckeisen diagram (Figure 6).

Belchertown Tonalite

In thin section, the tonalite of the Belchertown Complex is well foliated, with distinct gneissic layering of hornblende and biotite with quartz and feldspar. The quartz is colorless and unaltered, with a few serrated grain boundaries and local strained extinction. Microcline, up to 0.9 mm in size, has faint "scotch-plaid" twinning and relief lower than plagioclase. Plagioclase is very slightly zoned, with more calcic rims, and is An 19-22 based on Michel-Levy extinction angles (Table 4). It is up to 1.8mm long. Some grains contain secondary sericite.

Biotite is strongly pleochroic from greenish brown (Z=Y), to pale yellow (X) and has a subhedral elongate crystal habit. It defines defines the dominant metamorphic foliation. Zircon and allanite form pleochroic haloes in the biotite. Both iron-rich (positive elongation) and magnesium-rich (negative elongation) chlorite are alteration products of the biotite.

Table 4. Estimated modes of Fourmile Gneiss and Belchertown Tonalite from the Tailrace Tunnel and Northfield Mountain. Feldspar composition by the Michel-Levy method of extinction angles.

	Fourmile Gneiss				Belchertown	
	TR17+00	TR17+90	TR18+34	TR18+48	N164	TR25+06
Quartz	27	39	29	37	20	24
Plagioclase	44	33	39	40	51	46
Microcline	13	15	14	13	2	2
Hornblende					12	20
Biotite	13	9	12	6	15	8
Garnet	tr	tr				
Pistacite	3	4	6	4	tr	tr
Allanite	tr	tr	tr		tr	tr
Sphene					tr	tr
Apatite	tr	tr	tr	tr	tr	tr
Zircon	tr	tr	tr	tr	tr	tr
Opaques	tr	tr	tr	tr	tr	tr
Chlorite	tr	tr	tr	tr	tr	tr
Sericite	tr	tr	tr	tr		
Calcite		tr				
An content:	An_{26}	An_{26}	An_{24}	An_{23}	An_{22}	An_{19}

Specimens in Table 4

Fourmile Gneiss

TR17+00 - Light-gray fine-grained feldspar-biotite gneiss. Homogeneous except for rare 1mm thick white feldspar layers. Northfield Mountain Project, Tailrace Tunnel, 1700 feet from west end.

TR17+90 - Light-gray fine-grained feldspar-biotite gneiss with two pink and white feldspar layers each 3mm thick. Augen within the layers up to 1 cm long. Northfield Mountain Project, Tailrace Tunnel, 1790 feet from west end.

TR18+43 - Light-gray fine-grained feldspar-biotite gneiss. Two 8 mm thick layers slightly enriched in biotite. Northfield Mountain Project, Tailrace Tunnel, 1843 feet from west end.

TR18+48 - Light-gray fine-grained homogeneous feldspar-biotite gneiss with one 1 mm thick layer of white feldspar. Northfield Mountain Project, Tailrace Tunnel, 1848 feet from west end.

Belchertown Tonalite

N164 - Medium-gray biotite-feldspar gneiss. Homogeneous, except for scattered 2 mm grains of hornblende. Northfield Mountain Project junction of roads about 600 feet north of Access Tunnel portal area. A road cut on east side of road, twenty feet from Ashenden sample location 164, which is buried beneath the road.

TR25+06 - Medium-gray fine-grained homogeneous biotite-feldspar gneiss. Northfield Mountain Project, Tailrace Tunnel, 2506 feet from west end.

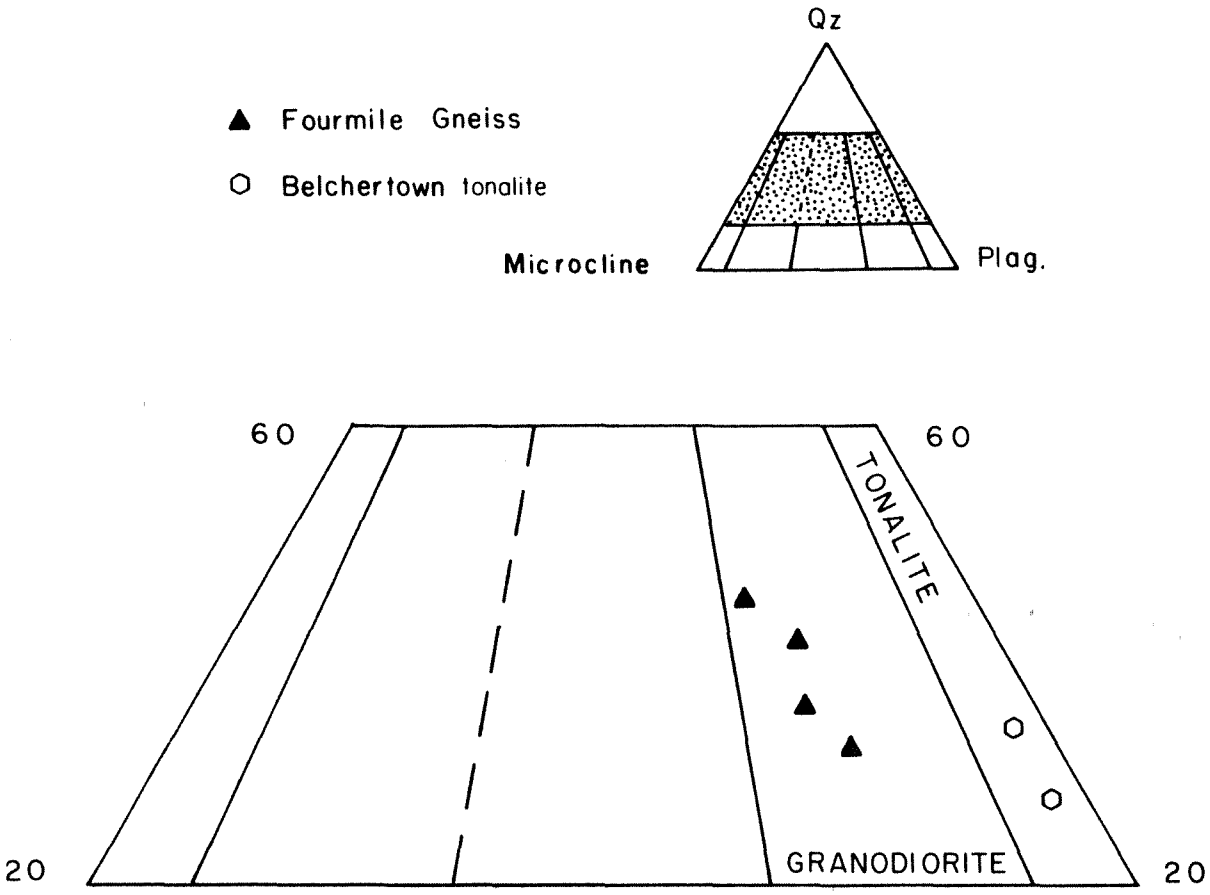

Figure 6. Estimated modes of Fourmile Gneiss and the sill of tonalite related to the Belchertown Complex, plotted in volume percent on a modified Streckeisen diagram. Two unrelated units are combined on this figure for convenience.

Hornblende is strongly pleochroic with Z>Y>X from slightly bluish green (Z) to slightly olive green (Y) to pale yellow (X), and has a 2V of 70°. The grain length is up to 4.2mm. The amphibole is poikilitic with quartz and usually occurs in intergrowths with sphene, chlorite, and biotite. A slight color change indicates minor zoning of the mineral.

Allanite is radioactive, anhedral, slightly pleochroic orange brown, and overgrown by pistacite. One grain of allanite shows (100) twinning. Both pistacite and zoisite occur in the formation. Sphene is euhedral, radioactive, and is a pleochroic brownish golden color. A few grains are twinned. Apatite occurs as small, colorless, subhedral grains.

The modes of the Belchertown sill plot in the tonalite field of a modified Streckeisen diagram (Figure 6). Although the unit as a whole has been called the Belchertown Quartz Monzodiorite (Ashwal, et al., 1979) this mode is consistent with tonalites described by Guthrie (1972) in the northern part of the pluton.

MINERAL CHEMISTRY OF THE DRY HILL GNEISS

Based on optical studies, a typical sample of Dry Hill Gneiss Hornblende Member, TR 44+50, was selected for analysis with the ETEC Autoprobe at the University of Massachusetts. Major element chemistry of the dominant phases: amphibole, biotite, plagioclase, microcline, and garnet was determined. A grain mount of fifteen amphiboles from the Hornblende Member of the Dry Hill Gneiss and three amphiboles from the felsic gneiss within the Poplar Mountain Gneiss was analysed for major elements on the ETEC Autoprobe at the University of Massachusetts. This was done to study the chemistry of the minerals and to try to relate that chemistry to the small 2Vs of the amphiboles.

Amphibole

The results of the amphibole study are presented in Table 5. Each listed analysis represents an average of 3 to 7 best analysed grains. Structural formulae were calculated on the basis of 23 oxygens and 15 cations in the formula exclusive of Na and K (Robinson et al., 1982). This particular formulation assumes that all Na and K are assigned to the A crystallographic site, and Ca is excluded from the site. The formulation gives the minimum reasonable amount of Fe that should be assigned to Fe3+.

The amphiboles in the Dry Hill Gneiss have a high ratio of Fe2+/(Fe2+ + Mg), from 0.544 to 0.909 (Table 5). Tetrahedral aluminum in the structural formula ranges from 1.664 to 2.040. A-site occupancy is high and sums from 0.748 to 0.917. The amphiboles from felsic gneiss in the Poplar Mountain Gneiss have a slightly more limited range of

Table 5. Electron microprobe analyses of fifteen amphiboles from the Dry Hill Gneiss and three amphiboles from the felsic gneiss within the Poplar Mountain Gneiss. Structural formulae are based on 23 oxygens. FeOT is total iron as FeO. *Ferric iron correction calculated to 15 cations exclusive of Na and K.

Sample no.	0+50	9+40F	11+83	TR31+79	TR33+40	TR35+00
No. of Analyses:	5	5	6	4	5	5
SiO2	37.12	37.51	36.68	39.93	40.18	40.76
TiO2	0.99	0.83	0.84	1.02	0.98	0.71
Al2O3	12.86	12.04	12.47	11.88	11.97	10.02
FeOT	28.14	27.58	29.73	23.50	23.60	21.49
MnO	0.77	0.64	0.80	0.85	0.93	0.72
MgO	2.87	3.67	2.17	5.73	5.39	8.38
ZnO	0.42	0.46	0.49	0.30	0.36	0.33
CaO	10.79	10.88	10.42	10.90	11.40	11.28
Na2O	1.73	1.69	1.57	1.53	1.56	1.84
K2O	1.73	1.65	1.66	1.40	1.61	1.46
Total	97.42	96.95	96.83	97.04	97.98	95.99
Structural Formulae:						
Si	5.964	6.025	5.960	6.270	6.273	6.336
Al	2.036	1.975	2.040	1.730	1.727	1.664
Sum	8.000	8.000	8.000	8.000	8.000	8.000
Al	0.399	0.304	0.348	0.469	0.476	0.172
Ti	0.120	0.101	0.103	0.120	0.115	0.083
Fe3+*	0.505	0.603	0.647	0.277	0.230	0.482
Mg	0.687	0.878	0.526	1.342	1.255	1.941
Zn	0.049	0.054	0.059	0.035	0.042	0.038
Fe2+	3.240	3.060	3.317	2.757	2.851	2.284
Mn	0	0	0	0	0.031	0
Sum	5.000	5.000	5.000	5.000	5.000	5.000
Fe2+	0.036	0.042	0.076	0.052	0	0.027
Mn	0.105	0.087	0.110	0.113	0.092	0.095
Ca	1.858	1.872	1.814	1.834	1.907	1.878
Sum	1.999	2.001	2.000	1.999	1.999	2.000
Na	0.538	0.526	0.495	0.466	0.472	0.554
K	0.355	0.338	0.344	0.280	0.320	0.290
Sum	0.893	0.864	0.839	0.746	0.792	0.844
Fe/(Fe+Mg)	0.846	0.808	0.885	0.697	0.711	0.590
Fe2+/(Fe2++Mg)	0.827	0.779	0.866	0.677	0.694	0.544
Fe3+/(Fe3++Al)	0.628	0.665	0.650	0.371	0.326	0.737
2V (in degrees)	5	10	10	undet.	30	40

Table 5. continued.

Sample No.	TR37+82	TR38+29	TR40+85	TR41+95	TR42+23	TR43+46
No. of analyses:	5	5	5	5	5	5
SiO2	37.52	37.99	37.52	38.02	38.38	38.21
TiO2	1.05	0.10	0.95	0.74	1.02	0.77
Al2O3	12.83	12.35	12.06	12.35	11.98	12.45
FeOT	27.90	27.92	29.54	27.69	28.10	26.98
MnO	0.77	0.58	0.75	0.73	0.56	0.78
MgO	3.14	3.26	2.27	3.52	3.38	3.88
ZnO	0.40	0.31	0.36	0.41	0.41	0.34
CaO	10.86	10.42	10.16	10.45	10.43	10.51
Na2O	1.89	1.72	1.71	1.52	1.73	1.63
K2O	1.79	1.53	1.53	1.45	1.52	1.56
Total	98.15	96.18	97.05	96.88	97.43	97.11
Structural Formulae:						
Si	5.985	6.147	6.115	6.089	6.140	6.099
Al	2.015	1.853	1.885	1.911	1.860	1.901
Sum	8.000	8.000	8.000	8.000	8.000	8.000
Al	0.397	0.502	0.420	0.420	0.399	0.441
Ti	0.126	0.012	0.116	0.089	0.123	0.092
Fe3+	0.416	0.472	0.379	0.545	0.368	0.454
Mg	0.747	0.786	0.548	0.841	0.806	0.923
Zn	0.048	0.037	0.043	0.048	0.049	0.040
Fe2+	3.266	3.191	3.494	3.057	3.255	3.050
Sum	5.000	5.000	5.000	5.000	5.000	5.000
Fe2+	0.040	0.115	0.132	0.107	0.137	0.098
Mn	0.104	0.079	0.103	0.099	0.075	0.105
Ca	1.856	1.806	1.765	1.794	1.788	1.797
Sum	2.000	2.000	2.000	2.000	2.000	2.000
Na	0.585	0.539	0.538	0.472	0.537	0.504
K	0.365	0.316	0.316	0.296	0.310	0.318
Sum	0.950	0.855	0.854	0.768	0.847	0.822
Fe/(Fe+Mg)	0.833	0.828	0.880	0.815	0.823	0.796
Fe2+/(Fe2++Mg)	0.816	0.808	0.869	0.790	0.808	0.773
Fe3+/(Fe3++Al)	0.512	0.485	0.474	0.565	0.480	0.507
2V (in degrees)	30	30-40	10	10	10	undet.

Table 5 continued.

	---------Dry Hill--------			Felsic Gneiss in --Poplar Mountain Gneiss-		
Sample No.	TR44+50	TR44+90F	TR56+88	TR28+66	TR29+64	TR29+99
No. of analyses:	7	5	5	3	3	5
SiO2	37.85	37.54	37.39	38.04	39.95	40.09
TiO2	0.76	1.08	0.95	0.93	0.98	0.77
Al2O3	12.65	12.75	11.68	12.73	12.15	11.69
FeOT	28.84	27.55	30.68	25.72	21.89	22.90
MnO	0.84	0.78	0.68	0.84	0.66	0.83
MgO	2.25	3.28	1.56	4.30	6.61	6.36
ZnO	0.05	0.33	0.42	0.44	0.35	0.34
CaO	10.54	10.42	10.04	10.96	11.28	11.01
Na2O	1.66	1.71	1.63	1.60	1.74	1.56
K2O	1.84	1.61	1.54	1.61	1.47	1.32
Total	97.28	97.05	96.57	97.16	97.08	96.87
Structural Formulae:						
Si	6.115	6.031	6.120	6.042	6.237	6.276
Al	1.885	1.969	1.880	1.958	1.763	1.724
Sum	8.000	8.000	8.000	8.000	8.000	8.000
Al	0.523	0.445	0.374	0.425	0.472	0.432
Ti	0.092	0.131	0.117	0.111	0.115	0.090
Fe3+	0.280	0.400	0.433	0.494	0.242	0.375
Mg	0.542	0.785	0.380	1.018	1.593	1.484
Zn	0.006	0.039	0.051	0.051	0.041	0.040
Fe2+	3.557	3.200	3.645	2.901	2.591	2.579
Sum	5.000	5.000	5.000	5.000	5.000	5.000
Fe2+	0.059	0.101	0.146	0.021	0.025	0.043
Mn	0.115	0.106	0.094	0.133	0.088	0.110
Ca	1.825	1.793	1.760	1.865	1.887	1.847
Sum	1.999	2.000	2.000	2.019	2.000	2.000
Na	0.519	0.532	0.517	0.492	0.527	0.473
K	0.380	0.330	0.322	0.326	0.292	0.264
Sum	0.899	0.862	0.839	0.818	0.819	0.737
Fe/(Fe+Mg)	0.878	0.825	0.917	0.770	0.642	0.669
Fe2+/(Fe2++Mg)	0.870	0.808	0.909	0.742	0.622	0.639
Fe3+/(Fe3++Al)	0.349	0.473	0.537	0.538	0.339	0.465
2V (in degrees)	20	5	20	30	50	60

0.622 to 0.742 Fe2+/(Fe2+ + Mg) and 1.724 to 1.985 tetrahedral aluminum. In a similar manner to the Dry Hill Gneiss, the A-site in the amphiboles of the felsic gneiss are quite full, from 0.737 to 0.819.

An attempt was made to classify the amphiboles from the Dry Hill Gneiss and the felsic gneiss within the Poplar Mountain Gneiss by plotting the analyses on standard classification diagrams (Figures 7 and 8). In Figure 7a, all of the analyses are shown in a plot of A-site versus tetrahedral Al, and all contain more than 0.5 cations in the A-site. Of these, those with tetrahedral Al greater than 1.75 fall in the general category of either hastingsite (H) or pargasite (P), depending on the Fe3+/AlVI ratio. Those with tetrahedral Al less than 1.75 fall into the general category of either hastingsitic hornblende (HH) or pargasitic hornblende (PH), again dependent on Fe3+/AlVI ratio. Adjectives and prefixes to be applied to the names of these amphiboles are dependent on whether the Fe2+/(Fe2+ + Mg) ratio is greater than or less than 0.70 (Figure 7b). For those with the higher ratio, the appropriate names are hastingsite (H) and ferropargasite (F); and hastingsitic hornblende (HH) and ferropargasitic hornblende (FH). For those with the lower ratio, the appropriate names are magnesian hastingsitic hornblende (MHH) and ferroan pargasitic hornblende (FPH). The decision between the names hastingsite (H) and hastingsitic hornblende (HH); and pargasite (P) and pargasitic hornblende (PH), is dependent on whether the ratio of Fe3+/(Fe3+ + Al) is greater than or less than 0.5 as shown in Figure 7c. In the two parts of Figure 8, the two ratios Fe2+/(Fe2+ + Mg) and Fe3+/(Fe3+ + Al) are plotted against each other for the two groups of amphiboles, those with tetrahedral Al > 1.75 and those with tetrahedral Al < 1.75 (and > 1.25). For those with tetrahedral Al > 1.75 (Figure 8a), eight analyses are assigned to hastingsite (H), five to ferropargasite (F), one to ferroan pargasite (FP), and none to magnesian hastingsite (MH). For those with tetrahedral Al < 1.75, none are assigned either to hastingsitic hornblende (HH) or to ferropargasitic hornblende (FH), three are assigned to ferroan pargasitic hornblende (FPH), and one to magnesian hastingsitic hornblende (MHH). Thus, of the eight possible names that could be used in this small region of amphibole composition space, only five are actually used. A combined examination of plots in Figures 7 and 8 shows that, with the exception of the one magnesian hastingsitic hornblende, the amphiboles fall on a broad general trend in which increasing tetrahedral Al is accompanied by increasing A-site occupancy (Figure 7a), increasing Fe2+/Mg ratio (Figure 7b) and increasing Fe3+/AlVI ratio (Figure 7c) approximately from ferroan pargasitic hornblende to hastingsite. In particular, Figure 7a shows a trend of A-site occupancy versus tetrahedral Al of about 0.44/1, somewhat higher than that observed in hornblendes in amphibolites and calc-alkaline granitic rocks (Dodge, et al., 1968 cited in Robinson and Jaffe, 1969), but similar to trends observed in alkalic granites and feldspathoidal syenites (Robinson, et al., 1971, p. 1019).

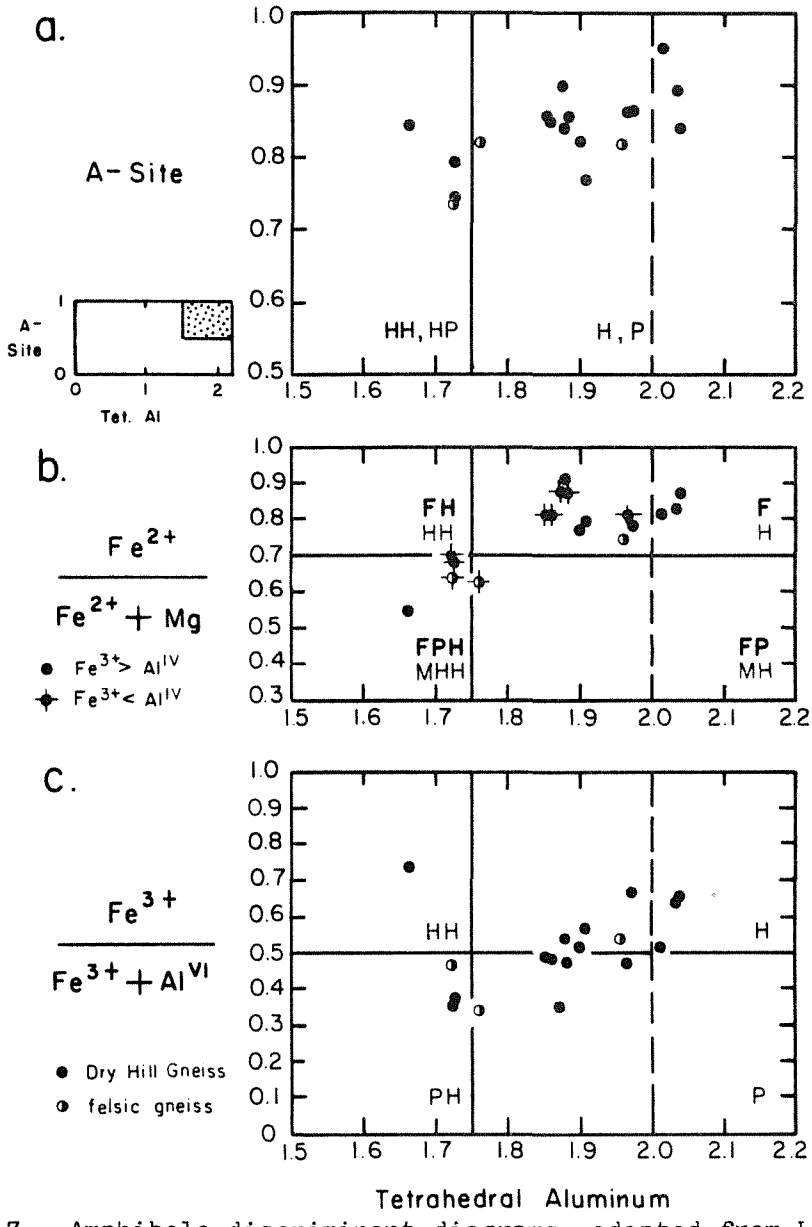

Figure 7. Amphibole discriminant diagrams, adapted from Leake (1978) and Hawthorne (1981). All diagrams are plotted against tetrahedral aluminum. In diagram b, bold face letters stand for names of amphiboles with Fe3+ less than AlVI and regular letters stand for names of amphiboles with Fe3+ greater than AlVI.

AMPHIBOLE NOMENCLATURE

HH hastingsitic hornblende
PH pargasitic hornblende
H hastingsite
P pargasite
FH ferropargasitic hornblende
F ferropargasite
FPH ferroan pargasitic hornblende
FP ferroan pargasite
MHH magnesian hastingsitic hornblende
MH magnesian hastingsite

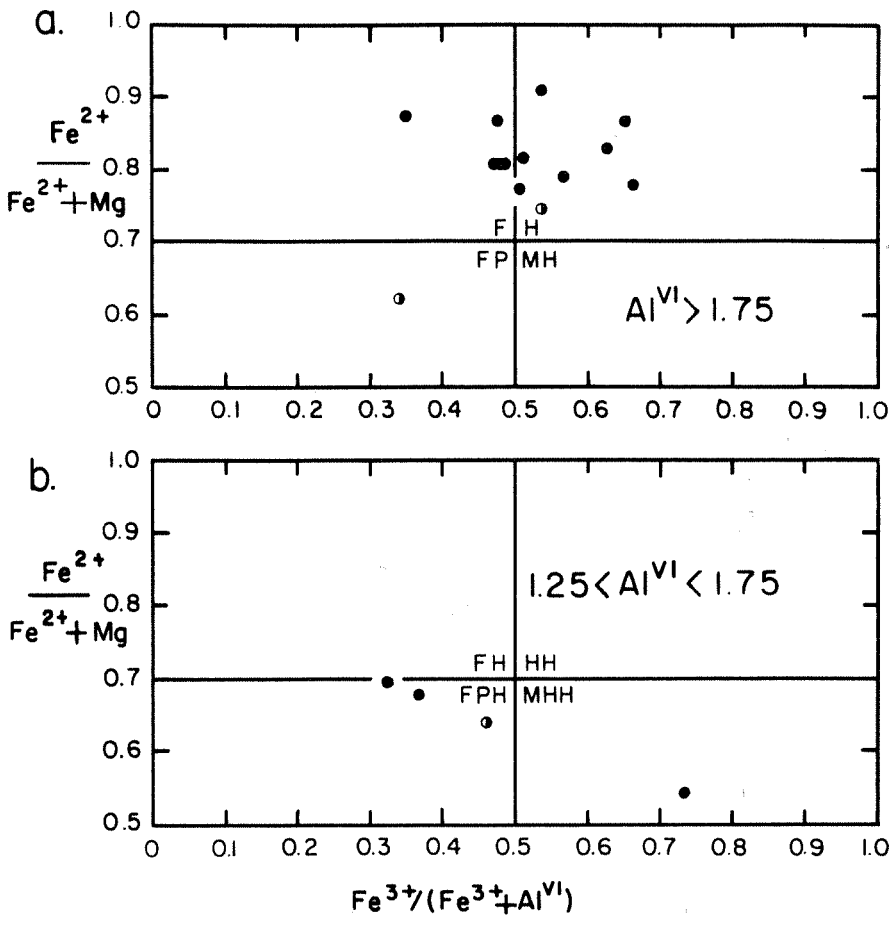

Figure 8. Amphibole classification diagram.

AMPHIBOLE NOMENCLATURE

F ferropargasite	FH ferropargasitic hornblende
H hastingsite	HH hastingsitic hornblende
FP ferroan pargasite	FPH ferroan pargasitic hornblende
MH magnesian hastingsite	MHH magnesian hastingsitic hornblende

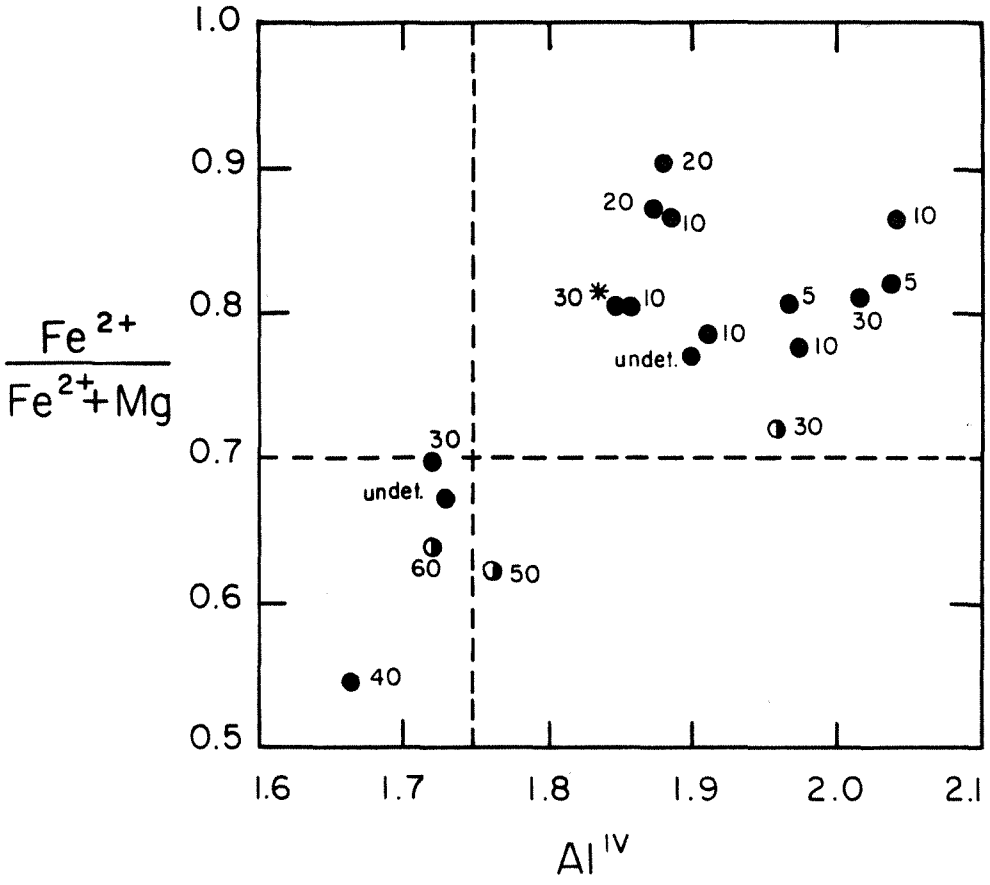

Figure 9. Visually estimated amphibole 2Vs plotted on a diagram of tetrahedral aluminum vs. a ferrous iron and magnesium ratio. * means uncentered figure.

Three samples from Dry Hill Gneiss plot apart from the rest of the Dry Hill amphiboles in Figure 7c, in the fields of hastingsitic hornblende and pargasitic hornblende, and they have a somewhat anomalous whole rock chemistry. Whole rock analyses of samples TR 31+79, TR 33+40, and TR 35+00 have about 4 times more MgO than the rest of the Dry Hill Gneiss and this is reflected in the amphibole chemistry.

All of the amphiboles have a pleochroism from dark blue-green (Z) to brownish green (Y) to pale yellow green (X), but TR 35+00, TR 29+64 and TR 29+99 have weaker pleochroism and dispersion than the others. According to Binns (1965), the dark blue-green (Z) color indicates high Fe3+ and low Ti content. These three samples also have the largest 2Vs of any of the samples studied (Table 5). A plot of Fe2+/(Fe2+ + Mg) vs. tetrahedral aluminum (Figure 9, similar to Figure 7b) shows that those samples with the lower ferrous iron ratio have higher 2Vs. The samples were also plotted on various other discriminant diagrams, but these did not separate the samples with high 2Vs from the samples with low 2Vs.

In comparison to the amphiboles in selected other anorogenic granites, (Figure 10) the hastingsites in the Dry Hill Gneiss and the felsic gneiss are richer in tetrahedral aluminum. Amphiboles from the Pliny Range in New Hampshire are also high in ferrous iron, but are not so high in tetrahedral aluminum as the ones from the Dry Hill Gneiss (Czamanske et al., 1977). The amphiboles from the Precambrian Wolf River Batholith of Wisconsin cover a very wide field(Anderson, 1983). They have a similar Fe/(Fe+Mg) ratio to the Dry Hill but not so much tetrahedral aluminum. Amphiboles from the Precambrian Montello Batholith of Wisconsin are most similar in composition to those of the Dry Hill Gneiss, although analyses are limited in number (Anderson, 1983). An amphibole from the green marginal variety of hornblende rapakivi of Finland also plots close to the cluster of analysed samples (Savolahti, 1962). The amphiboles from the Pikes Peak Batholith of Colorado, are peculiar in that they are rich in FeO, but deficient in tetrahedral aluminum, so that they plot within the ferroedenite field (Barker, et al., 1975).

Anorogenic granitic magmas are fairly rich in fluorine, which crystallizes in the hydroxide minerals and in the mineral fluorite. The amphiboles of the anorogenic granites can have up to 1 weight percent fluorine (Anderson, 1983), and it is possible that the amphiboles of this study contain high amounts of fluorine, although no analysis was made for it. The ratio of Fe/(Fe+Mg) in the hastingsites varies with the ratio Fe/(Fe+Mg) in the whole rock of the Dry Hill Gneiss (Figure 11). The whole rock gives the appearance of being slightly more iron-rich than the amphiboles especially at high ratios. However, most if not all of this trend is due to the fact that the XRF detection limit of MgO of 0.02 weight percent (Rhodes, personal communication, 1984) for the rock has been exceeded while MgO is still sufficiently abundant in amphibole grains to obtain valid analyses.

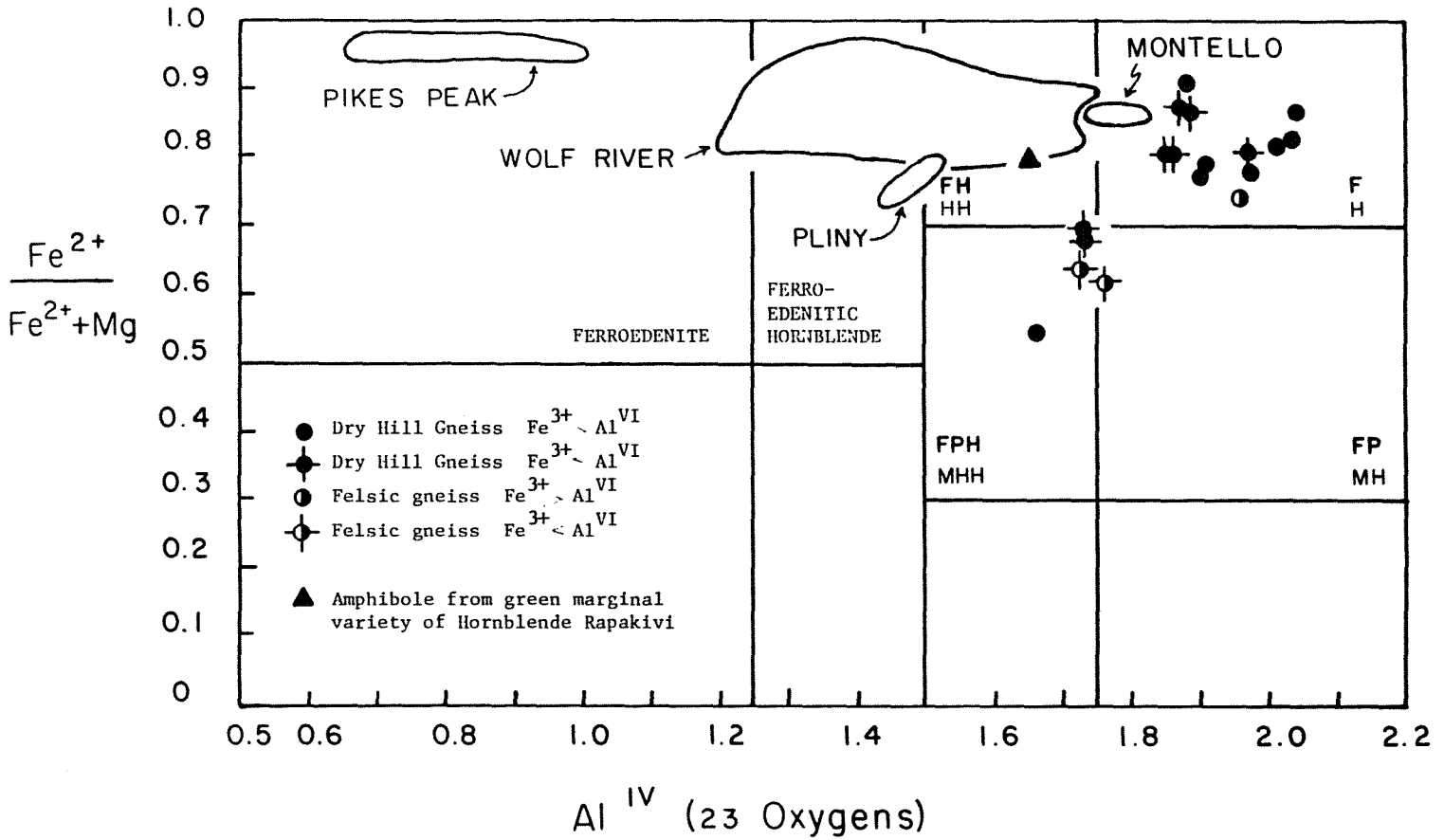

Figure 10. Amphibole identification diagram, adapted from Hawthorne (1981). Fields of amphiboles from Pikes Peak Batholith, Pliny hastingsite-biotite granite, and Wolf River Batholith and Montello Biotite Granite from Barker, et al. (1975), Czamanske, et al. (1977), and Anderson (1980, 1983), respectively. Triangle is amphibole from Hornblende Rapakivi (Savolahti, 1962). Wolf River and Montello amphiboles are plotted as if the left axis were Fe/(Fe+Mg). Bold face letters refer to names of amphiboles with Fe3+ less than AlVI and regular letters refer to amphiboles with Fe3+ greater than AlVI. Letter abbreviations are the same as in Figure 9.

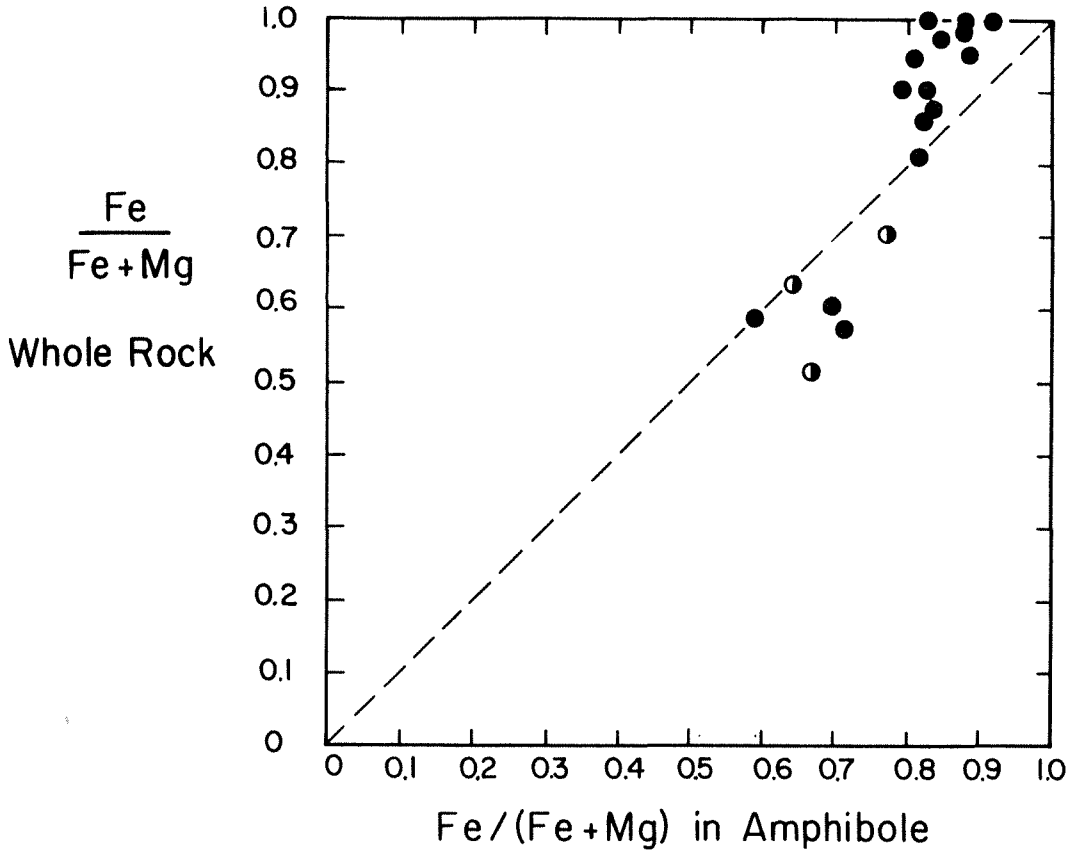

Figure 11. The cation ratio of total Fe to total Fe plus Mg in amphiboles vs. the same ratio in corresponding whole rocks.

The amphiboles with higher levels of MgO tend to plot closer to that of the corresponding bulk composition, or even to have a higher Fe ratio than the corresponding rock. This would be consistent with the probability that the biotite is more magnesian than the coexisting amphibole as suggested by the Fe/(Fe+Mg) ratios of the analysed biotite (0.816) and amphibole (0.878) in sample TR 44+50.

Biotite

Biotite analysed from one sample of the Dry Hill Gneiss Hornblende Member is very iron-rich with a ratio of Fe/(Fe+Mg) of 0.816 (Table 6). It is strongly pleochroic from dark greenish brown (Z=Y) to light greenish yellow (X). Hayama (1959) cited in Guidotti (1984) links the relative amounts of Ti4+ and Fe3+/FeT to the color of a biotite. A red color appears to be a result of high Ti4+ and low Fe3+/FeT. A green color results from low amounts of Ti4+ and high Fe3+/FeT. Although no wet chemistry was done of the probed biotite to determine the relative amount of ferric iron to total iron, the total amount of titanium in the sample is very small compared to the amount of iron.

The analysed biotite is compared to biotites in other granitic rocks with chemistries similar to the Dry Hill Gneiss (Figure 12). Although the biotite in the Dry Hill is metamorphic and the biotite in the other rocks is primary, biotite composition is strongly dependent on rock composition and mineral assemblage (Anderson, 1983). Similar granitoid rocks with anorogenic affinities for which biotite analyses are available include the Wolf River Granite and the Montello Batholith of Wisconsin, the Pikes Peak Granite of Colorado, and the Pliny hastingsite biotite granite of the White Mountain Magma Series of New Hampshire.

The biotite of this study plots closer to the annite end member than to the siderophyllite end member (Figure 12). It plots within the Wolf River Granite field and very near the biotite from the Hornblende Rapakivi. Biotites from the Pikes Peak Batholith plot very close to the annite corner of the diagram. It is common for the mafic silicates in anorogenic granites to be rich in iron, and a large annite component is commonly found in the biotites (Wones, Fahey, and Ayuso, 1977).

Anderson (1980) found that biotites rich in aluminum coexisted with albite and sodic oligoclase, whereas biotites depleted in aluminum occured with calcic oligoclase and andesine. Anorthite component in plagioclase may concentrate aluminum at the expense of biotite (Anderson, 1980, 1983 and Shand, 1927). The composition of the plagioclase which occurs with the probed sample of Dry Hill biotite is An 17 (Table 7). This may be one reason why that the biotite is relatively poor in aluminum.

The biotite in the Dry Hill Gneiss was not tested for fluorine, but significant amounts of fluorine commonly occur in anorogenic

Table 6. Electron microprobe analysis of a biotite from Dry Hill Gneiss Hornblende Member sample TR 44+50. Formula calculated on a basis of 11 oxygens. FeOT is total iron as FeO. Difference between analysis total and 100 is probably composed mostly of H2O, with some fluorine and chlorine.

Biotite

No of Analyses: 4

SiO2	35.16
TiO2	2.36
Al2O3	16.03
FeOT	29.03
MnO	0.63
MgO	3.68
ZnO	0.07
CaO	0
Na1O	0.05
K2O	8.82
Sum	95.83
Diff.	4.17
Total	100.00

Structural Formula:

IV Site	Si	2.798
	Al	1.202
		4.000
VI Site	Al	0.301
	Ti	0.141
	Mg	0.437
	Zn	0.004
	Fe	1.932
	Mn	0.043
		2.858
A Site	K	0.895
	Na	0.008
		0.903
	Total	7.762
	OH-	2.214
Fe/(Fe+Mg)		0.816
K/(K+Na)		0.991
$\frac{Fe+Mn}{Fe+Mn+Mg}$		0.819

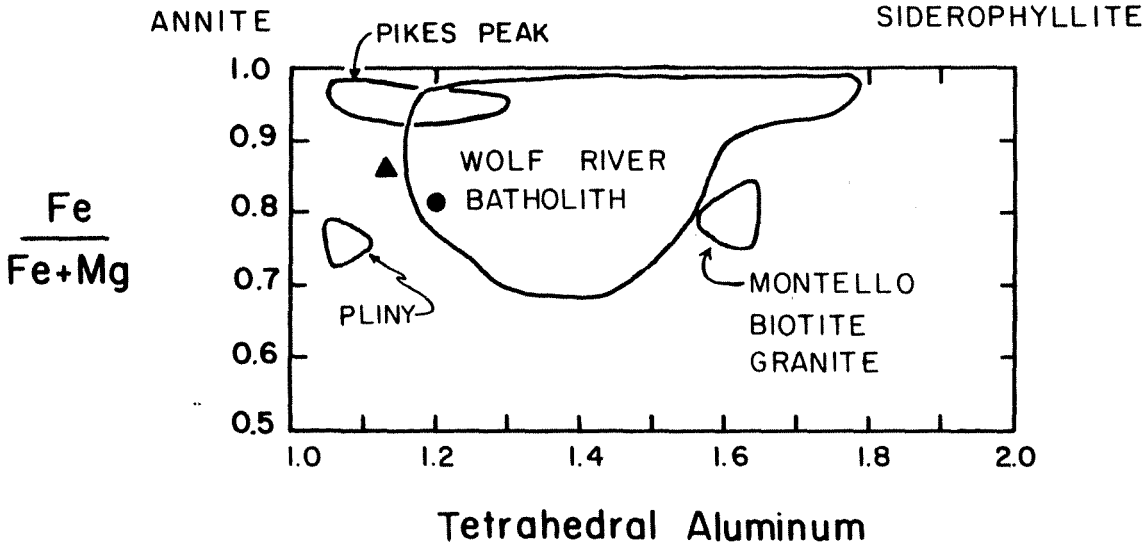

Figure 12. Biotite classification diagram. Circle is biotite from the Dry Hill Gneiss Hornblende Member TR 44+50. Triangle is biotite from the green marginal variety of the Hornblende Rapakivi (Savolahti, 1962). Field of biotite from Anderson (1980, 1983). Barker, et al., (1975), and Czamanske, et al. (1977) for Wolf River and Montello, Pikes Peak, and Pliny, respectively.

granites. The fluorine content of biotite in other anorogenic granitic rocks can be greater than 1.5 weight percent (Anderson, 1983).

Plagioclase

Plagioclase feldspar has cores of oligoclase with more sodic rims. The feldspar analysed in sample TR 44+50 has a core of An 17.2 Ab 81.8 Or 1.0 and a rim of albite An 5.7 Ab 93.7 Or 0.6 (Table 7). The details of the rimming relationship are worthy of note. The albite rims only appear next to microcline, not next to any other phase. On a microprobe traverse across the partial rims, the last part of the traverse was always off of the edge of the grain onto a potassium feldspar. It is likely that the microcline is exsolving albite, which is preferentially crystallizing onto nearby oligoclase grains. This relationship has been noted in other New England granitic rocks (c.f. Maczuga, 1981; Toulmin, 1964).

Microcline

The potassium feldspar has a composition of Or 91.5 Ab 7.6 An 0.1 Cn 0.8 (Table 7). Laird (1974) did X-ray diffraction studies on the microcline in the Dry Hill Gneiss and determined that it is quite close to maximum microcline. If the Dry Hill Gneiss ever contained orthoclase, the reordering to maximum microcline may have been caused by the kyanite grade metamorphism (Laird, 1974). The microcline contains a moderate amount of BaO, and the total amount of Ba in the rock is high. A calculation of the amount of BaO in the feldspar times the modal percentage of microcline estimated in thin section in TR 44+50, when converted to ppm Ba, gives a result of 1331 ppm Ba, which is very close to the amount of 1257 ppm Ba determined for the whole rock.

Garnet

On the basis of analyses from one specimen, the garnets are chiefly composed of almandine, with lesser amounts of grossular, spessartine, pyrope, and probably andradite (Table 8). If the garnet formulae are calculated assuming all Fe as FeO, then the amount of aluminum found is too small to fill the aluminum site completely (Table 8, Column A). However, if the formulae are normalized to 8 cations (Table 8, Column B), and corrected for Fe^{3+}, a small andradite component appears. Although the garnets are uniform in color, and relatively free of inclusions, they are zoned. Rims contain more iron, and less manganese and calcium relative to the cores (Figure 13).

An amphibole from the same rock as the garnet was plotted on the garnet diagram (Figure 13) and it lies quite near the extension of the core to rim garnet trend. It is likely that the garnet rim formed at the expense of amphibole during prograde metamorphism. The aluminum source was probably plagioclase.

Table 7. Electron microprobe analyses of feldspars from sample TR 44+50. Structural formulae calculated on a basis of 8 oxygens. Formulae are calculated from the average of the seven best analyses.

	Plagioclase		Microcline	
	n=7	n=7	n=7	
	Core	Rim		
SiO2	63.72	67.08	SiO2	64.96
Al2O3	22.39	20.42	Al2O3	17.98
CaO	3.81	1.15	CaO	0.01
Na2O	9.65	10.97	Na2O	0.83
K2O	0.17	0.11	K2O	15.21
BaO	0.01	0.03	BaO	0.42
Total	99.75	99.76	Total	99.41
Structural Formulae:				
Si	2.824	2.945	Si	3.015
Al	1.170	1.057	Al	0.983
Sum	3.994	4.002	Sum	3.998
Ba	0	0.001	Ba	0.008
K	0.010	0.006	K	0.901
Na	0.829	0.934	Na	0.075
Ca	0.181	0.054	Ca	0.001
Sum	1.020	0.995	Sum	0.985
Total	5.014	4.997	Total	4.983
An	17.2	5.7	Or	91.5
Ab	81.8	93.7	Ab	7.6
Or	1.0	0.6	An	0.1
			Cn	0.8

Table 8. Representative electron microprobe analyses of garnet from Dry Hill Gneiss sample TR 44+50. Structural formulae are based on 12 oxygens. Column A is all iron as FeO, column B is normalized to 8 cations and corrected for Fe2O3.

	Core	Intermediate	Rim
	n=1	n=1	n=1
SiO2	37.69	37.65	37.81
Al2O3	20.18	20.17	20.13
FeO	20.40	26.13	27.13
MnO	6.60	5.62	5.09
MgO	0.37	0.43	0.40
CaO	11.43	10.78	10.59
Total	100.67	100.78	101.15

Structural Formulae:

		A	B	A	B	A	B
Si site	Si	3.017	3.005	3.014	3.004	3.021	3.009
Al site	Al	1.905	1.898	1.904	1.898	1.897	1.890
	Fe3+		0.092		0.095		0.092
		1.905	1.990	1.904	1.993	1.897	1.982
M2+ site	Fe2+	1.635	1.537	1.750	1.649	1.814	1.715
	Mn	0.448	0.446	0.382	0.381	0.345	0.344
	Mg	0.045	0.045	0.051	0.051	0.047	0.047
	Ca	0.981	0.977	0.926	0.923	0.907	0.904
		3.109	3.005	3.109	3.004	3.113	3.010
Total		8.031	8.000	8.027	8.001	8.031	8.001
Almandine		52.6	51.9	56.3	55.8	58.3	57.9
Spessartine		14.4	15.1	12.3	12.9	11.1	11.6
Pyrope		1.4	1.5	1.6	1.7	1.5	1.6
Grossular		31.6	28.4	29.8	26.4	29.1	25.8
Andradite			3.1		3.2		3.1
Total		100.0	100.0	100.0	100.0	100.0	100.0

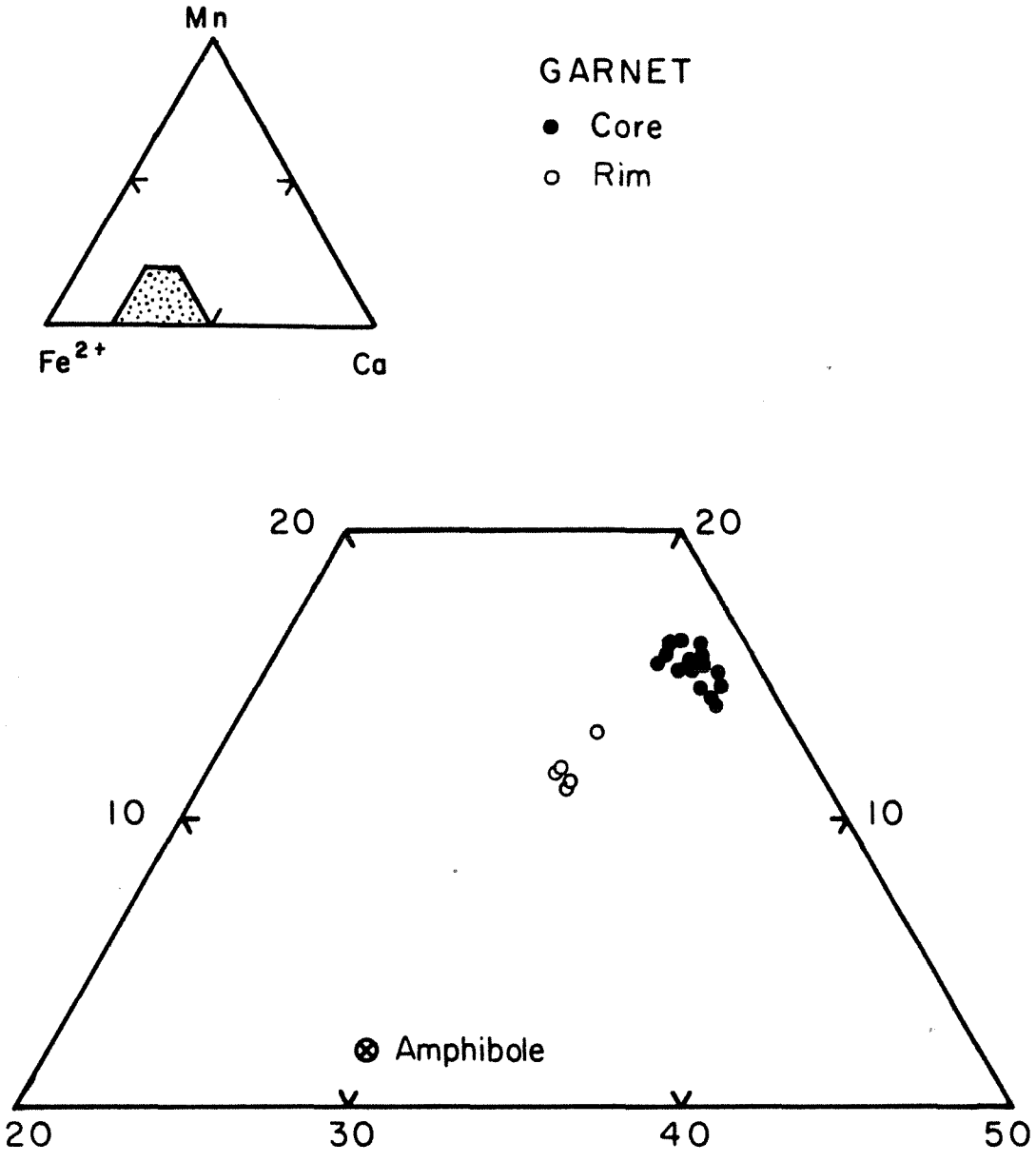

Figure 13. Plot of garnet core and rim compositions from Dry Hill Gneiss sample TR 44+50. Core to rim zoning trend points toward amphibole from TR 44+50, indicating a possible reaction. Mg component of the amphibole was added to the Fe2+ apex. Mg in the garnet is negligible.

Chemographic Relations

In order to understand the relationship between the mineralogy and the bulk chemistry of the Dry Hill Gneiss, a method of plotting both rocks and minerals was developed. The fact that the Biotite Member does not contain hastingsite, but the Hornblende Member does, is an especially intriguing part of the problem.

A tetrahedron that has Al2O3, CaO, K2O, and (FeO+MgO) at its four corners, includes many of the major minerals in the Dry Hill Gneiss, but is awkward to plot. A phase which is ubiquitous in both members is plagioclase, so a simplified plagioclase projection was selected (Figure 14).

The probed minerals from Hornblende Member sample TR 44+50 are plotted on the projection, as are all analysed amphiboles. The biotite location is not exact, since it is not possible to distinguish between FeO and Fe2O3 using the electron microprobe. The formula was calculated using one half of the cation ratio $Fe^{3+}/(Fe^{3+} + Fe^{2+})$ of the corresponding amphibole, and is therefore subject to uncertainty. Sample TR 44+50 whole rock plots slightly outside of the microcline-biotite-hornblende field, so the amount of ferric iron may be underestimated. Another problem is that the minerals of rocks of slightly different whole rock chemistry from TR 44+50 probably do not have quite the same chemistry as those from the probed sample. The diagram is qualitative, rather than quantitative.

The biotite member of the Dry Hill Gneiss plots outside of the microcline-biotite-hornblende field, or very close to the edge. Rocks of the Hornblende Member which contain only trace amounts of hastingsite plot near to the biotite-microcline tie line and in some cases, across it. The leucogneiss layers (F) of the Dry Hill Gneiss plot near the microcline-amphibole tie lines, and the biotite gneiss layers (M) plot near the microcline-biotite tie line. The relative enrichment of K2O in the leucogneiss layers can be clearly seen on this diagram. Samples from the granite gneiss within the Poplar Mountain Quartzite show a similar relationship. They contain no hastingsite. The two samples of felsic gneiss that plot closest to the microcline-biotite tie line contain no modal amphibole, whereas the three that plot farthest from the tie line are rich in amphibole. A few samples of Hornblende Member which contain appreciable amounts of amphibole plot outside the microcline-biotite-hornblende field, but that may be a result of varying biotite chemistry. Most whole rock analyses of samples which contain hastingsite and biotite, do plot within the microcline-biotite-hornblende field.

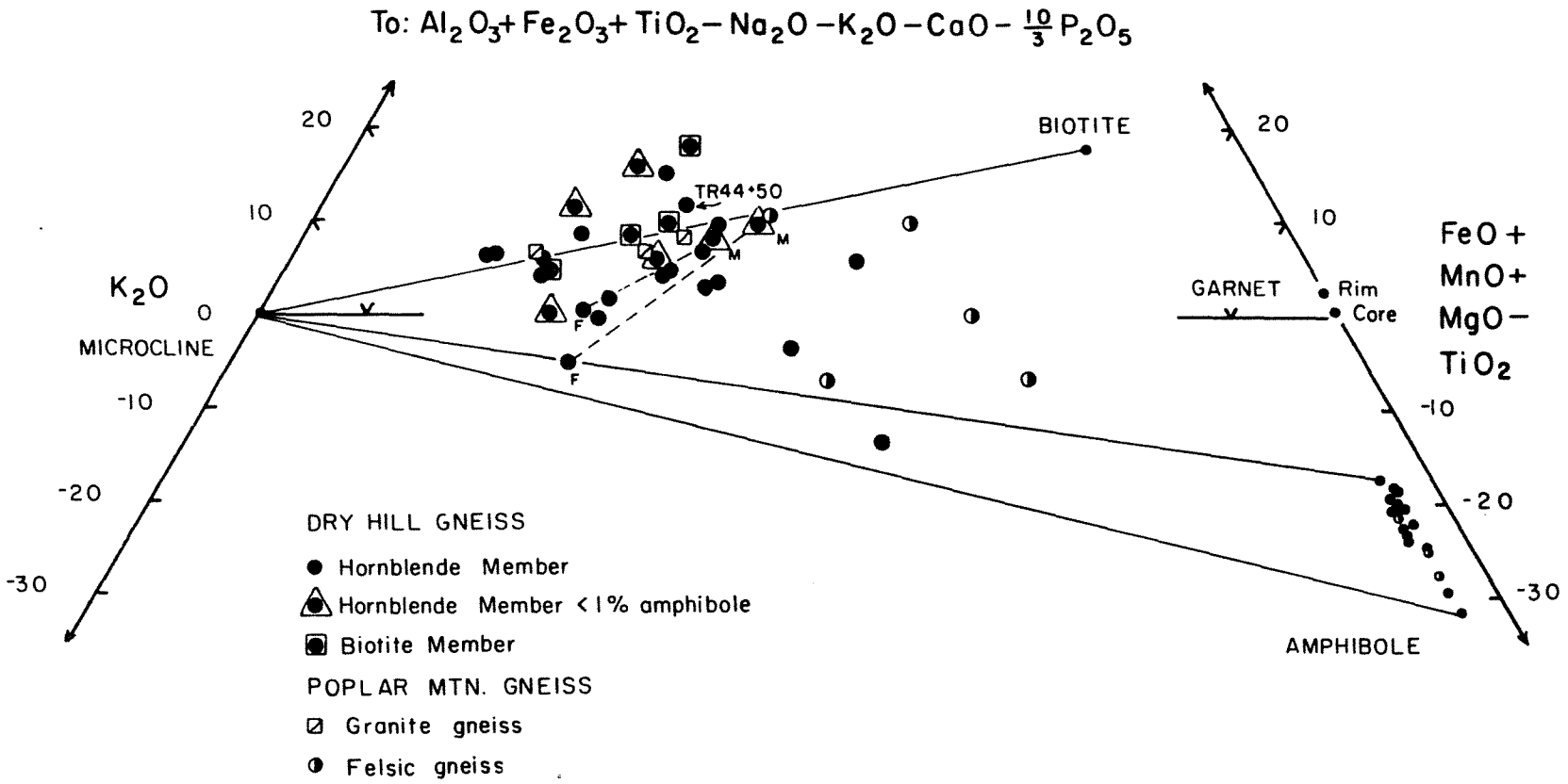

Figure 14. AKFm diagram, plotted in molar proportions, showing bulk compositions of rocks plotted vs. minerals in Dry Hill Gneiss Hornblende Member sample TR 44+50. Biotite formula calculated to one half the amount of Fe3+/(Fe3++Fe2+) in corresponding amphibole.

GEOCHEMISTRY AND PETROLOGY

Methods of Study

Fifty-two rock samples have been carefully selected and powdered for analysis. These include thirty samples of Dry Hill Gneiss from the Biotite and Hornblende Members, three samples of granite gneiss within the Poplar Mountain Quartzite, five samples of felsic gneiss within Poplar Mountain gneiss that resemble Dry Hill Gneiss, eight samples of Poplar Mountain Gneiss proper, four samples of Fourmile Gneiss, and two samples of Belchertown tonalite.

The sampling problems inherent in the study are three-fold. First, the tunnels only cut through a limited exposure of the formations studied, compared to the total rock volume of the dome. However, the tunnels cut through a complete stratigraphic section of the Dry Hill Gneiss and the upper level of the Poplar Mountain Gneiss. Second, samples were obtained by Robinson and Ashenden under difficult conditions, in areas that were generally poorly lit, and their sample selection was commonly based on ease of removal, rather than on how representative the sample was of each rock layer. Third, the samples are medium- to coarse-grained, and a fairly large sample, approximately two kilograms, would be necessary to ensure that the samples were representative of each rock layer as a whole.

One of the major reasons that the tunnel samples were selected for study is that they are extremely fresh, having been subjected to little or no weathering. Individual samples were selected for homogeneity, even foliation, and sufficient size. Because the tunnel samples are irreplaceable and cannot be entirely powdered for analysis, two one-hundred gram slabs were cut off each sample and were treated as two discrete samples, to serve as a check for sampling size problems. Samples were cut from adjoining areas, perpendicular to the foliation to attempt to minimize variation due to layering. This subject will be treated in more detail below.

Samples were cut on a steel rock saw. The resulting slabs were inspected for trace metal from the saw and were cleaned first on a rotating fresh silicon carbide grinding lap and second in a sonic cleaner. The rocks were reduced to gravel-sized pieces in a carbon-steel cylinder with a hammer and chisel. The pieces were ground into a powder in a tungsten carbide shatterbox. Possible sources of contamination are trace amounts of tungsten, cobalt, and iron.

Major element analysis was done by X-ray fluorescence spectroscopy on fused glass discs, with a chromium X-ray tube. The samples were first ignited for approximately eight hours at 1000^{o}C to oxidize all of the iron to Fe_2O_3 and to remove H_2O and CO_2. Then 0.28 grams of a each sample were mixed with 1.5 grams of lanthanum-doped lithium tetraborate flux and fused into glass discs at 1020^{o}C using the technique developed

by Norrish and Hutton (1969). Samples were fused to assure homogeneity and to eliminate problems with differing grain size of the various minerals. The ratio of flux to sample was selected to reduce matrix effects. Lanthanum in the flux absorbs heavy element interferences. A disc was made for each of the two 100 gram splits and the results of the two analyses were averaged. The samples were run with U. S. Geological Survey standards BCR-1 and GSP-1(Flanagan, 1976) as unknowns to monitor precision and accuracy.

Ferrous iron determinations have been made on all samples, using the cold-acid digestion method of A. D. Wilson (1955), cited in Maxwell (1968). Knippa Basalt and Fitchburg Granite, which has a similar amount of iron to Dry Hill Gneiss were analysed as unknowns, together with the Dry Hill Gneiss samples to monitor precision and accuracy.

Pressed powder pellets were made of unoxidized samples for trace element analysis, using a modification of the method of Norrish and Chappell (1967). Powdered boric acid was used to hold the discs together. They were run with a molybdenum X-ray tube for Y, Sr, Rb, Th, Pb, and Ga and a gold X-ray tube for Nb, Zr, Sr, Zn, Ni, Cr, V, Ce, and Ba. BCR-1 and GSP-1 were run as unknowns to monitor accuracy and precision.

One exception was made to the sampling procedure. Two sub-samples of sample TR 17+00 were made by the above procedures, but the plastic vial which contained one of the sub-samples was accidentally broken and the sample contaminated. Insufficient rock remained to prepare another sub-sample and the major element analysis had already been run on the original pair, so both powder discs were formed of only one sub-sample. The glass discs had already been prepared from both sub-samples.

Discussion of Paired-Sample Statistics

The sampling process of this study can be tested with paired-sample standard deviation calculations. This tests the validity of slicing two small slices off of the hand sample. It is not possible to test statistically how well the hand sample represents the outcrop.

Paired samples were accepted providing they agreed to within 1 per cent and totalled to between 99.00 and 101.00 for major elements. Some sample halves had totals that were too high or too low and for that reason were discarded. Time did not permit rerunning them. They are starred (*) in the tables where the results are reported. The bad halves were figured into the statistical data, although they were not used, to determine how effective the sampling method was.

Standard deviation of the pairs was calculated (Table 9). The differences between each pair were calculated, summed, and used in the standard deviation formula. The process was repeated for each element, for each formation. SiO2 and Al2O3 standard deviation are both

Table 9. Standard Deviation of Sample Pairs.

	Dry Hill Gneiss Hbde. Member	Dry Hill Gneiss Biot. Member	Granite Gneiss in Pop. Mtn. Qrtzt.	Felsic Gneiss in Pop. Mtn. Gneiss	Poplar Mtn. Gneiss	Fourmile Gneiss	Belcher-town tonalite
No. of Samples	26	4	3	5	8	4	2
SiO2	0.68	1.62	0.71	0.44	1.04	0.54	0.38
TiO2	0.02	0.08	0.01	0.04	0.02	0.01	0.03
Al2O3	0.21	0.55	0.15	0.23	0.27	0.16	0.22
Fe2O3*	0.16	0.41	0.07	0.16	0.27	0.07	0.10
MnO	0.01	0.01	0.01	0.01	0.01	0.01	0.01
MgO	0.05	0.13	0.05	0.12	0.13	0.04	0.22
CaO	0.06	0.23	0.01	0.08	0.14	0.04	0.08
Na2O	0.23	0.34	0.09	0.07	0.16	0.05	0.16
K2O	0.13	0.25	0.11	0.05	0.19	0.04	0.11
P2O5	0.01	0.04	0.02	0.02	0.02	0.01	0.01
Total	0.87	0.39	0.65	0.44	0.78	0.54	0.92
FeO	0.24	0.14	0.25	0.32	0.22	0.23	0.06
Rb	3.73	6.04	0.72	5.54	5.33	3.21	2.12
Pb	1.54	1.07	1.83	0.79	2.13	1.77	4.27
Sr1	2.33	3.26	1.20	7.09	6.59	7.02	15.01
Sr2	3.08	3.79	3.86	6.40	6.43	6.28	21.79
Ba	32.60	42.14	19.63	67.98	67.12	23.94	86.18
Ce	13.00	11.24	11.92	6.29	8.78	8.42	3.68
Y	3.55	2.04	2.20	2.59	3.50	0.92	0.10
Nb	1.99	7.30	0.47	2.18	0.94	0.61	1.09
Zr	21.03	26.74	21.88	14.70	12.66	8.13	51.64
Th	1.33	1.95	2.40	1.29	1.60	1.11	1.22
Ga	0.69	0.74	0.77	0.80	0.78	0.70	0.76
Zn	4.92	3.18	8.52	3.77	5.29	2.87	10.30
Ni	4.31(8)	3.51(3)	--	--	--	3.01	3.51
Cr	7.29(8)	3.37(3)	--	--	--	4.92	1.64
V	2.78	3.10	2.22	2.75	8.56	3.84	4.76

Standard deviation (two sigma) at the 95% confidence level. Sr1 was detected using the molybdenum x-ray tube; Sr2 by the gold tube. Nickel and chromium were determined for only eleven samples of Dry Hill Gneiss, since both elements were at or below detection levels. Fe2O3* is all iron as Fe2O3. FeO was determined by the Wilson cold acid digestion method.

disappointingly high, although lower for the finer-grained formations: Fourmile Gneiss and Belchertown tonalite. In general, the finer grained formations have lower standard deviation of pairs. The standard deviation of the major elements of the Biotite Member are high, since one of the pairs of sample 17+82 was anomalous, but it was added into the standard deviation calculations, and there were only four rocks of the Biotite Member sampled. Geochemistry of samples is reported in Tables 11-14, such that the number of decimal places reflects the standard deviation of the pairs.

The agreement on trace elements is adequate, with a few exceptions. The standard deviation of barium is high for two reasons. The amount of potassium feldspar in the rocks of the Dry Hill Gneiss and the Poplar Mountain Gneiss is large and the crystals range in size up to seven centimeters. The standard deviation for zirconium is high also. The Dry Hill Gneiss contains a trace amount of zircon, which has a hardness of seven and one half. Two powder pellets were made for each sample. Possibly small pieces of zircon, not adequately crushed, were present in greater amounts at the surface of one of the powder pellets than the other. Similar reasoning may hold true for the large standard deviations of rubidium in the more biotite-rich formations. A crystal of biotite, which readily accepts Rb into its crystal structure, could have lain flat on a cleavage plane (001) at the surface of one of the powder pellet pairs, and thus given somewhat higher Rb numbers in one of the pairs. Cerium numbers are higher than satisfactory, which may be a result of unequal distribution of allanite or sphene crystals in the paired powder pellets.

For Dry Hill Gneiss, elements such as nickel and chromium are present in such small amounts that they are at or below detection limits, and their standard deviations may be high due to the difficulty of analysing such small amounts.

Either U. S. G. S. standard BCR-1 or GSP-1 were run as unknowns with all samples (Table 10). Agreement was good with published values (Flanagan, 1976) with the exception of barium and cerium.

Major Element Chemistry of the Dry Hill Gneiss

The SiO_2 values of the Dry Hill Gneiss range from 72.9 to 78.5 weight percent (Table 11). There is no appreciable difference in the amount of silica between the Biotite Member and the Hornblende Member. The major element chemistry is displayed on Harker diagrams (Figure 15), because SiO_2 is so abundant in all formations. In order to conserve space, all other analysed formations are also plotted on the diagrams, but a consanguineous origin is not necessarily implied.

The Dry Hill Gneiss is high in K_2O. It is low in Al_2O_3 and CaO and strikingly low in MgO. Some MgO values are below the X-ray fluorescence detection limit, which is 0.02 weight percent

Table 10. Standards.

GSP-1				BCR-1			
Element	Avg.	Std. Dev.	Accepted Value	Element	Avg.	Std. Dev.	Accepted Value
Chrome X-ray Tube n=8				Chrome X-ray Tube n=5			
SiO2	67.62	0.42	67.38	SiO2	54.32	0.64	54.50
TiO2	0.67	0.01	0.66	TiO2	2.24	0.18	2.20
Al2O3	15.10	0.12	15.25	Al2O3	13.51	0.15	13.61
Fe2O3*	4.29	0.25	4.33	Fe2O3*	13.32	0.12	13.40
MnO	0.04	0.02	0.04	MnO	0.19	0.02	0.18
MgO	0.77	0.16	0.96	MgO	3.37	0.02	3.46
CaO	2.00	0.04	2.02	CaO	6.91	0.06	6.92
Na2O	2.78	0.38	2.80	Na2O	3.29	0.30	3.27
K2O	5.48	0.05	5.53	K2O	1.73	0.02	1.70
P2O5	0.29	0.02	0.28	P2O5	0.36	0.04	0.36
Total	99.04		99.25	Total	99.24		99.60
Molybdenum X-ray Tube n=12				Molybdenum X-ray Tube n=1			
Y	23.4	0.52	30.4	Y	33.8		37.1
Sr	235.5	2.06	233	Sr	327.3		330
Rb	252.7	2.48	254	Rb	46.7		46.6
Th	90.4	1.82	104	Th	6.3		6.0
Pb	54.2	1.92	51.3	Pb	15.4		17.6
Ga	20.7	1.24	22	Ga	22.9		20
Gold X-ray Tube n=12				Gold X-ray Tube n=1			
Nb	25.3	0.8	29	Nb	12.7		13.5
Zr	518.3	11.6	500	Zr	194.2		190
Sr	234.6	3.2	233	Sr	326.7		330
Zn	114.7	15.7	98	Zn	126.9		120
Ni(4)	12.5	12.6	12.5	Ni	13.8		15.8
Cr(4)	10.7	4.5	12.5	Cr	9.3		17.6
V	45.9	3.2	52.9	V	336.2		399
Ce	292.4	10.8	394?	Ce	35.6		53.9
Ba	1257.9	21.5	1208	Ba	730.5		675

Accepted values for U. S. G. S. standards GSP-1 and BCR-1 are from Flanagan (1976). Standard deviation (two sigma) is to the 95% confidence level. Only 4 runs were made for nickel and chromium using GSP-1 for comparative purposes.

Table 11. X-ray Fluorescence Analyses and CIPW Norms of Dry Hill Gneiss Hornblende Member. Sr was determined using the molybdenum X-ray tube. n.d. is not detected. * means only one of the pairs was used for majors.

	0+50	8+45	9+07	9+40F*	9+40M	11+83	15+84
SiO2	76.2	73.2	76.7	73.9	74.1	74.4	75.7
TiO2	0.16	0.32	0.16	0.31	0.32	0.26	0.16
Al203	12.7	13.8	12.4	12.7	13.5	13.2	13.1
FeO	1.0	2.0	1.5	2.0	2.2	2.3	1.4
Fe203	0.3	0.4	0.1	0.4	0.1	0.5	0.2
MnO	0.04	0.06	0.07	0.05	0.03	0.05	0.06
MgO	0.02	0.33	n.d.	0.07	0.20	0.08	n.d.
CaO	1.32	1.65	1.17	1.75	1.57	1.60	1.12
Na20	2.9	3.5	2.9	2.3	3.3	3.1	3.2
K20	5.0	4.5	5.3	5.7	4.3	4.9	4.7
P205	0.03	0.10	0.03	0.07	0.08	0.06	0.03
TOTAL	99.67	99.86	100.33	99.25	99.70	100.45	99.67
Rb	119	162	144	153	162	137	143
Pb	21	19	17	22	18	17	17
Sr	175	137	101	123	125	115	94
Ba	1542	816	1023	1455	855	1227	1010
Ce	127	106	136	188	134	145	132
Y	23	36	27	49	24	32	38
Nb	11	24	12	30	20	19	12
Zr	168	218	201	379	216	305	191
Th	11	17	11	18	16	11	12
Ga	13	16	13	14	17	16	15
Zn	24	46	32	48	58	58	32
V	7	19	2	16	20	8	3
K/Rb	345	229	305	310	222	301	275
Rb/Sr	0.68	1.17	1.42	1.24	1.29	1.19	1.52
Ba/Sr	8.71	5.93	10.10	11.82	6.82	10.63	10.76
			CIPW Norms				
Q	36.76	30.68	36.16	33.87	32.98	32.73	35.57
Or	29.26	26.43	31.24	33.74	25.65	29.31	27.95
Ab	24.79	29.53	24.37	19.46	28.26	25.89	27.25
An	6.37	7.60	5.37	7.52	7.32	7.50	5.38
C	0.20	0.40	0	0	0.64	0	0.70
Di							
En	0	0	0	0.02	0	0	0
Fs	0	0	0.17	0.33	0	0.04	0
Wo	0	0	0.15	0.31	0	0.04	0
Hy							
En	0.05	0.82	0	0.15	0.50	0.20	0
Fs	1.45	2.89	2.43	2.58	3.62	3.33	2.22
Mt	0.41	0.51	0.17	0.51	0.03	0.78	0.32
Il	0.30	0.61	0.29	0.59	0.61	0.49	0.30
Ap	0.07	0.22	0.07	0.15	0.17	0.13	0.07
TOTAL	99.66	99.70	100.33	99.24	99.78	100.44	99.76

Table 11, continued.

	15+96	TR31+79	TR32+18	TR33+23	TR33+40	TR34+91	TR35+00
SiO2	74.1	74.3	74.1	76.4	74.5	75.6	78.5
TiO2	0.24	0.34	0.23	0.24	0.31	0.16	0.22
Al2O3	13.4	13.1	13.4	12.6	12.4	13.6	10.3
FeO	2.2	2.6	1.7	1.1	1.9	1.1	2.0
Fe2O3	0.3	0.1	0.1	0.1	0.1	0.1	0.1
MnO	0.07	0.07	0.05	0.02	0.07	0.01	0.06
MgO	0.09	0.96	0.12	0.04	0.83	0.16	0.84
CaO	1.38	1.76	1.40	1.07	1.69	1.15	1.77
Na2O	3.4	3.0	3.5	3.0	3.2	3.5	2.9
K2O	4.7	4.2	4.7	5.1	4.3	5.0	3.4
P2O5	0.06	0.09	0.06	0.03	0.08	0.04	0.05
TOTAL	99.94	100.52	99.36	99.70	99.38	100.32	100.07
Rb	151	167	179	172	165	147	99
Pb	15	20	26	21	18	19	10
Sr	121	103	91	96	101	87	87
Ba	1322	481	653	771	594	438	606
Ce	147	77	92	83	70	72	76
Y	40	43	41	28	44	24	34
Nb	24	28	24	15	31	13	19
Zr	315	135	181	129	159	99	189
Th	13	12	12	12	9	11	9
Ga	16	16	15	13	15	15	12
Zn	58	56	42	23	49	24	43
V	6	25	11	7	18	5	9
K/Rb	261	211	220	247	217	281	282
Rb/Sr	1.25	1.62	1.94	1.79	1.63	1.66	1.13
Ba/Sr	10.99	4.66	7.08	8.03	5.86	4.95	6.91
			CIPW Norms				
Q	31.40	33.74	31.18	36.37	33.56	32.86	43.30
Or	28.01	25.12	28.01	30.26	25.47	29.37	19.92
Ab	29.11	25.30	29.87	25.39	27.08	29.53	24.12
An	6.49	8.20	6.59	5.13	6.08	5.47	5.33
C	0.23	0.59	0.03	0.23	0	0.42	0
Di							
En	0	0	0	0	0.19	0	0.51
Fs	0	0	0	0	0.28	0	0.82
Wo	0	0	0	0	0.47	0	1.32
Hy							
En	0.22	2.39	0.30	0.10	1.88	0.40	1.58
Fs	3.49	4.22	2.67	1.57	2.74	1.72	2.51
Mt	0.36	0.09	0.16	0.10	0.14	0.03	0.19
Il	0.46	0.65	0.44	0.46	0.59	0.30	0.42
Ap	0.13	0.20	0.13	0.07	0.17	0.09	0.11
TOTAL	99.91	100.49	99.38	99.67	99.37	100.20	100.12

Table 11, continued.

	TR37+82	TR38+29	TR39+40	TR40+85	TR41+95*	TR42+23*	TR43+46*
SiO2	72.9	73.6	76.7	75.6	72.3	73.5	72.9
TiO2	0.29	0.34	0.14	0.19	0.32	0.31	0.31
Al2O3	13.6	13.3	12.5	12.8	13.7	13.7	13.6
FeO	1.8	2.7	1.2	1.6	2.0	2.2	1.7
Fe2O3	0.8	0.5	0.3	0.4	0.8	0.4	0.8
MnO	0.09	0.06	0.03	0.07	0.07	0.04	0.04
MgO	0.20	0.19	n.d.	n.d.	0.35	0.23	0.15
CaO	1.79	1.60	1.08	1.37	1.76	1.71	1.62
Na2O	3.4	3.1	3.5	2.8	3.7	3.3	3.0
K2O	4.7	4.9	4.4	5.0	4.5	4.4	4.7
P2O5	0.07	0.09	0.03	0.04	0.09	0.08	0.09
TOTAL	99.64	100.38	99.85	99.87	99.59	99.87	98.91
Rb	140	149	111	149	150	136	166
Pb	18	16	14	20	17	16	20
Sr	149	129	96	109	148	143	138
Ba	1334	1230	1129	1151	1231	1255	880
Ce	163	149	107	171	126	128	122
Y	40	30	19	35	32	26	34
Nb	23	21	9	17	25	20	23
Zr	297	292	174	259	272	297	242
Th	13	13	13	13	12	12	17
Ga	16	16	13	14	16	15	16
Zn	53	65	31	35	64	62	50
V	16	14	5	5	20	15	18
K/Rb	277	277	330	280	250	268	237
Rb/Sr	0.93	1.16	1.14	1.36	1.01	0.95	1.20
Ba/Sr	8.83	9.55	11.55	10.45	8.29	8.73	6.32
CIPW Norms							
Q	30.47	30.96	36.33	36.42	28.50	32.33	33.14
Or	27.60	29.31	26.06	29.67	26.71	25.94	28.01
Ab	28.52	26.57	29.70	23.36	31.14	27.76	25.05
An	8.27	7.41	5.18	6.56	7.62	8.01	7.51
C	0	0.01	0.07	0.40	0	0.59	0.89
Di							
En	0.02	0	0	0	0.06	0	0
Fs	0.07	0	0	0	0.19	0	0
Wo	0.08	0	0	0	0.24	0	0
Hy							
En	0.48	0.47	0	0	0.81	0.57	0.37
Fs	2.29	4.10	1.88	2.43	2.44	3.35	1.95
Mt	1.17	0.65	0.36	0.54	1.10	0.54	1.22
Il	0.55	0.65	0.27	0.36	0.61	0.59	0.59
Ap	0.15	0.20	0.07	0.09	0.20	0.17	0.20
TOTAL	99.68	100.33	99.92	99.82	99.62	99.85	98.93

Table 11, continued.

	TR44+50	TR44+90F	TR44+90M*	TR47+75	TR56+88
SiO2	73.0	74.1	73.1	73.6	75.1
TiO2	0.28	0.25	0.36	0.30	0.17
Al2O3	13.5	12.8	13.9	13.6	13.0
FeO	2.4	2.0	2.5	1.9	1.8
Fe2O3	0.7	0.2	0.5	0.5	0.1
MnO	0.08	0.25	0.05	0.06	0.06
MgO	0.03	n.d.	0.35	0.16	n.d.
CaO	1.73	1.71	1.83	1.54	1.07
Na2O	2.9	2.3	3.3	2.9	3.6
K2O	4.7	6.2	4.4	4.7	5.0
P2O5	0.06	0.06	0.10	0.09	0.04
TOTAL	99.38	99.87	100.39	99.35	99.84
Rb	145	155	155	160	164
Pb	17	25	20	18	17
Sr	132	152	147	142	81
Ba	1257	1952	1093	883	1170
Ce	159	190	121	134	69
Y	44	88	33	31	47
Nb	22	28	24	17	22
Zr	325	392	274	207	227
Th	14	15	12	21	14
Ga	15	12	17	16	15
Zn	48	18	60	43	50
V	12	10	21	21	3
K/Rb	270	334	237	245	252
Rb/Sr	1.08	1.02	1.05	1.18	2.01
Ba/Sr	9.39	12.85	7.39	6.16	14.30
CIPW Norms					
Q	32.90	32.40	31.26	34.03	31.74
Or	27.89	36.88	26.12	27.89	29.37
Ab	24.62	19.12	27.76	24.62	30.13
An	8.23	6.27	8.49	7.11	4.81
C	0.54	0	0.63	1.11	0
Di					
En	0	0	0	0	0
Fs	0	0.88	0	0	0.12
Wo	0	0.78	0	0	0.11
Hy					
En	0.07	0	0.87	0.40	0
Fs	3.40	2.63	3.70	2.71	3.06
Mt	1.06	0.35	0.71	0.72	0.04
Il	0.53	0.47	0.68	0.57	0.32
Ap	0.13	0.13	0.22	0.20	0.09
TOTAL	99.38	99.91	100.44	99.37	99.80

Table 11: X-ray Fluorescence Analyses and CIPW Norms of Dry Hill Gneiss Biotite Member.

	17+82*	18+43	18+72	TR57+88
SiO2	74.4	75.0	74.9	73.6
TiO2	0.28	0.21	0.20	0.31
Al2O3	13.7	13.5	13.3	13.6
FeO	1.9	1.8	1.4	2.1
Fe2O3	0.3	0.2	0.2	0.4
MnO	0.06	0.06	0.03	0.05
MgO	0.15	0.07	0.08	0.15
CaO	1.55	1.04	1.11	1.42
Na2O	3.3	3.7	3.2	2.7
K2O	4.6	4.7	5.3	4.7
P2O5	0.09	0.06	0.09	0.10
TOTAL	100.33	100.34	99.81	99.13
Rb	136	153	215	180
Pb	17	18	23	16
Sr	103	76	81	125
Ba	1016	737	534	1224
Ce	90	95	80	107
Y	27	31	25	31
Nb	11	12	17	23
Zr	155	216	154	254
Th	11	14	18	16
Ga	14	16	15	16
Zn	28	51	35	58
V	4	7	8	15
K/Rb	279	253	206	216
Rb/Sr	1.32	2.01	2.66	1.42
Ba/Sr	9.82	9.67	6.59	9.66
		CIPW Norms		
Q	33.01	32.11	32.44	35.25
Or	27.01	27.54	31.56	27.72
Ab	27.92	31.48	27.33	23.19
An	7.16	4.81	4.98	6.46
C	0.70	0.57	0.38	1.60
Di				
En	0	0	0	0
Fs	0	0	0	0
Wo	0	0	0	0
Hy				
En	0.37	0.17	0.20	0.37
Fs	2.95	2.81	2.10	3.17
Mt	0.42	0.29	0.35	0.57
Il	0.53	0.40	0.38	0.59
Ap	0.20	0.13	0.20	0.22
TOTAL	100.28	100.32	99.91	99.13

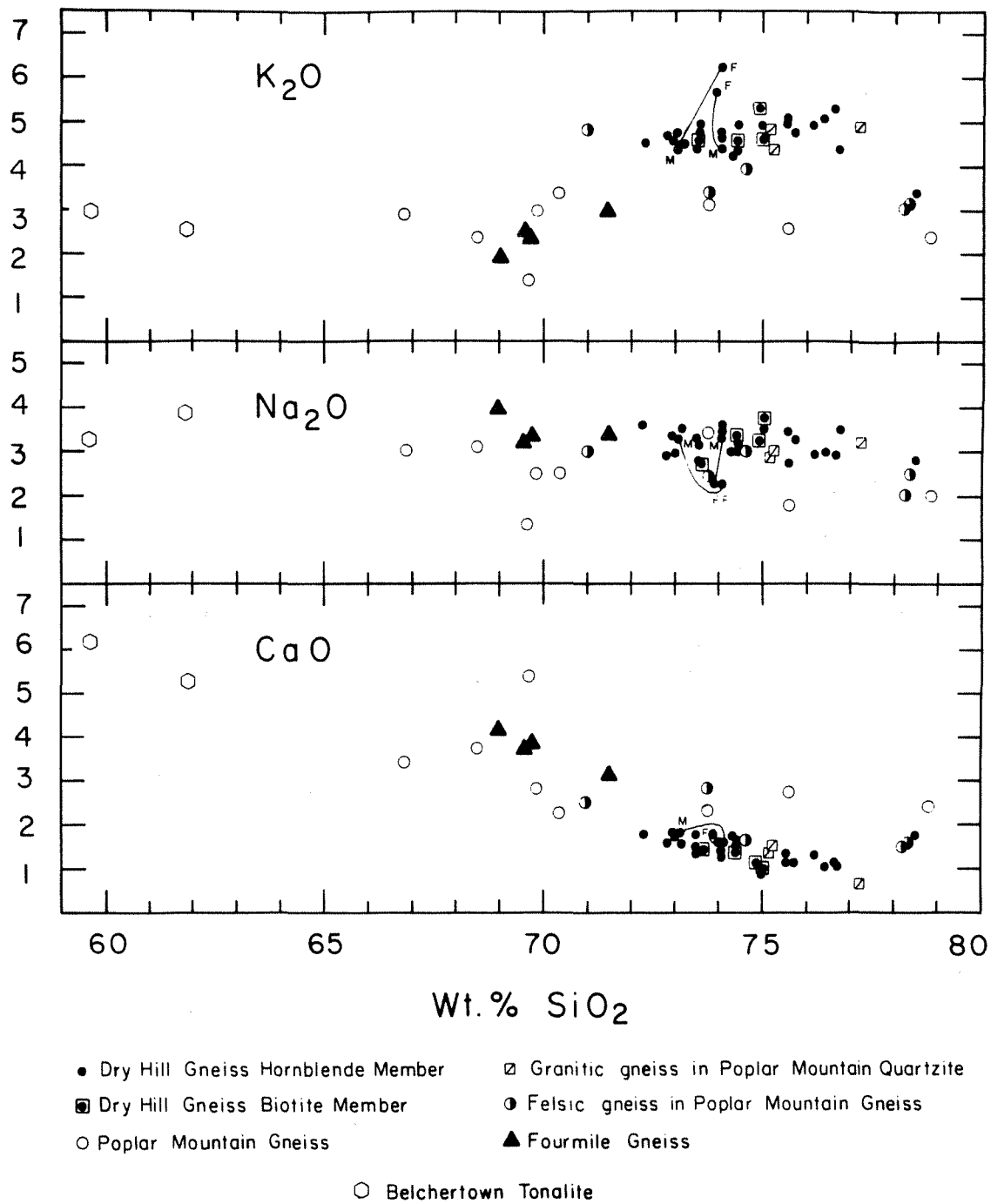

Figure 15. Harker diagram showing major oxides plotted against SiO2 for all samples. All formations are included in order to conserve space.

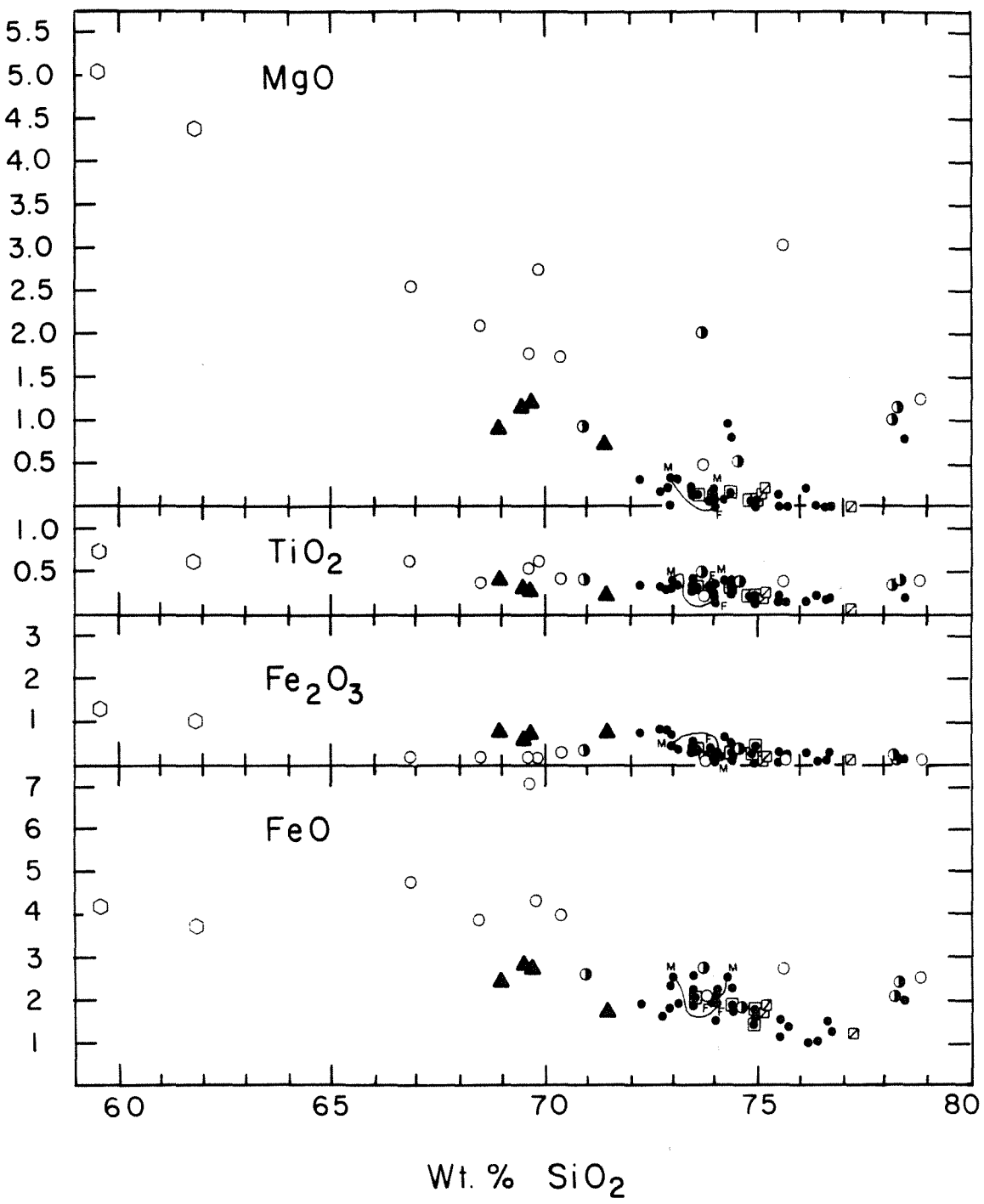

Figure 15, continued.

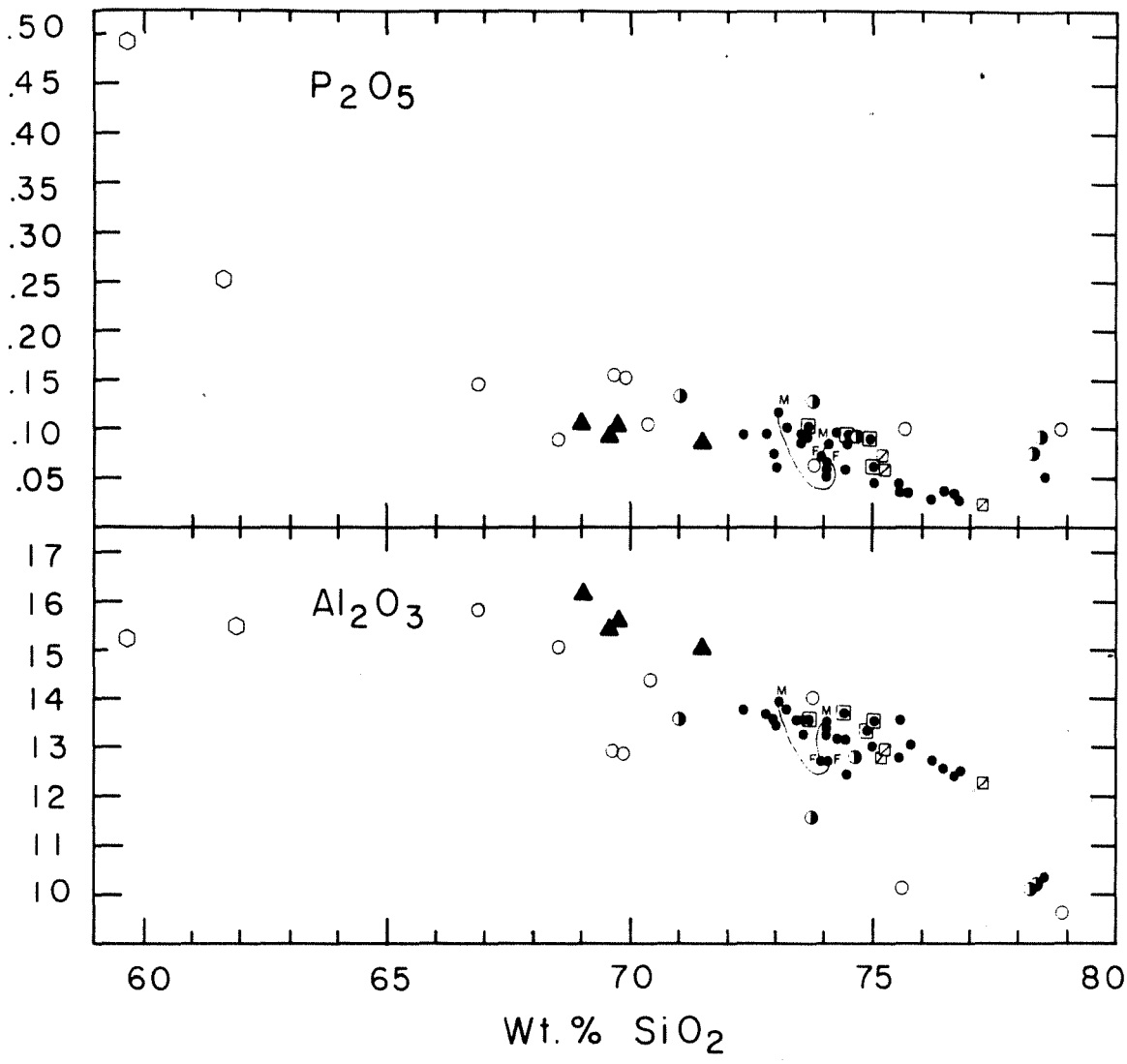

Figure 15, continued.

(J.M.Rhodes, personal communication, 1984). With increasing SiO2, and presumably more differentiation, the amounts of FeO, MgO, TiO2, CaO, Al2O3, Fe2O3, and P2O5 decrease, a not unusual differentiation trend for granitic rocks (Anderson et al., 1980, Emslie, 1978, and others). K2O and Na2O do not vary much with increasing silica.

Norms of the Dry Hill Gneiss plot in the granite (rhyodacite) field of a modified Streckeisen diagram (Figure 16). Dry Hill Gneiss sample TR 35+00 plots apart from the rest of the Dry Hill samples, because it is enriched in quartz. It plots close to the Poplar Mountain Gneiss compositions, which are sedimentary. Most of the samples of Dry Hill Gneiss plot in the tholeiitic field of a calc-alkaline/tholeiite diagram (Figure 17), and most are extremely enriched in iron relative to magnesium. Three samples of the gneiss, TR 31+79, TR 33+40, and TR 35+00 plot in the calc-alkaline field. They have slightly larger amounts of MgO than the rest of the formation.

The extreme MgO depletion trend can also be seen on a standard AFM diagram (Figure 18). The Dry Hill Gneiss plots on the MgO-poor edge, quite close to the alkali corner. The classic tholeiitic/calc-alkaline boundary is plotted on the diagram for comparison. The three previously mentioned Dry Hill Gneiss samples plot apart from the rest of the Dry Hill samples, close to the felsic gneiss analyses. Sample TR 35+00 probably was contaminated by sedimentary material. It does not plot on the igneous trend of Figure 15, because it is enriched in SiO2, CaO and MgO. The protolith may have been contaminated by quartz sand and dolomite. For these reasons, sample TR 35+00 will be omitted on subsequent diagrams of Dry Hill Gneiss, unless a sedimentary formation, such as the Poplar Mountain Gneiss, is also included. The other two anomalous samples do plot on the igneous trend of the Harker diagram and do not contain high SiO2 and CaO.

The Dry Hill Gneiss does not fit well into the classification scheme of Chappell and White (1974). Chappell and White developed the scheme to describe quantitatively the chemistry of two distinct suites of granitic rocks in eastern Australia. One group was melted from a sedimentary source, and the other was derived from an igneous source. Chappell and White designated the rocks S-type and I-type, respectively. I-type rocks have Na2O weight percent > 3.2, have molecular Al2O3/(Na2O + K2O + CaO) < 1.1, and are diopside normative or have less than 1% normative corundum. S-type rocks have Na2O < 3.2, have molecular Al2O3/(Na2O + K2O + CaO) > 1.1, and have more than 1% normative corundum. The Dry Hill Gneiss fits many of the characteristics for I-type granites, but it plots on the sedimentary side of a K2O vs. Na2O diagram (White et al., 1977).

The Dry Hill Gneiss fits much better into the anorogenic granite classification of Loiselle and Wones (1979), as explored in detail below. They describe anorogenic granites as those found in rift zones or within thick stable continental crust. Chemically, the granites are

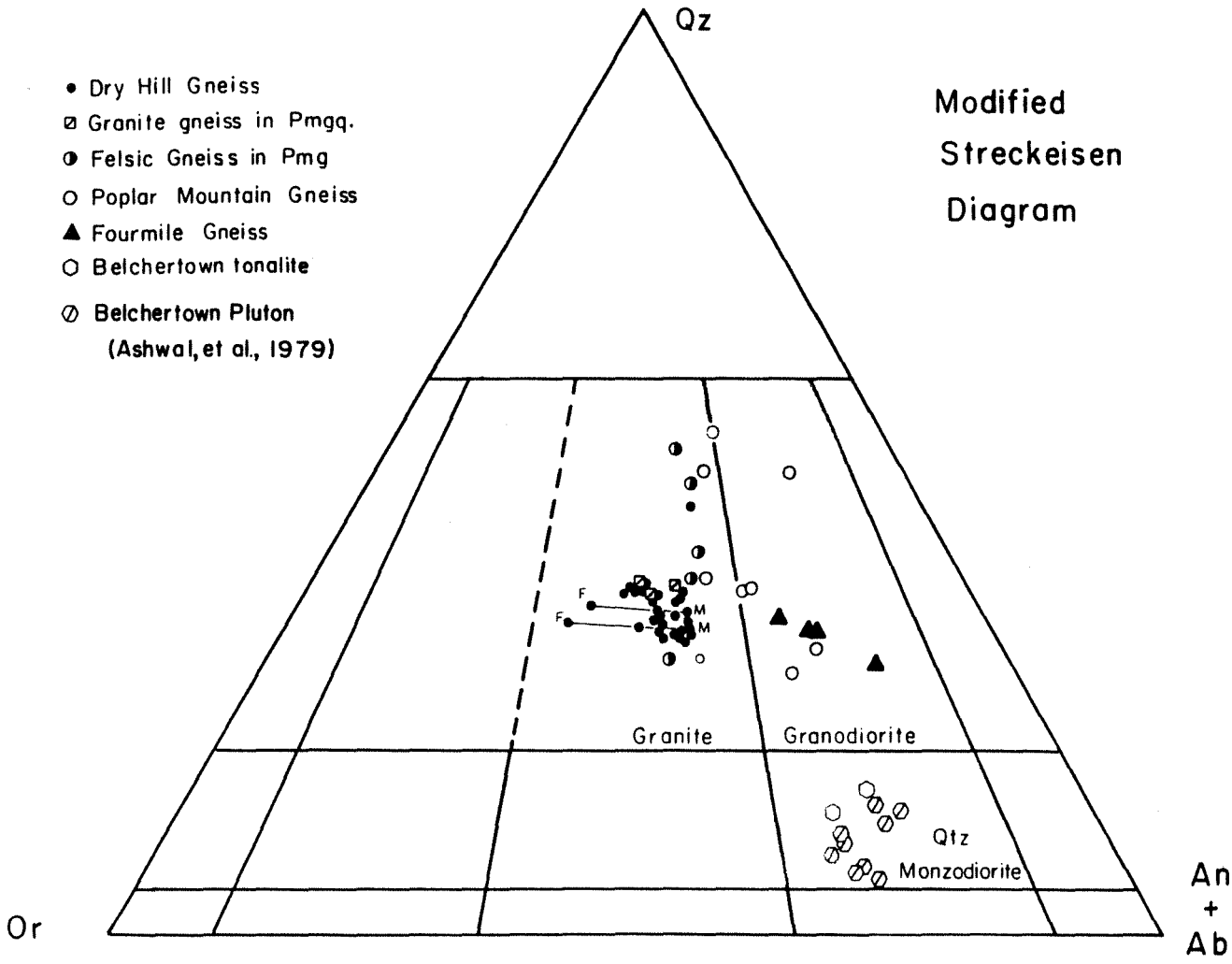

Figure 16. Norms plotted in volume percent on a modified Streckeisen diagram. Norms of quartz, orthoclase, anorthite, and albite were recalculated by density before plotting. Note that most analyses of Dry Hill Gneiss plot between the split samples "F" and "M".

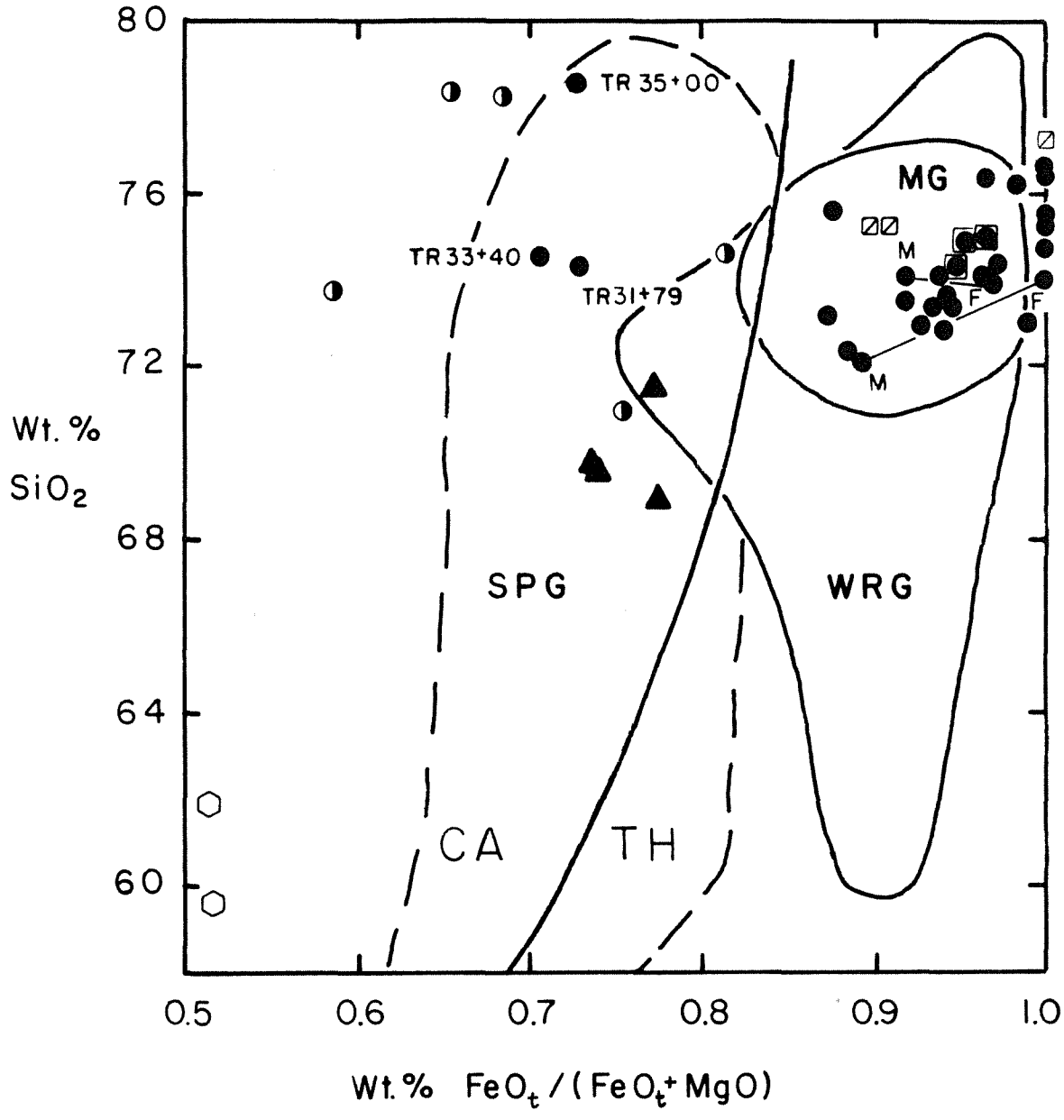

Figure 17. Calc-alkaline/tholeiite discriminant diagram, modified from Miyashiro (1974). Note that three samples of Dry Hill Gneiss: TR 31+79, TR 33+40, and TR 35+00, plot in the calc-alkaline field. Dry Hill Gneiss is compared to rocks of the Montello Batholith (MG), Wolf River Granite (WRG), and the synorogenic Penokean Granite (SPG). Data from Anderson, et al. (1980) and Anderson and Cullers (1978). Curved diagonal line separates calc-alkaline field from tholeiitic field.

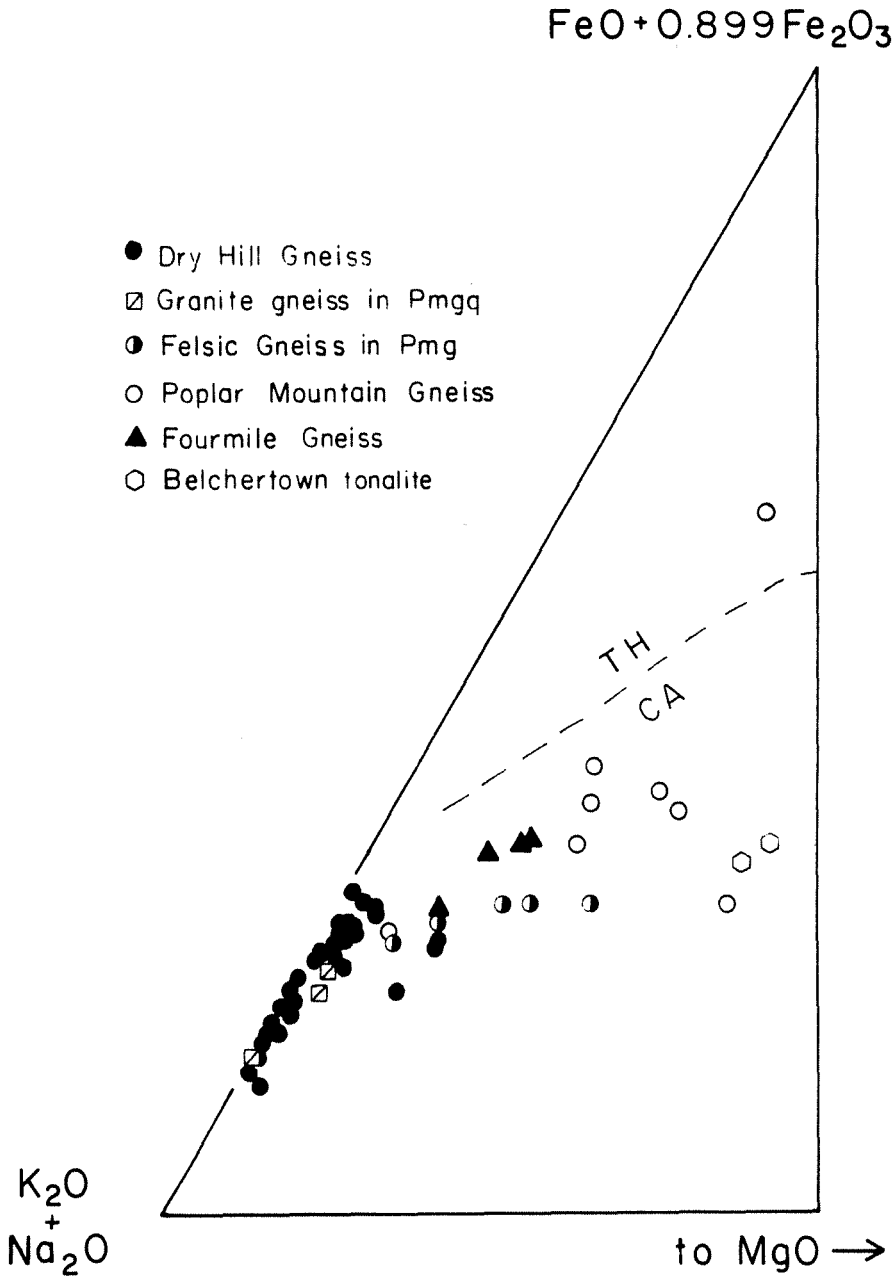

Figure 18. AFM diagram.

slightly alkaline with high K2O, K2O/Na2O and Fe/Fe+Mg and low CaO and Al2O3. The rocks crystallized under conditions of low H2O fugacity and low to moderate oxygen fugacity, i.e., a dry and reducing environment. Loiselle and Wones theorize an origin by melting of lower crust, possibly with an alkali basalt initiating melting. They suggest that an episode of continental rifting or fracturing would be the best tectonic regime to produce anorogenic granites.

Comparison of Dry Hill Gneiss with Anorogenic Granites

Although the protolith of the Dry Hill Gneiss was probably rhyolite lavas or tuffs, based on field evidence, it is appropriate to compare the chemistry of the Dry Hill Gneiss to that of anorogenic granite batholiths. In North America, the period from 1500my to 850 my was characterized by the generation of anorogenic igneous rock (Anderson, et al., 1980). A so-called "trinity" of gabbro, anorthosite, and rapakivi granite has been recognized by several workers (c.f. Emslie 1978, Anderson 1983). Anderson (1983) has identified 79 anorogenic granite suites in North America including the Pikes Peak Batholith of Colorado, the Wolf River Batholith of Wisconsin, the Montello Batholith of Wisconsin and the St. Francois Mountains Igneous Complex of Missouri. The rapakivi granites of Finland are archetypal anorogenic granites (Simonen, 1960).

The Pikes Peak Batholith is composed of biotite granite, and biotite-hornblende granite, with lesser amounts of quartz syenite, fayalite granite and riebeckite granite and is about 1040 $\pm$ 13my (Hedge, 1970). The rocks are high in K2O and low in CaO and MgO, and contain from 0.3 to 0.6 weight percent fluorine(Barker et al., 1975). Barker et al. (1975) hypothesize that melting was initiated by an alkali olivine basalt intruding the lower crust which melted to form a quartz syenitic liquid. The two dominant granite types were produced when the syenitic magma partially melted and reacted with crustal rocks of intermediate levels. Thus, the formation of the batholith was an anorogenic process that required a thick crustal sequence.

The dominant rock types of the 1500 my Wolf River Batholith are biotite granite and biotite-hornblende granite (Anderson and Cullers, 1978). The Wolf River rocks are high in silica, Fe/Mg and alkalies and low in alumina, calcium and magnesium. On a ternary diagram of normative quartz, albite and orthoclase the granites plot near minimum melt composition, in vapor undersaturated conditions, at a pressure of 7-10 kilobars. Based on those estimates, Anderson and Cullers (1978) suggest that the rocks formed at lower to intermediate crustal levels by partial fusion of tonalitic to granodioritic rocks. They suggest that the surrounding calc-alkaline Penokean granodiorites and tonalites would be a reasonable source. The Wolf River Batholith probably formed in an extensional tectonic regime.

The Montello batholith of Wisconsin is approximately 1.76by old and is dominantly composed of biotite granite (Anderson et al., 1980). Some mantles of plagioclase on K-feldspar occur. The mineralogy, which might be similar to that of the protolith of the Dry Hill Gneiss before metamorphism, consists of quartz, two feldspars, hastingsite, biotite, sphene and allanite. In the case of the Montello Batholith, the more silica-rich rocks have no hastingsite, whereas the amount of silica appears to have no bearing on the presence or absence of amphibole in the Dry Hill Gneiss.

The rocks of the Montello batholith are subalkaline, high in iron relative to magnesium and usually contain more than 5 weight % K20. With increasing differentiation the rocks decrease in Fe, Mg, Ti, Ca, AL, Ba and Sr, but increase in Si and Rb. The trend is similar to that of the Dry Hill except that Ba does not increase with increasing SiO2 in the Dry Hill Gneiss. Anderson et al. (1980) suggest a lower crustal source with a 10% melting of tonalite to granodiorite, accompanied by fractional crystallization of biotite and hornblende. They suggest that the Penokean calc-alkaline magmatic activity ended by 1760 my and magmatism may have henceforth been a result of 1) collision and melting of a tectonically thickened crust or 2) anorogenic extensional tectonics.

The rocks of the St. Francois Mountains of Missouri are rhyolites, tuffs and epizonal granites and are approximately 1500 my old (Bickford and Mose, 1975). Except for granites interpreted as parental, the granites and rhyolites of the St. Francois Mountains are low in Al2O3 and CaO and moderately high in K2O(Bickford, et al., 1981). There are two main sources of the granites and rhyolites, the Butler Hill Caldera and the Taum Sauk area. Cullers and Koch (1981) theorize that the rocks of the Butler Hill Caldera were formed by 30% aggregate melting of a lower crustal source of metamorphosed quartz diorite, graywackes, or subgraywackes. The rocks of the Taum Sauk area may have originated by 30% equilibrium melting of arkose to subarkose.

All of the above anorogenic suites are usually compared to the Finnish rapakivi granites, which were among the first rocks in the world to be labelled anorogenic granites (Sahama, 1945 cited in Emslie, 1978). The rapakivi granites are characterized by extremely high K2O values, high total alkalis, low CaO and high $FeO_{total}/(FeO_{total} + MgO)$ (Emslie, 1978).

Dry Hill Gneiss fits well into the rapakivi granite field on a plot adapted from Shand (1927) which contrasts peraluminous and metaluminous rocks (Figure 19). Both formations straddle the peraluminous/metaluminous boundaries. The anorogenic Wolf River Granite plots very close to the rapakivi granite. A calc-alkaline series from the Sierra Nevada is plotted for contrast. The Biotite Member and the more biotite-rich samples of the Hornblende Member of the Dry Hill Gneiss plot in the peraluminous field. The samples of

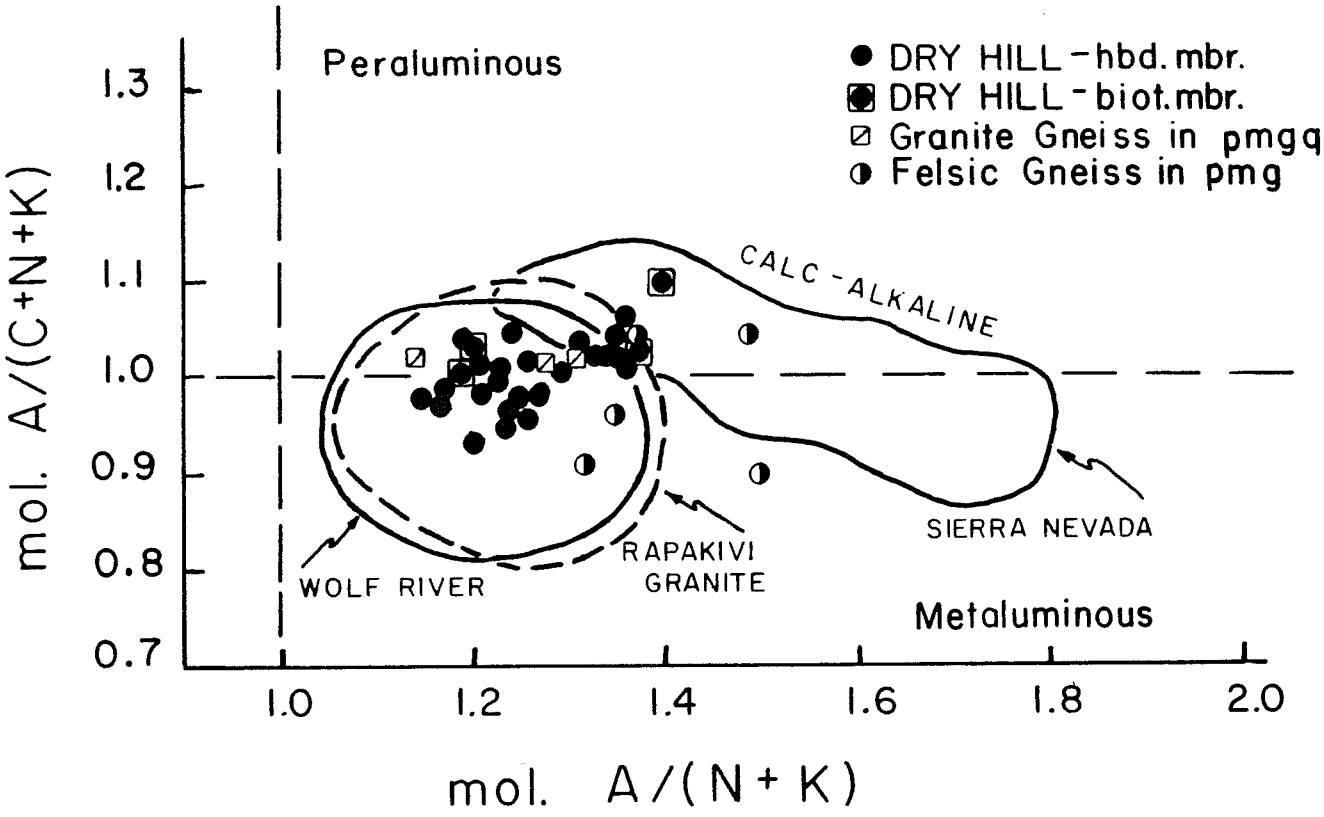

Figure 19. Shand alumina saturation diagram, adapted from Lidiak and Denison (1983). Rapakivi field from Sahama (1945), Wolf River field from Anderson and Cullers (1978), and Sierra Nevada field from Bateman, et al. (1963). Pmgq is Poplar Mountain Quartzite and pmg is Poplar Mountain Gneiss. A is molecular Al203, C is molecular CaO, N is molecular Na20, and K is K20.

granite gneiss from the Poplar Mountain Quartzite also plot in the peraluminous field, and that fact combined with field evidence, implies a cogenetic relationship to the Dry Hill Gneiss. Samples of felsic gneiss from the Poplar Mountain Gneiss are more scattered and have a less clear relationship to the Dry Hill. They may have a sedimentary component.

Referring to Figure 17, the Dry Hill is chemically similar to both the Montello Granite and the Wolf River Granite. All are extremely evolved with respect to magnesium. The synorogenic Penokean rocks in the calc-alkaline field are plotted for contrast.

Emslie (1978) has written a synthesis of anorogenic granite evolution. He envisions a heat source in the mantle, such as a mantle plume producing an olivine tholeiitic magma which rises until it hits the base of the crust where it begins to crystallize. The heat produced by the crystallization of the tholeiitic rocks could partially melt the granodiorite to quartz diorite rocks of the lower crust, forming an anorogenic magma (Emslie 1978).

Clemens (1984) has experimentally determined a crystallization sequence for an A-type granite from southeastern Australia. Since field evidence indicates that the magma was emplaced as a liquid at a shallow depth, then crystallized, he ran his experiments at one kilobar. His sequence is magnetite ($T > 950^{o}C$), quartz plus plagioclase ($T \geq 830^{o}C$), followed by clinopyroxene, and potassium feldspar. Biotite crystallizes also, if 0.5 weight percent fluorine is added or if the oxygen fugacity is reduced. His evidence contradicts some of that which has been accepted for A-type granites because he implies an amount of water in the melt that is greater than 2 weight percent. Clemens envisions an origin from melt-depleted I-type rocks by high-temperature anatexis.

The Dry Hill Gneiss has no directly discernable crystallization sequences of a similar type to those described by Clemens except for possible magnetite crystallization and fractionation. Indirect evidence, in the form of the leucogneiss/biotite gneiss layering, does remain. Early magnetite fractionation could account for part of the fractionation trend on the AFM diagram (Figure 18).

It is likely that the protoliths of the Dry Hill Gneiss were rhyolite lavas or tuffs of anorogenic affinities, based on chemical similarities with anorogenic granites and related rhyolites. The layering in the present day Dry Hill Gneiss suggests that part of the protoliths may have been layered tuffs, a concept which will be discussed below.

Trace Element Chemistry of the Dry Hill Gneiss

On a plot of K2O vs. Rb (Figure 20), the K2O values of the Dry Hill Gneiss remain approximately constant as the rubidium values increase. Dry Hill Gneiss Biotite Member sample 18+72 is greatly enriched in Rb, relative to the rest of the formation. Because Rb substitutes in biotite, the powder pellets were inspected for any obvious large flakes of biotite resting on the surface, which would anomalously raise the Rb count. None were detected. The hand sample does not contain an unusually large amount of biotite, either. Probably, the protolith was enriched in Rb. Perhaps the glassy portion of the protolith was enriched in Rb, or some small amount of biotite had crystallized before eruption of the rock, and was erupted with the ash. Both of the microcline-hornblende-rich leucogneiss layers of the split samples have a marked increase in K2O for the same amounts of Rb. The leucogneiss layers were probably enriched in orthoclase, perhaps by crystal setting during eruption. Because the Rb values do not change in the split samples, large amounts of biotite fractionation are unlikely. Probably most of the Rb remained in the liquid. The three samples of granitic gneiss plot within the Dry Hill Gneiss cluster, although they contain a little less Rb. The felsic gneiss samples plot between the Dry Hill Gneiss and the Poplar Mountain Gneiss, perhaps due to removal of K2O from the protolith by sedimentary processes, or perhaps due to smaller accumulations of orthoclase in the protolith. Poplar Mountain Gneiss contains much less K2O then the Dry Hill Gneiss and somewhat less Rb, possibly as a result of weathering.

Zr varies by a factor of 3 with essentially no change in silica, on a plot of Zr vs. SiO2 (Figure 21). The leucocratic layers of the split samples contain more Zr than the other layers. Zircon can crystallize early in a granitic magma. Pre-eruption zircon crystallization and removal from the magma of the Dry Hill protolith should have caused Zr to decrease with increasing silica. The change in Zr must be explained by another process. This problem will be addressed below.

The Zr/Nb ratio varies from just under 5 to 20 on Figure 22. Perhaps some mafic, Nb-bearing mineral fractionated slightly, but any trend is obscure. The two anomalous Dry Hill Gneiss samples, TR 31+79 and TR 33+40, are enriched in Nb. Some of the scatter in the Dry Hill samples may be due to varying amounts of sphene, which can contain Nb in trace amounts (Jaffe, 1947).

The Dry Hill Gneiss exhibits a coherent linear trend on a diagram of Ba vs Zr (Figure 23). The Poplar Mountain Gneiss, the felsic gneiss, and the granite gneiss all plot along the same trend. The ratio of Ba/Zr is about 4. Poplar Mountain Gneiss has lower amounts of Ba and Zr, perhaps due to loss by weathering of glass. The leucogneiss layers (F) of the split samples are enriched in both Ba and Zr relative to the biotite gneiss layers (M). This suggests that whatever process

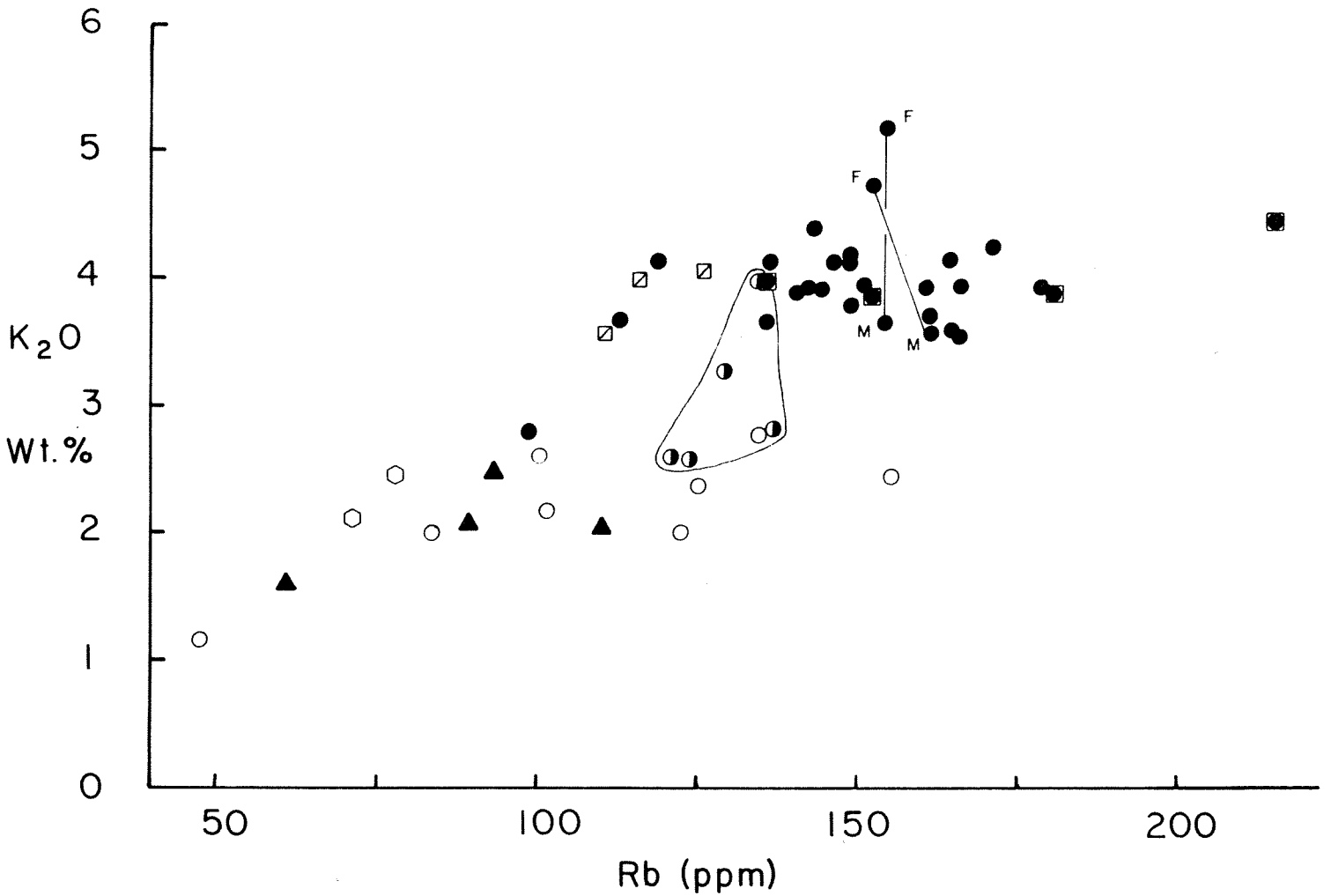

Figure 20. Plot of Rb vs. K20. Note that Poplar Mountain Gneiss has consistently lower K20 and Rb than the Dry Hill Gneiss.

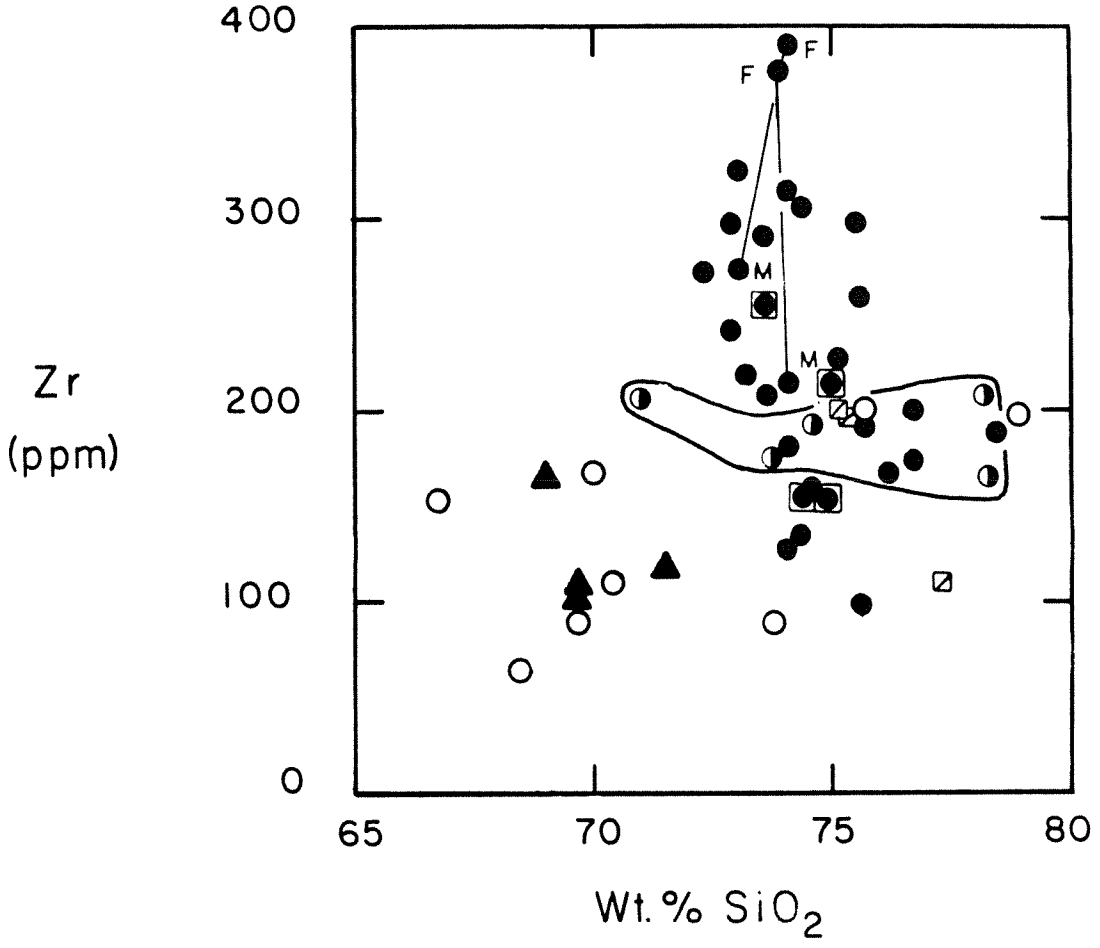

Figure 21. Plot of Zr vs. SiO2. Field of felsic gneiss within the Poplar Mountain Gneiss is outlined.

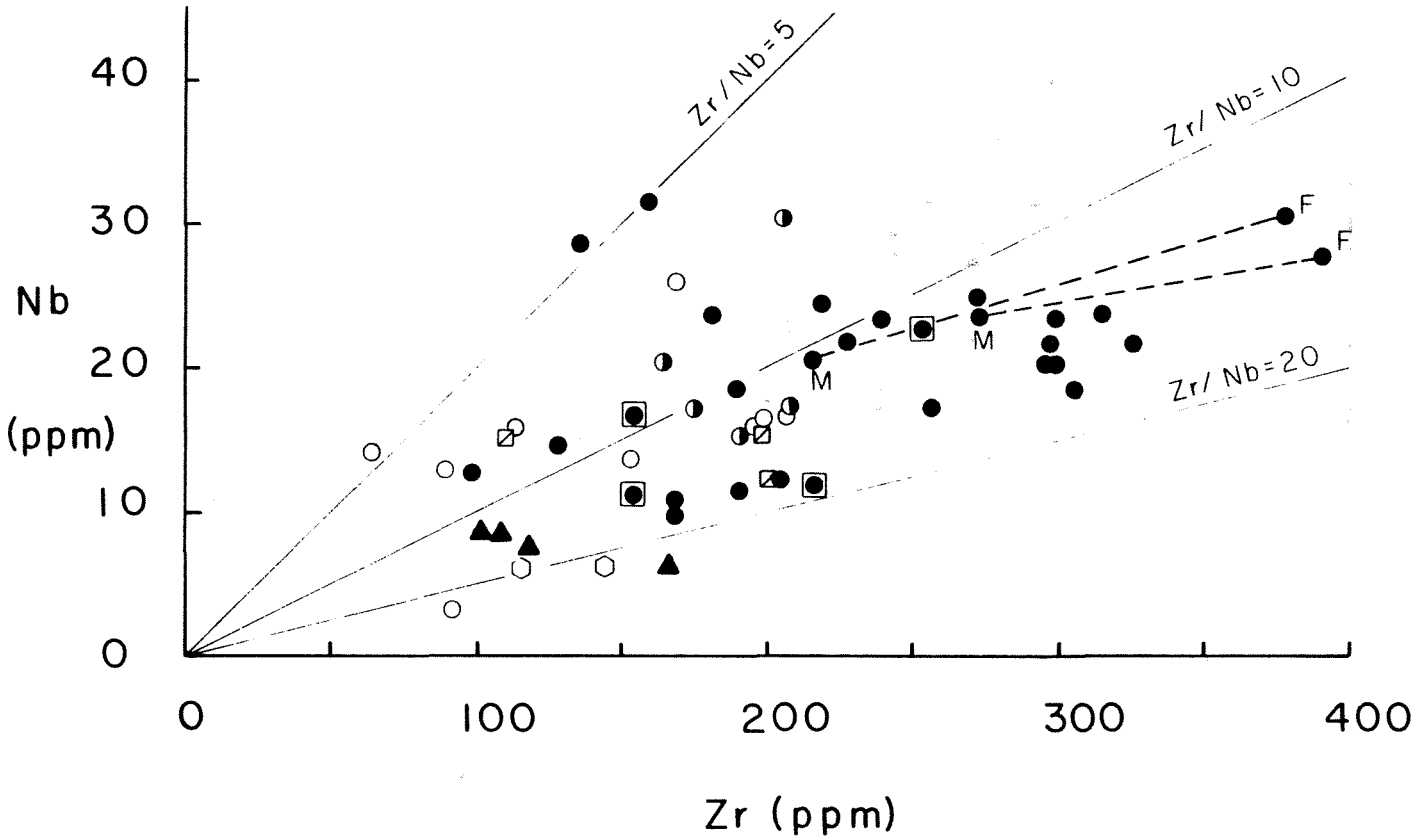

Figure 22. Plot of Nb vs. Zr.

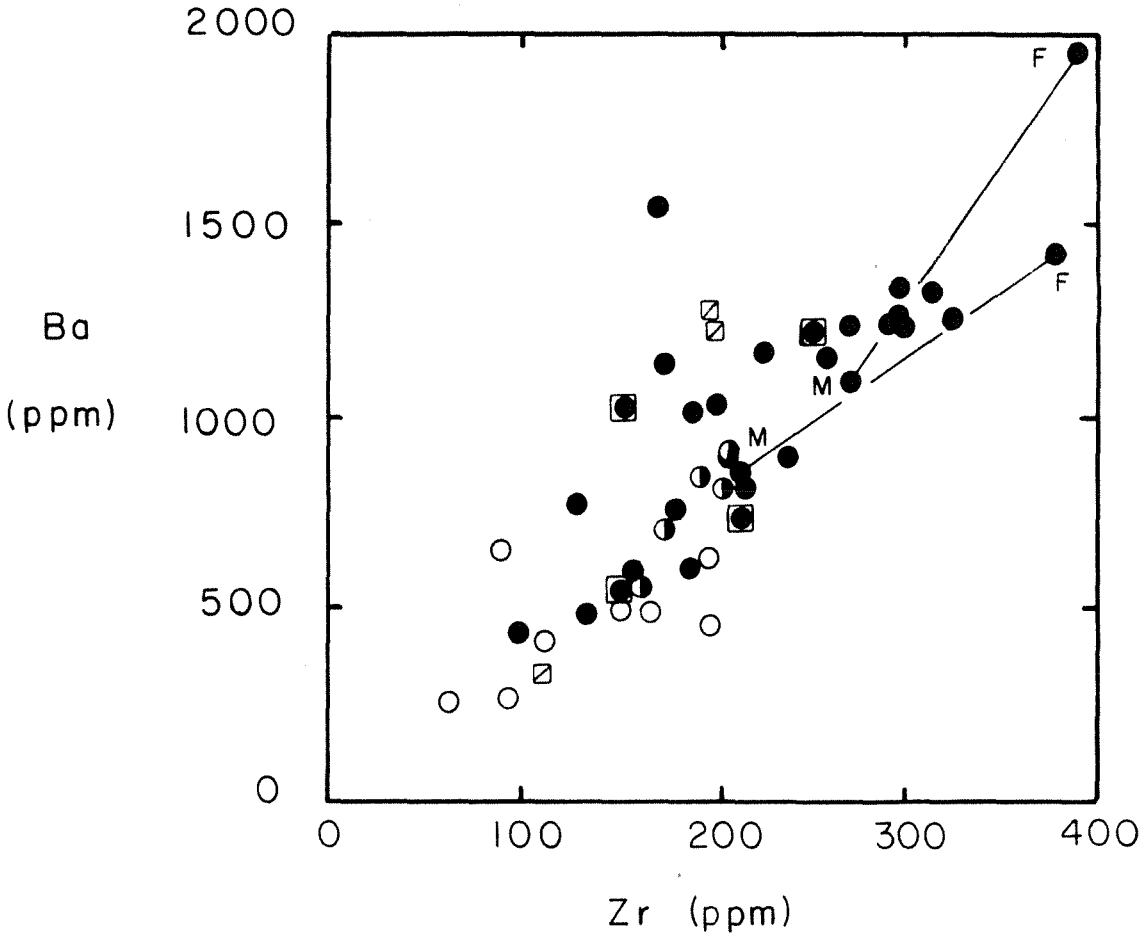

Figure 23. Plot of Ba vs. Zr for Dry Hill Gneiss and Poplar Mountain Gneiss, including felsic gneiss and granite gneiss.

is differentiating the leucogneiss layers from the biotite gneiss layers is responsible for the whole trend. A plot of Ce vs Zr has a similar trend (not shown). A plot of Ba vs. SiO2 (not shown) has a strong variation in Ba with essentially no change in silica, suggesting that whatever process was enriching some layers in potassium feldspar, was not conformably changing the amount of silica.

Introduction to Poor Man's Rare Earth Elements

One of the best ways to get an idea of the origin of an igneous rock is by rare earth element (lanthanum to lutetium) analysis, henceforth referred to as REE. They are useful because they are stable under most geologic conditions and behave in a chemically systematic manner (Hanson, 1980). Such processes as metamorphism, hydrothermal alteration, or weathering should not greatly affect either patterns or abundances of REE, unless the processes are extreme (Hanson, 1980). Studies of igneous fractionation, enrichment, melting and other processes should still be possible after metamorphism. Unfortunately, the process of analysing for REEs is expensive and no facilities exist for the technique at the University of Massachusetts. For those reasons, a technique was used that can serve as an analog, using X-ray fluorescence analysis at the University (Bougault, 1980; Bougault and Treuil, 1980). Because it is relatively inexpensive, the technique has come to be called informally poor man's rare earth element (PMREE) analysis. The elements are incompatible ($Kd \leq 1$), belong to a transition series, and are not volatile under conditions of planetary accretion. Bougault selected Ti, V, Y, Zr, Hf, Ta, and Th, of which all except Hf and Ta are routinely analysed at the University of Massachusetts.

Two rare earth elements can be readily analysed by X-ray fluorescence analysis, cerium and lanthanum. REEs are normalized to chondritic meteorites, which are theorized to be analogous to original cosmic abundances of the elements, and may reflect the composition of the primitive earth. The method eliminates the Oddo-Harkins effect and produces a smooth curve. The chondritic values determined by Haskin, et al. (1968), were used to normalize the two elements. Sr was used in place of divalent europium because the ionic radii are very close in size and the two behave in a similar manner chemically (Hanson, 1980).

The agreement between REE and PMREE is fairly good, but exact correlations cannot be drawn between the two. The PMREE must be interpreted cautiously. Specifically, three problems may occur. The first is that the technique was developed for basaltic rocks but the rocks of this study are granitic. The second is that certain minerals, such as allanite and zircon, are ubiquitous in the study rocks, and those minerals concentrate REE and PMREE. They may cause scatter in the data. The third is that metamorphism may affect some PMREEs, although the process normally does not affect REEs.

Dry Hill Gneiss PMREE

On a PMREE diagram, (Figure 24), the Dry Hill Gneiss has uniform and generally parallel trends, suggesting that the process which formed it did not change much through time. The steep slope of the trend is typical for a granitic rock. By analogy with REE, the Dry Hill Gneiss is probably light rare earth (LREE) enriched. Cerium, a LREE, is quite high. Perhaps the source rocks of the Dry Hill Gneiss were also enriched in light rare earth elements. Alternatively, the trend may be due to crystal fractionation. The gneiss may be heavy rare earth (HREE) depleted, if vanadium is behaving analogously to a HREE, such as lutetium. Garnet has large Kd's for HREE, so perhaps there was garnet in the residue after melting. Alternatively, V may substitute into a mafic mineral such as magnetite, in which case the trend may be due to magnetite fractionation or magnetite in the residue.

The diagram has both a pronounced negative niobium anomaly and a strong negative titanium anomaly. Possibly an oxide phase, such as ilmenite, which contains both Ti and Nb, fractionated to produce the anomalies. Alternatively, the source rocks from which the Dry Hill Gneiss melted may have been depleted in Ti and Nb.

Strontium substitutes in trace amounts in plagioclase feldspar, in much the same way that divalent europium does (Hanson, 1980). There may be a very slight Sr anomaly, due to plagioclase fractionation.

Dry Hill Gneiss Biotite Member PMREE

The Biotite Member compared to the Dry Hill Gneiss as a whole, contains less Ce, Zr, Ti, and Y (Figure 25). Ce substitutes in allanite. Perhaps the protolith of the Biotite Member was depleted in allanite before eruption, or allanite crystals were winnowed out during emplacement. Another possibility is that sphene was removed, because it can contain minor amounts of Ce, Y, and Nb (Jaffe, 1947). It can also contain minor amounts of Zr (Sahama, 1946). Titanium is a major structural component of sphene. The Biotite Member contains little or no garnet or hornblende, which have a large Kd for Y, so smaller amounts of Y are reasonable. Probably the protolith of the Biotite Member contained less Y than the protolith of the Hornblende Member, due to deposition of smaller amounts of hornblende or sphene. In general, the Biotite Member protolith seems to have had a greater glass component than the Hornblende Member protolith.

Comparison of Dry Hill Gneiss with Average Crustal Rocks

An average of the combined Hornblende Member and the Biotite Member of the Dry Hill Gneiss was computed for comparison with average crustal composition (Taylor and McLennan, 1981). The Dry Hill Gneiss is enriched in Rb, Pb, Ba, Ce, Y, and Th, relative to both the upper and lower crust (Table 12). Relative to both, the Dry Hill Gneiss is

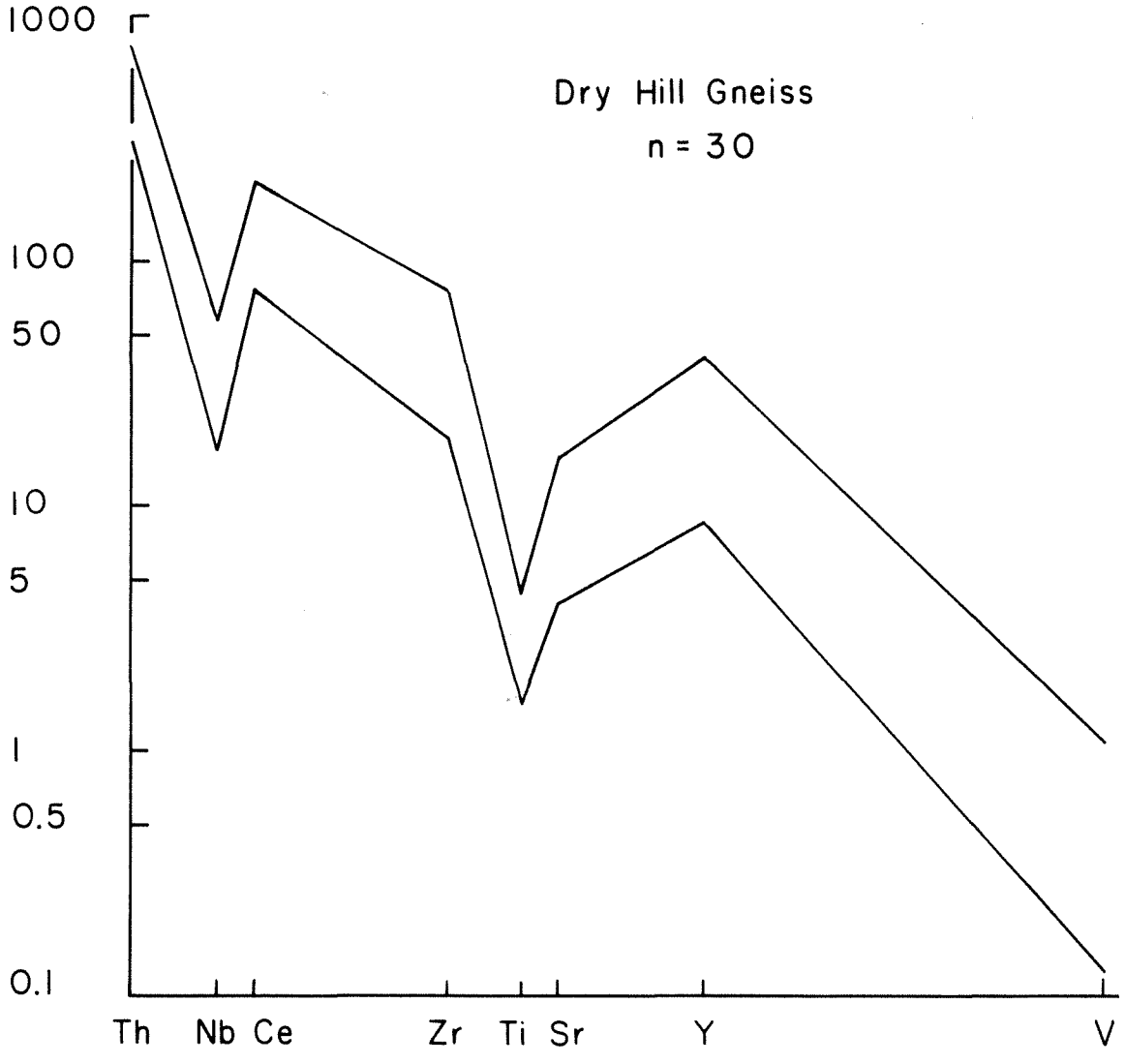

Figure 24. Plot of "Poor Man's" Rare Earth Element (PMREE) analyses for Dry Hill Gneiss. Trace elements are normalized by normalizing factors of Bougault (1980). Trend of the Dry Hill Gneiss is indicated by an envelope around 30 samples.

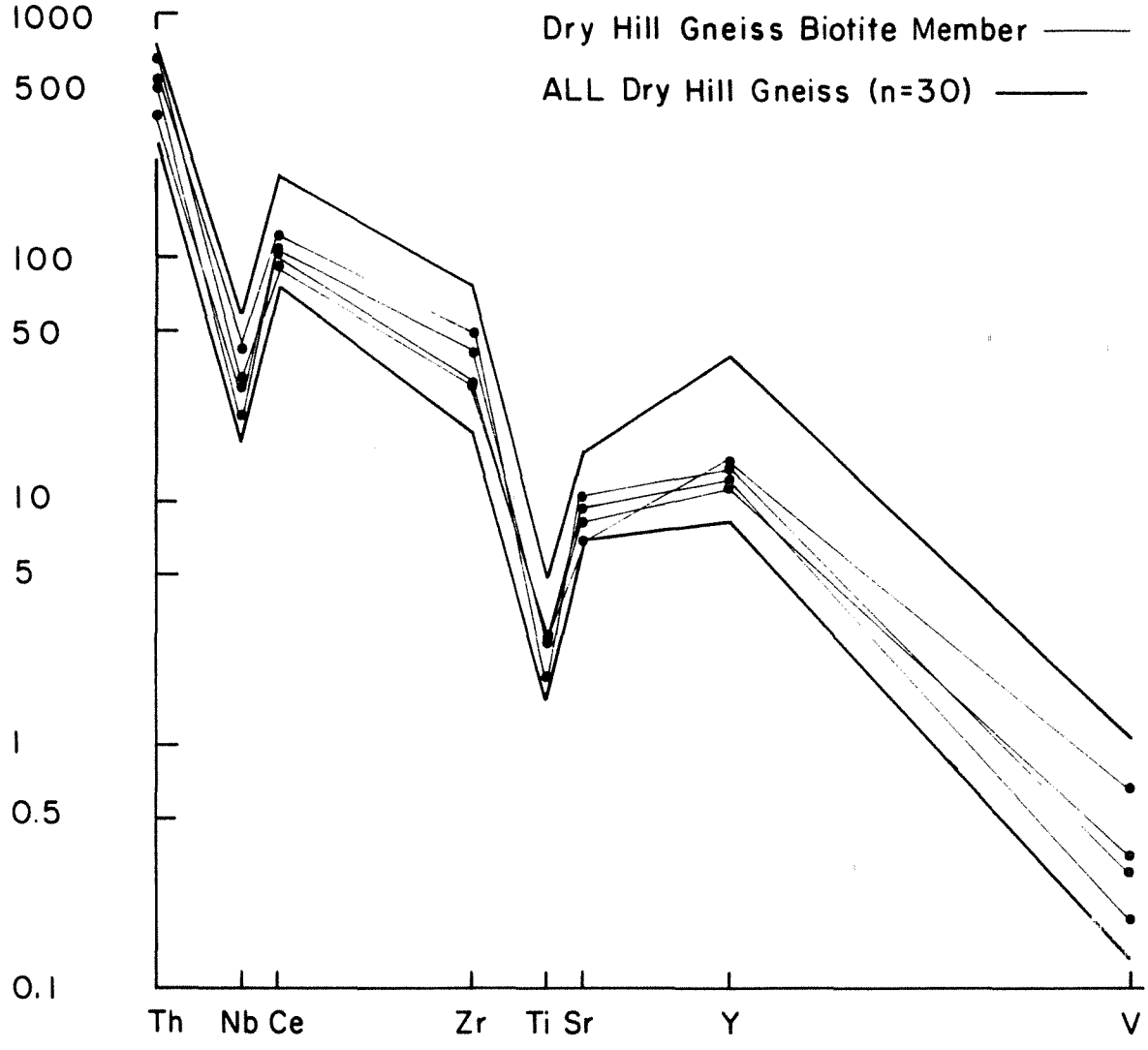

Figure 25. PMREE diagram of four samples of Dry Hill Gneiss Biotite Member (thin lines) plotted against the Dry Hill Gneiss envelope (heavy lines).

depleted in strontium. The Dry Hill contains more Nb and Zr than the lower crust, but marginally less of the two elements than upper crust.

Taylor and McLennan theorize that the upper crust is derived from intracrustal partial melting of lower crust. The Dry Hill Gneiss could have been derived in a similar manner.

Table 12. Average crustal amounts of selected trace elements compared to those of the average of thirty samples of Dry Hill Gneiss. Table adapted from Taylor and McLennan (1981).

	Present Upper Crust	Present Lower Crust	Archaen Upper Crust	Dry Hill Gneiss Average
Rb	110	8	25	152
Pb	15	7.5	10	18
Sr	350	425	300	117
Ba	700	175	170	1029
Ce	64	25	26.8	120
Y	22	22	15	35
Nb	25	4	5	20
Zr	240	30	100	231
Th	10.5	1.95	2.9	13

On the Problem of Layering in Dry Hill Gneiss

One of the most striking features of the Dry Hill Gneiss in outcrop is the hundreds of meters of alternating pink leucogneiss and light-gray biotite gneiss layers, ranging in thickness from millimeters to 20 or 30 centimeters. The lighter-colored layers are richer in potassium feldspar and hastingsite, and the darker-colored layers are richer in biotite. One of the purposes of this study is to characterize chemically the layers and to present a reasonable hypothesis for their origin. Two samples, 9+40 and TR44+90, were carefully split into a leucogneiss layer and a biotite gneiss layer, and the layers were analysed separately.

The leucogneiss layers are richer in K_2O, but contain less Na_2O and Al_2O_3 than the biotite gneiss layers. The biotite gneiss layers contain marginally more MgO, TiO_2 and FeO. Barium, cerium, and zirconium, are drastically increased in the light-colored layers; yttrium and niobium are also slightly higher. The rubidium and strontium values are similar for each type of layer, as are those of SiO_2.

The PMREE of the split leucogneiss and biotite gneiss pairs were plotted against the Dry Hill as a whole (Figure 26). The leucogneiss layers contain more Nb, Ce, Zr, and Y; the biotite gneiss layers contain more Ti and V. In the minerals of the present Dry Hill Gneiss, perhaps the Nb substitutes for Ti in the sphene (Sahama, 1946 and Jaffe, 1947). In the microcline-hastingsite-rich layers, Y substitutes in garnet and hastingsite, and Zr is an essential structural component of zircon. Garnet and hastingsite are in greater abundance in the microcline-hastingsite-rich layers; there are no garnets and only trace amounts of hastingsite in the sampled biotite gneiss layers. A mechanism is needed to relate the chemical variation between the layers of the present rock to the chemistry of the protolith.

Robinson (personal communication, 1980) suggested pre-Acadian partial melting to explain the layering, during conditions of sillimanite-orthoclase grade metamorphism (Robinson, Tracy, and Ashwal, 1975). In this model, the leucogneiss layers would be the products of melt, and the biotite gneiss layers would be the restite. Unfortunately, the Dry Hill Gneiss has been subsequently metamorphosed and recrystallized under kyanite-staurolite grade conditions, obscuring direct mineralogical evidence which would bear on this question. Lappin and Hollister (1980) described petrographic textures and mineral zoning in the Central Gneiss Complex near Prince Rupert, British Columbia, that they interpreted to indicate that quartz, plagioclase, and biotite melted to produce amphibole plus granite melt. Robinson (1979) reasoned that peritectic melting of biotite gneiss in the Dry Hill Gneiss would produce hornblende and liquid. The theory of partial melting in the Dry Hill Gneiss was plausible before geochemical data were available.

Geochemical data, now available, cast serious doubt on the partial melting hypothesis. First, the Sr amounts in the leucogneiss and in the biotite gneiss are nearly the same. With partial melting of plagioclase, the melt, now leucogneiss, should be enriched in Sr. Also, the normative plagioclase in the melt should be more albitic, but both leucogneiss and biotite layers have oligoclase of nearly the same An content and the normative anorthite of the leucogneiss layers exceeds that of the biotite gneiss layers in both examples. If the feldspar reequilibrated during the kyanite-staurolite grade metamorphism, that still does not explain why the biotite gneiss or "restite" contains 1 weight percent more Na_2O than the leucogneiss or "melt". Second, the amount of Rb in both types of layers is nearly identical. Melting of biotite, which usually contains trace amounts of Rb, should change the proportions of that element in the melt and restite. Therefore, it must be assumed that the biotite did not melt.

Another problem develops in the reasoning, when the matter of zirconium is considered. The leucogneiss contains over 100 ppm more Zr than the biotite gneiss. At the estimated temperatures and pressures of sillimanite-orthoclase metamorphism, the bulk distribution

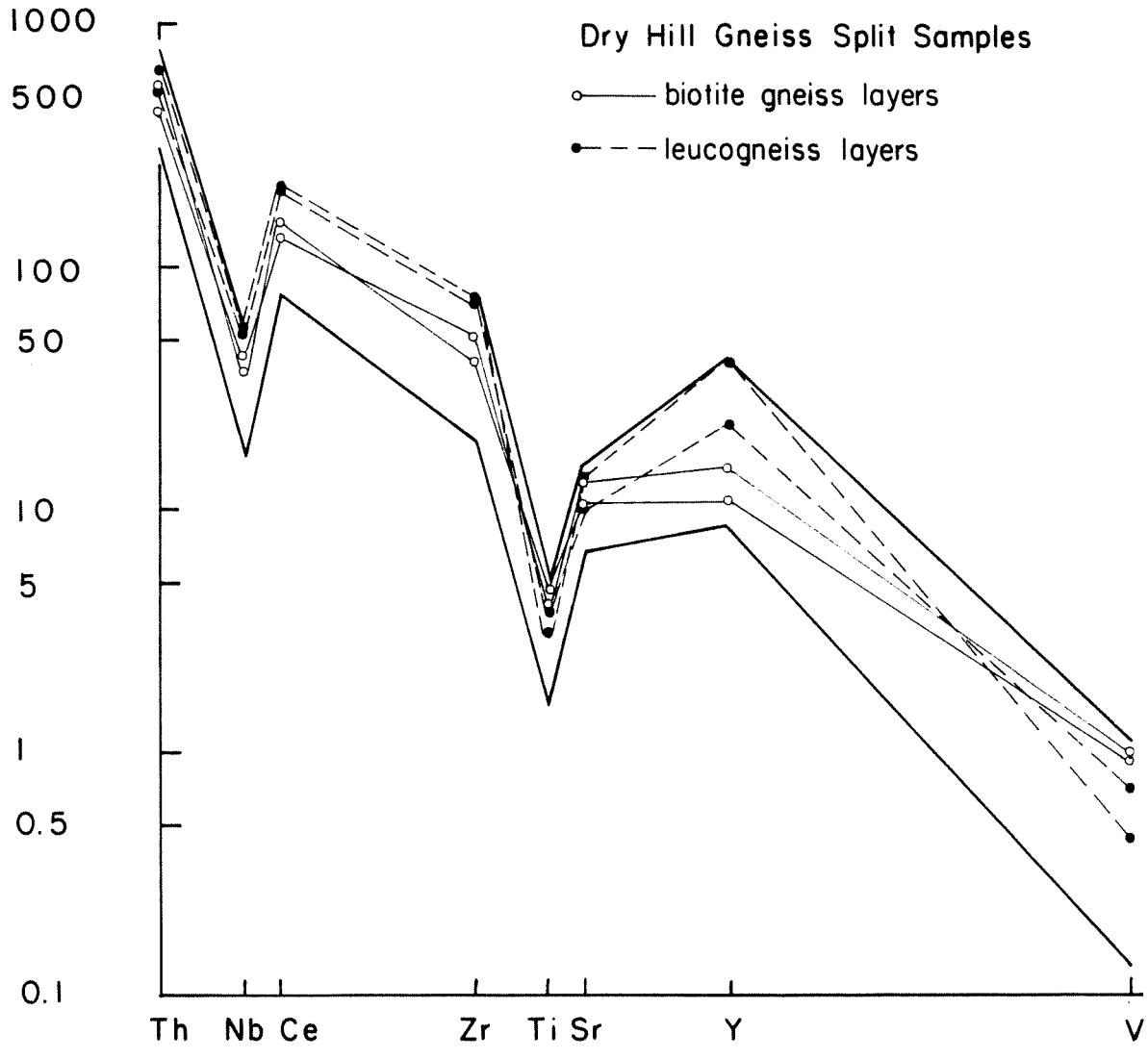

Figure 26. PMREE diagram of leucogneiss layers (dashed lines) and biotite gneiss layers (solid lines) of split samples of Dry Hill Gneiss. Split samples are plotted against the Dry Hill Gneiss envelope (heavy lines).

coefficient (D) of zirconium in zircon to that in the melt is approximately 3000 (Watson and Harrison, 1983). In other words, zirconium is a very highly compatible element, and is extremely likely to stay in the residue during partial melting. Only melting of 100% would mobilize it, which is impossible. On this basis, the enrichment of zirconium in the leucogneiss layers versus biotite gneiss layers rules out the possibility that the leucogneiss layers are the product of partial melting.

With the partial melting hypothesis apparently ruled out, an alternative hypothesis is that the chemical variation in the present rock is a relic of the protolith chemistry. A likely possibility is that the protolith was a layered tuff.

There are various processes by which tuffs are layered. Sheridan (1979) described flow units in pyroclastic eruptions with thin layers (10 cm to 50 cm thick) of differing chemistry due to concentrations of lithic inclusions near the bases of the layers, and concentrations of pumice fragments at the tops. This was due to sorting by mechanical means. Varying chemistry between ignimbrite flows could also be the result of settling out of denser crystals as hot ash clouds surge outward from a caldera (e.g. Hildreth, 1979). Moll (1981) described textures of 20% fine-grained phenocrysts to 40% coarse-grained phenocrysts in the Agua de Mayo Tuff of Chihuahua, Mexico, which she attributed to numerous separate ash flows from one heterogeneous magma chamber.

The process which best explains the Dry Hill Gneiss chemical data is one in which the crystals were separated from glassy shards due to differences in density, such that the denser crystals settled out and part of the glass was winnowed away. In order to explain the process in detail, a brief description of the granite system is necessary (Figure 27). Most granites are composed primarily of anorthite, albite, quartz, and orthoclase (James and Hamilton, 1969; von Platen, 1965; Winkler, 1976). Therefore, those four components are placed on the corners of a regular tetrahedron, with H2O in excess, to approximate granites in nature (Figure 27a). The small leucite field at the Or apex is ignored. Plane E1-E2-E5-P is the cotectic surface of quartz + plagioclase + melt + vapor. Plane P-E5-E3 is the cotectic surface of quartz + orthoclase + melt + vapor. Plane E6-P-E5-E4 is the cotectic surface of orthoclase + plagioclase + melt + vapor (Winkler, 1976). The planes intersect at the line of three-phase saturation P-E5. The cotectic surface of interest to this study is the one where orthoclase + quartz + melt + vapor are present. To display the relations graphically, a slice through the tetrahedron at Qz100 An100 Or50 Ab50 was constructed (Figure 27d). The orthoclase and albite corners were compressed into one corner. In the construction of this plot, the projection of the cotectic line P-E5 was plotted onto two ternary diagrams, Qz-Ab-Or and An-Ab-Or (Figures 27b and 27c).

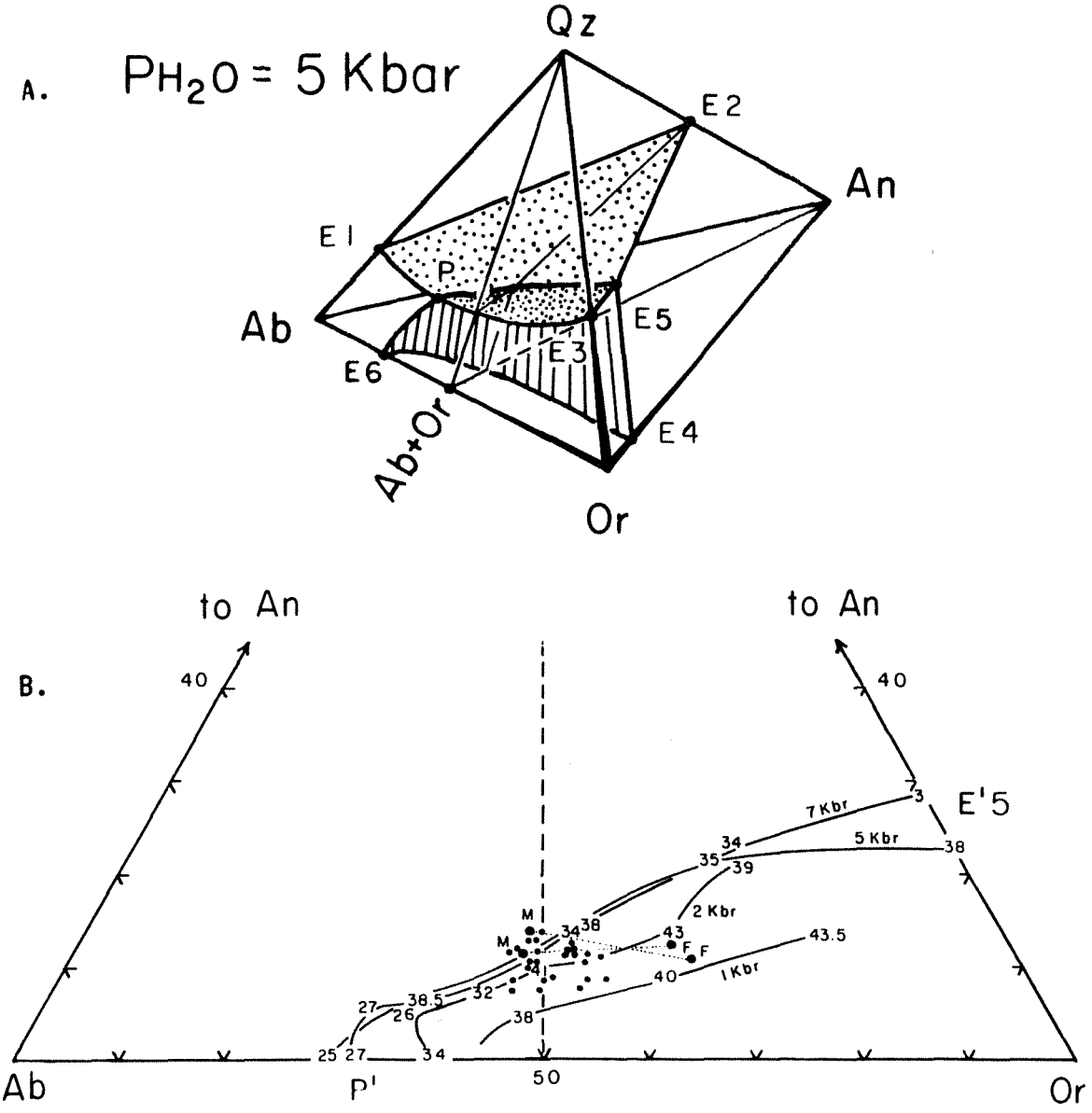

Figure 27A. Sketch of the granite system at 5 kilobars water pressure. Adapted from Winkler (1976, p. 286). Plotting coordinates from Winkler et al. (1975).

B. Projection from the quartz apex of Figure 27A of line P-E5 (three phase saturation) onto ternary diagram An-Ab-Or at various water pressures. Note that the 1 kbar line does not reach the Ab-Or-Qz plane of Figure 27A and hence not the Ab-Or line of Figure 27B. The diagram is plotted in weight percent of normative components. Small numbers give the weight percent normative quartz. Data for 1 kbar from James and Hamilton (1969), 2 kbar from von Platen (1965), 5-7 kbar from Winkler et al., (1975) and Winkler (1976).

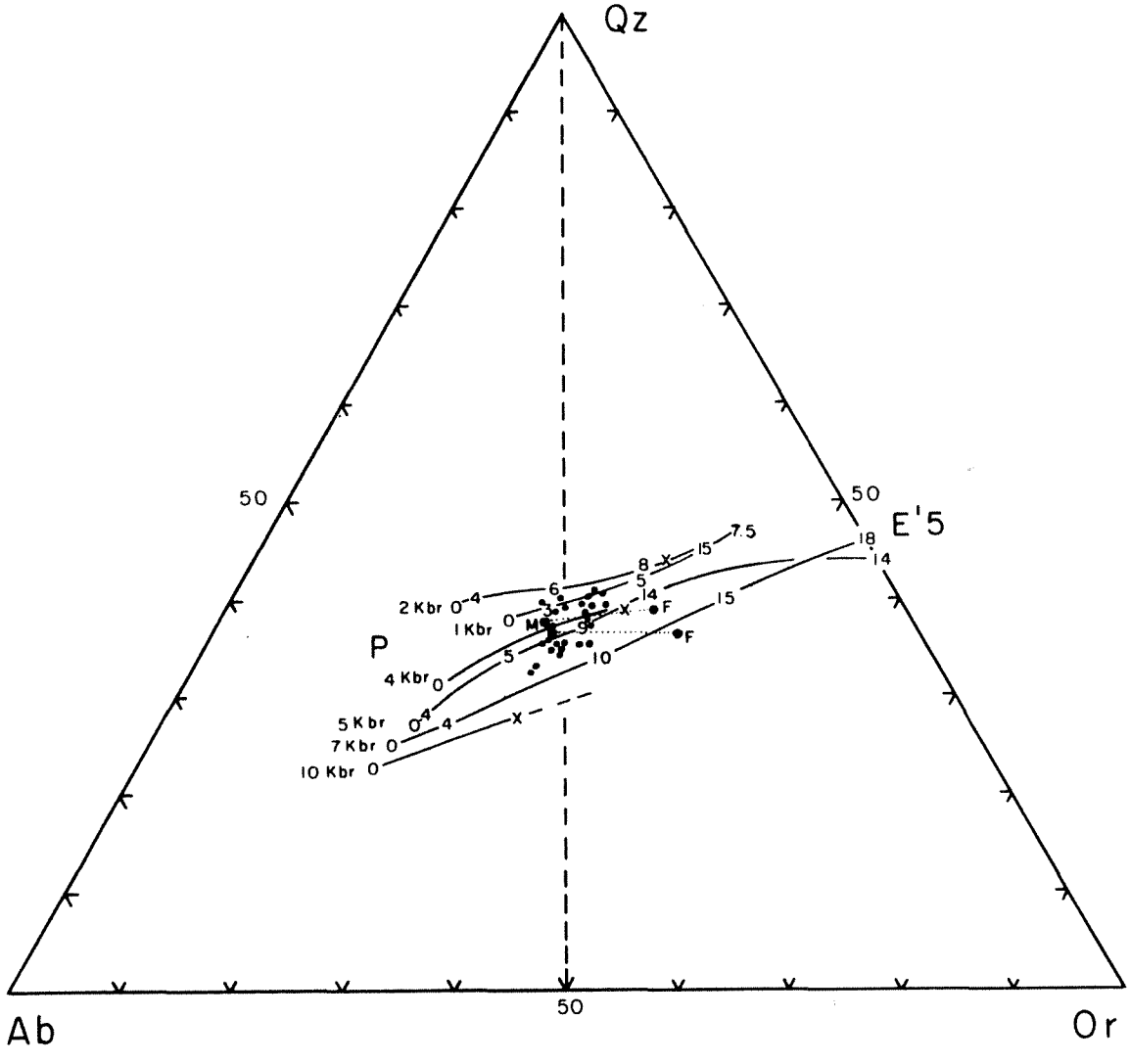

Figure 27C. Projection from the An apex of Figure 27A of line P-E5 (three phase saturation) ternary diagram Qz-Ab-Or at various water pressures. Small numbers give weight percents of normative anorthite. Sources same as in Figure 27B, with the addition of 4 kbar data from von Platen and Holler (1966), cited in Winkler (1976). Points P at An=0 from Tuttle and Bowen (1959) and Luth, et al. (1964).

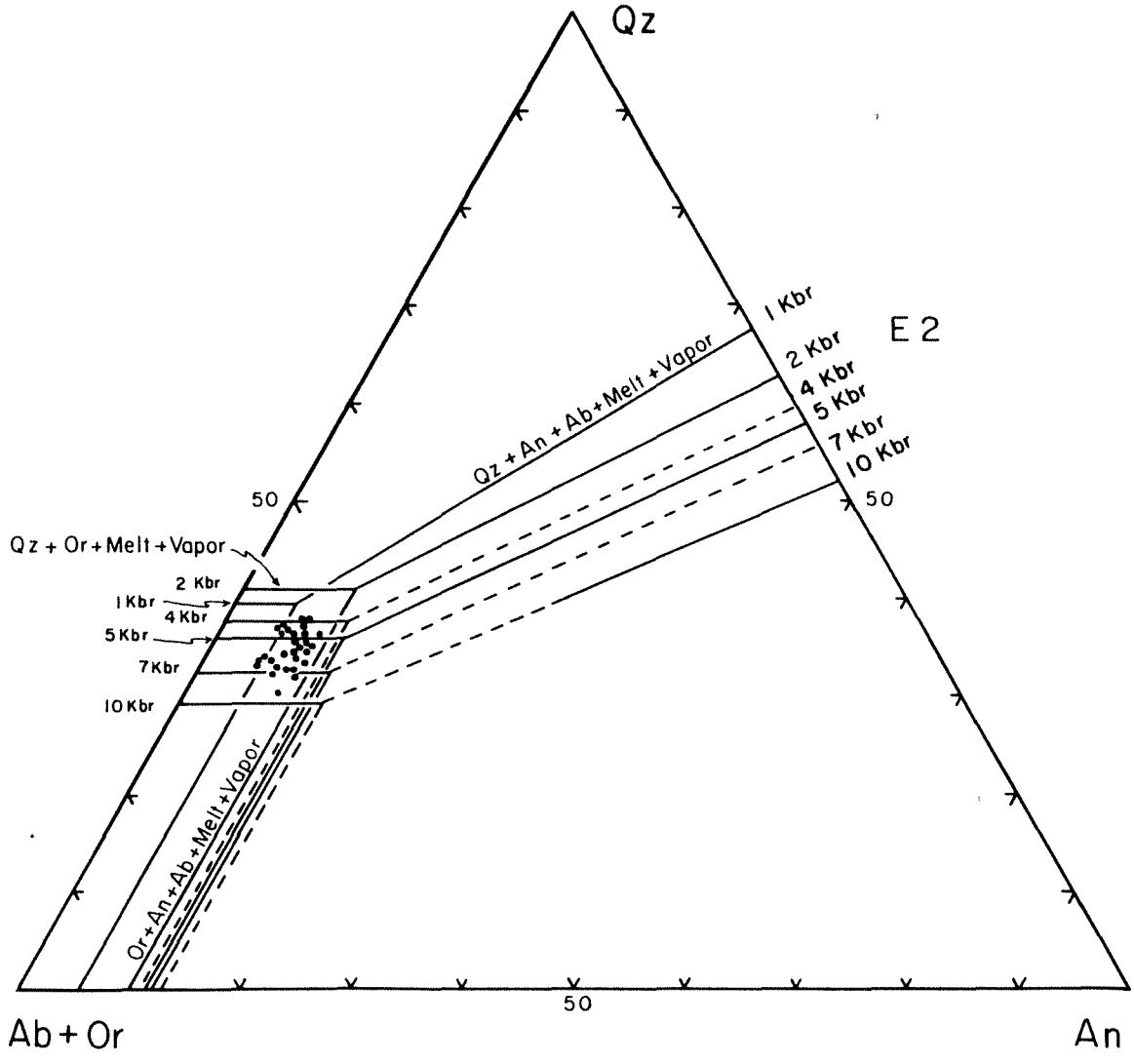

Figure 27D. Plane through the granite tetrahedron (Figure 27A) at Qz100 An100 Or50 Ab50, where the Or and Ab apices are compressed into one apex. An/(Ab+Or) edge at 4 kbar extrapolated from 2 and 5 kbar edges. Points E2 on Qz-An edge are from Stewart (1967).

At water pressures above 7 kilobars, (Figure 27d) the Dry Hill Gneiss plots in the quartz volume above the projection of the Qz-Or-melt-vapor surface. If the water pressure were lowered by an eruption the bulk composition of the Dry Hill Gneiss would intersect the Qz-Or-melt-vapor surface at some lower pressure, perhaps 5 kilobars, and crystallize quartz + orthoclase. The melt would be driven along the cotectic surface away from the crystals coming out, toward more sodic compositions. This is shown on Figures 27b and 27c, where "M" approximates the melt composition and "F" approximates the crystal composition. Note that the amount of quartz and anorthite in the crystals and melt would stay the same.

This is a reasonable crystallization sequence for a magma with the composition of an anorogenic granite. The Rapakivi granite of Finland, for example, plots near the eutectic, and contains large potassium feldspar phenocrysts (Simonen, 1960). The Dry Hill protolith melt probably did not quite reach the three-phase saturation line P-E5 for two reasons. First, if the melt had reached the cotectic, it would have crystallized quartz, potassium feldspar and plagioclase there, not just quartz and potassium feldspar. Second, Sr values do not vary between the leucogneiss (F) and the biotite gneiss (M) layers, as would be expected if the plagioclase were crystallizing. Before eruption, the protolith was in the form of a melt of approximately "M" composition containing crystals of quartz and potassium feldspar of crudely "F" proportions (Figures 27b and 27c). The melt probably also contained crystals of allanite, hornblende, zircon, and perhaps sphene, for reasons which will be explained below.

During some eruptions, the crystals and the melt (now glass) tended to separate mechanically. The force of the blasts removed much of the glass shards, but the denser crystals with subordinate glass settled out and became the leucogneiss layers of the Dry Hill Gneiss. During eruptions when there was much less separation of crystals and glass, the combination of crystals and liquid in the primary magma was erupted to produce the more normal biotite gneiss layers.

Ce is enriched in the leucogneiss, so allanite was probably deposited in the crystal accumulations. Y and Zr are also higher in the "F" layers, so small amounts of hornblende and zircon, respectively, are reasonable. Primary hornblende and/or Ca pyroxene is also suggested by the normative diopside in the leucogneiss layers as compared to normative corundum in the biotite gneiss layers. Sphene may have crystallized too, because it can contain trace amounts of Ce, Y, and Nb, all of which are enriched in the leucogneiss relative to the biotite gneiss.

The reason that the amount of SiO_2 in the biotite gneiss layers is the same as that in the leucogneiss layers is because the melt lay on the quartz-feldspar cotectic surface and was crystallizing quartz and K-rich feldspar in eutectic proportions (Figure 27). Melt, moving

away from the more potassic feldspar crystals, became enriched in Na2O, so the biotite gneiss layers have more sodium than the leucogneiss layers. A plot of normative orthoclase versus Ba (Figure 28) has parallel trends between the two "M" and "F" split samples, strongly suggesting that the high Ba in the two "F" samples is directly related to concentrations of magmatic orthoclase. The chemistry of each sample is different, but the process is the same. The scatter in the rest of the samples is probably due to varying mixes of crystals and glass and to variations in gross Dry Hill magmatic chemistry through the full eruptive history.

Granitic Gneiss within the Poplar Mountain Quartzite

The silica values of the granitic gneiss within the Poplar Mountain Quartzite vary between 75.2 and 77.3 weight percent (Table 13). They fit within the range of the Dry Hill Gneiss. The trends of the major element chemistry of the granitic gneiss are parallel to and plot within the trends of the Dry Hill (Figure 15).

The granitic gneiss has a similar trend on an AFM diagram (Figure 18) and plots within the Dry Hill Gneiss field on a peraluminous/metaluminous diagram (Figure 19). One way of distinguishing the granite gneiss from the Dry Hill Gneiss is that the former has less Rb than all except three samples of the latter. All other trace element abundances are similar to those of the Dry Hill Gneiss.

A PMREE plot of granite gneiss has a similar overall pattern to the Dry Hill Gneiss and fits within the envelope of the Dry Hill Gneiss, which implies that the two had a similar origin (Figure 29). For the above reasons, the granitic gneiss can be considered to have a nearly identical chemistry to the Dry Hill Gneiss. One sample of granitic gneiss, 21+60, has less Ti than the Dry Hill Gneiss samples and the rest of the granitic gneiss samples. It has less Ce, Zr, Sr, and V, but more Y than the other granitic gneiss analyses. The small variations in chemistry can be explained by differing accumulations of crystals and glass in the protolith of the unit. Probably 21+60 was less crystal-rich than the other two samples.

The granitic gneiss is interpreted to be metamorphosed tuffs produced during a reactivation of the same magma chamber that produced protoliths of the Dry Hill Gneiss after a period of volcanic quiescence and sedimentary deposition represented by the quartzite layers.

Felsic Gneiss within Poplar Mountain Gneiss

The SiO2 values of the felsic gneiss within the Poplar Mountain Gneiss range from 71.0 to 78.3 weight percent (Table 13). Two samples, TR 28+44 and TR 29+99, are anomalously high in silica and may contain a component of quartz sand. The trends of major element chemistry vs. SiO2 are parallel to those of the Dry Hill Gneiss for most elements

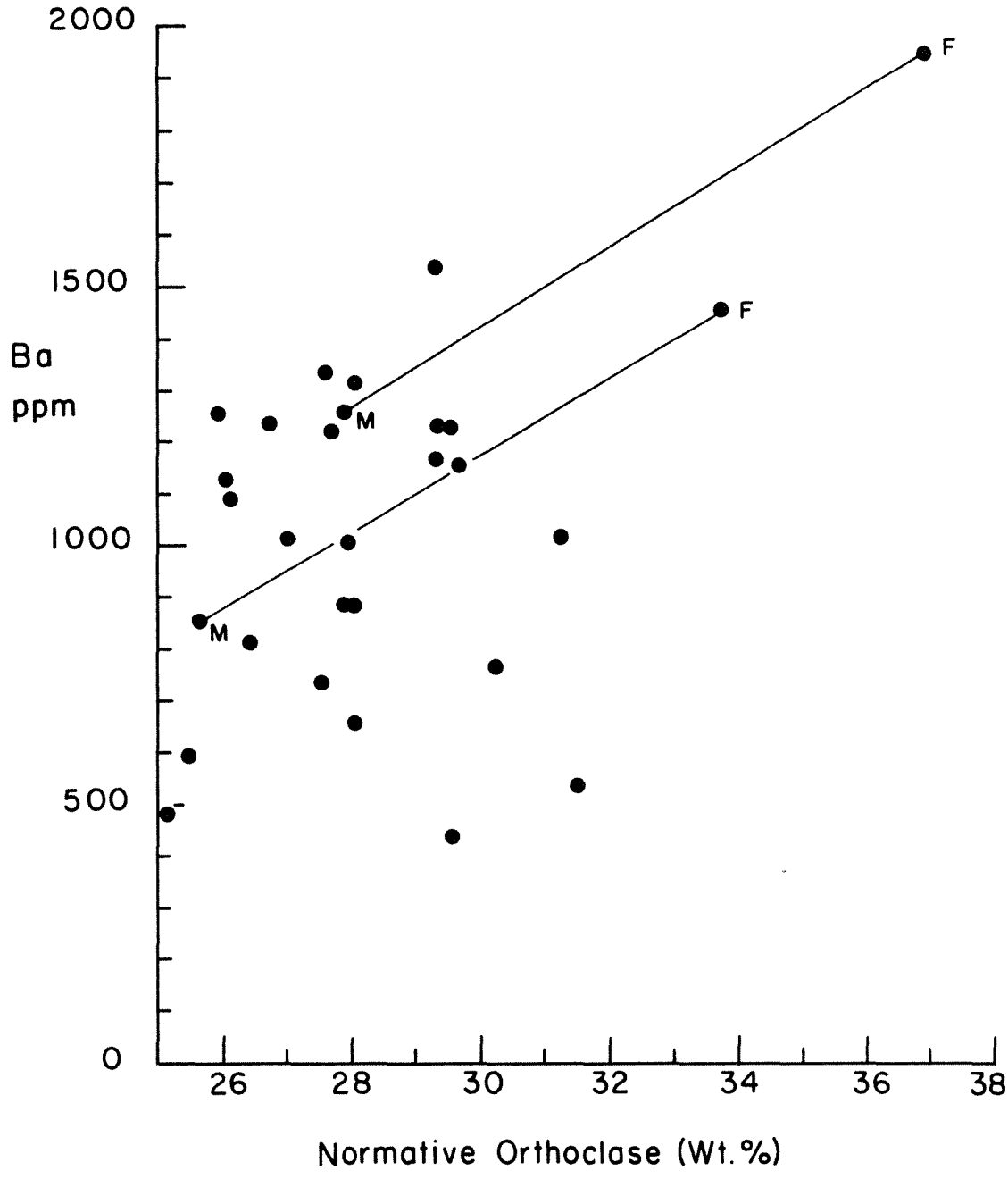

Figure 28. Plot of Ba vs. normative orthoclase.

Table 13. X-Ray Fluorescence Analyses and CIPW Norms of three samples of granite gneiss within Poplar Mountain Quartzite and five samples of felsic gneiss within Poplar Mountain Gneiss. Sr was determined using the molybdenum X-ray tube. n.d. is not detected.

	-----Granite Gneiss----			----------Felsic Gneiss----------				
	20+00	20+23	21+60	TR28+44	TR28+66	TR29+47	TR29+64	TR29+99
SiO2	75.3	75.2	77.3	78.2	74.6	73.7	71.0	78.3
TiO2	0.28	0.25	0.08	0.33	0.35	0.51	0.43	0.37
Al2O3	12.9	12.9	12.2	10.2	12.8	11.6	13.5	10.1
FeO	1.9	1.7	1.2	2.1	1.9	2.8	2.7	2.5
Fe2O3	0.2	0.2	0.1	0.3	0.5	0.1	0.3	0.1
MnO	0.04	0.06	0.05	0.05	0.06	0.07	0.09	0.08
MgO	0.21	0.21	n.d.	1.1	0.5	2.1	1.0	1.4
CaO	1.55	1.41	0.67	1.59	1.70	2.82	2.50	1.66
Na2O	3.1	2.9	3.2	2.08	3.05	2.41	3.01	2.46
K2O	4.3	4.8	4.9	3.09	3.94	3.40	4.81	3.14
P2O5	0.07	0.07	0.02	0.07	0.09	0.13	0.13	0.09
TOTAL	99.85	99.70	99.72	99.11	99.49	99.64	99.47	100.20
Rb	111	117	127	124	130	137	135	121
Pb	15	18	17	15	17	17	22	11
Sr	169	167	44	147	152	156	160	104
Ba	1261	1203	319	907	844	700	809	564
Ce	115	127	75	76	85	62	102	61
Y	22	24	33	20	25	18	55	25
Nb	16	12	15	17	16	17	30	21
Zr	197	200	110	208	193	176	207	164
Th	12	13	11	7	9	7	14	7
Ga	14	14	13	13	15	14	16	13
Zn	48	36	40	42	47	55	47	52
V	16	14	0	26	23	33	30	28
K/Rb	328	340	321	207	252	206	296	215
Rb/Sr	0.65	0.69	2.82	0.85	0.84	0.87	0.84	1.16
Ba/Sr	7.39	7.15	7.11	6.21	5.49	4.43	5.06	5.38
				CIPW Norms				
Q	36.00	35.54	37.42	48.01	36.33	36.53	27.27	44.94
Or	25.65	28.37	29.02	18.26	23.28	20.09	28.41	18.56
Ab	25.98	24.54	27.25	17.60	25.81	20.39	25.47	20.82
An	7.28	6.58	3.21	7.48	7.90	10.71	9.23	7.33
C	0.50	0.48	0.44	0.67	0.64	0	0	0
Di								
En	0	0	0	0	0	0.55	0.38	0.07
Fs	0	0	0	0	0	0.46	0.65	0.09
Wo	0	0	0	0	0	1.05	1.00	0.16
Hy								
En	0.52	0.52	0	2.64	1.34	4.55	1.99	3.31
Fs	2.96	2.74	2.07	3.20	2.72	3.82	3.43	3.87
Mt	0.28	0.23	0.16	0.36	0.65	0.19	0.46	0.17
Il	0.53	0.47	0.15	0.63	0.66	0.97	0.82	0.70
Ap	0.15	0.15	0.04	0.15	0.20	0.28	0.28	0.20
TOTAL	99.86	99.64	99.76	99.00	99.55	99.61	99.40	100.21

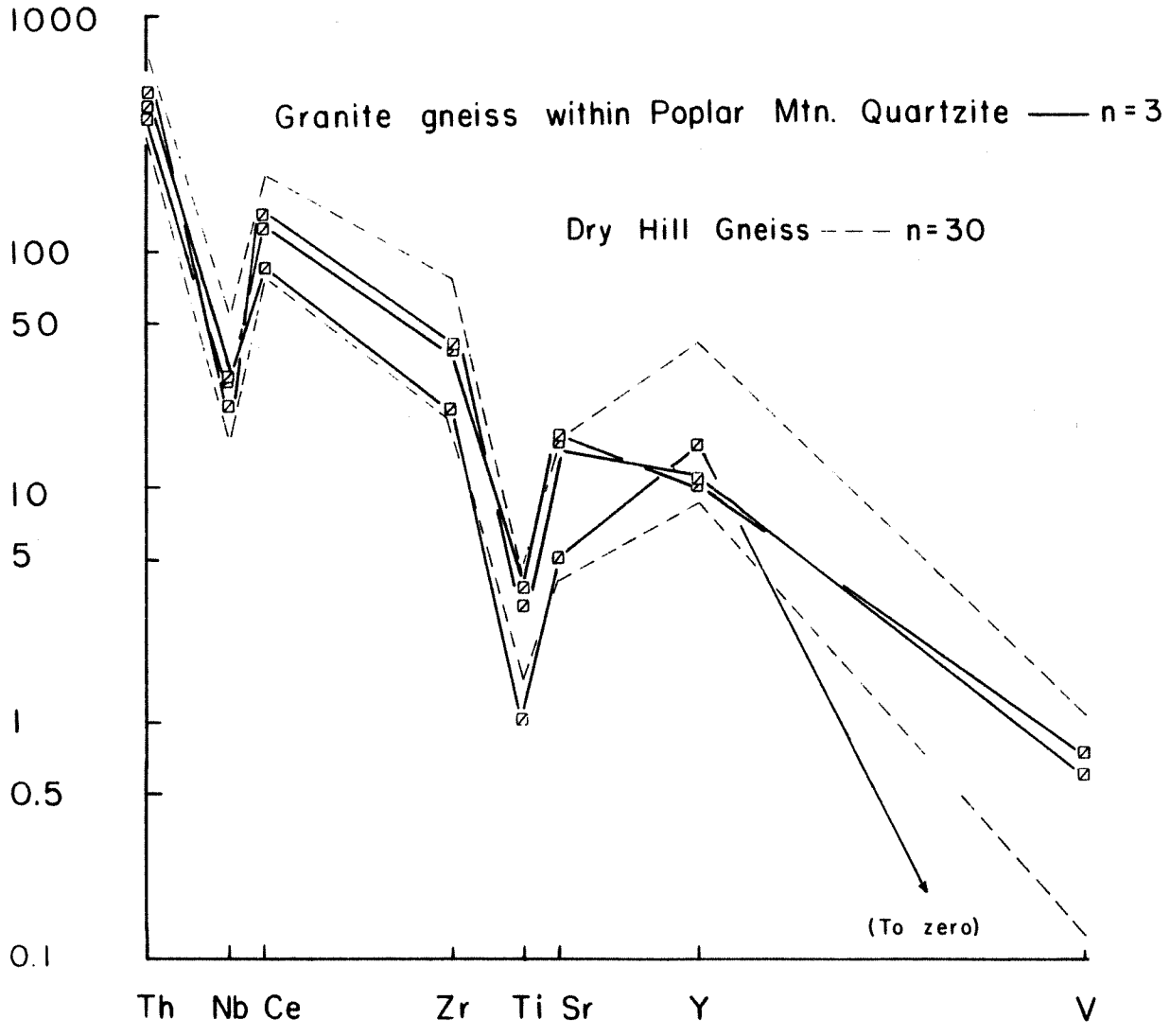

Figure 29. PMREE diagram of granite gneiss within the Poplar Mountain Quartzite (heavy lines) plotted against the Dry Hill Gneiss (dashed lines).

(Figure 15). K2O and Al2O3 values are slightly reduced for the felsic gneiss and MgO values are higher, possibly due to dolomite contamination. Three samples have higher CaO than the Dry Hill Gneiss.

The norms of the felsic gneiss plot within the granitic field on a modified Streckeisen diagram although they define a trend towards quartz (Figure 16). Most plot near the loose cluster of Poplar Mountain Gneiss samples. The felsic gneiss samples plot in the calc-alkaline field of Figure 17, near the three anomalous samples of Dry Hill Gneiss. The felsic gneiss has more MgO so it has a lower FeO/(FeO + MgO) ratio than the bulk of the Dry Hill. On a standard AFM diagram the felsic gneiss has a calc-alkaline trend, also (Figure 18).

The felsic gneiss has roughly the same amount of Zr for a varying amount of SiO2 on Figure 21. Simple fractionation cannot explain it because the trend is at right angles to normal fractionation trends. On a diagram of K2O vs. Rb (Figure 20), the felsic gneiss contains less K2O than the Dry Hill Gneiss, for a similar amount of Rb. If the felsic gneiss protolith was a later reactivation from the Dry Hill Gneiss magma chamber, it may be tapping, a lower, more primitive layer. Perhaps the orthoclase crystals rose to the upper level of the magma chamber and were erupted to form the protolith of the Dry Hill Gneiss, and subsequent eruptions drew upon a layer depleted in orthoclase.

A PMREE plot of the felsic gneiss has a similar trend to the Dry Hill Gneiss although it appears to be lower in elements which would preferentially go into crystals, except for those which would go into magnetite (Figure 30). Perhaps the protolith formed from a more mafic zone in the magma chamber. Titanium and vanadium are slightly higher in the felsic gneiss. Based on that diagram, a similar origin to the granite gneiss within the Quartzite Member is not unreasonable.

Poplar Mountain Gneiss

The SiO2 values of the Poplar Mountain Gneiss range from 66.8 to 78.9 weight percent (Table 14). The formation is characterized by erratic and variable chemistry, especially with respect to MgO, Al2O3 and CaO (Figure 15).

Ashenden (1973) theorized that the protolith of the Poplar Mountain Gneiss was a sedimentary rock and the present study does not conflict with that interpretation. Relative to Dry Hill Gneiss, the Poplar Mountain Gneiss has more FeOT, MgO, and CaO, but less Na2O and K2O (Figure 15). Perhaps the Poplar Mountain Gneiss was derived by sedimentary processes from a protolith similar to the Dry Hill Gneiss, but from a more calcic magma. The increase in CaO and MgO could be obtained by some dolomite addition to the protolith. Some samples of Poplar Mountain Gneiss are enriched in modal and normative quartz relative to Dry Hill Gneiss, which could be a result of weathering processes, since quartz is resistant to weathering. The formation is

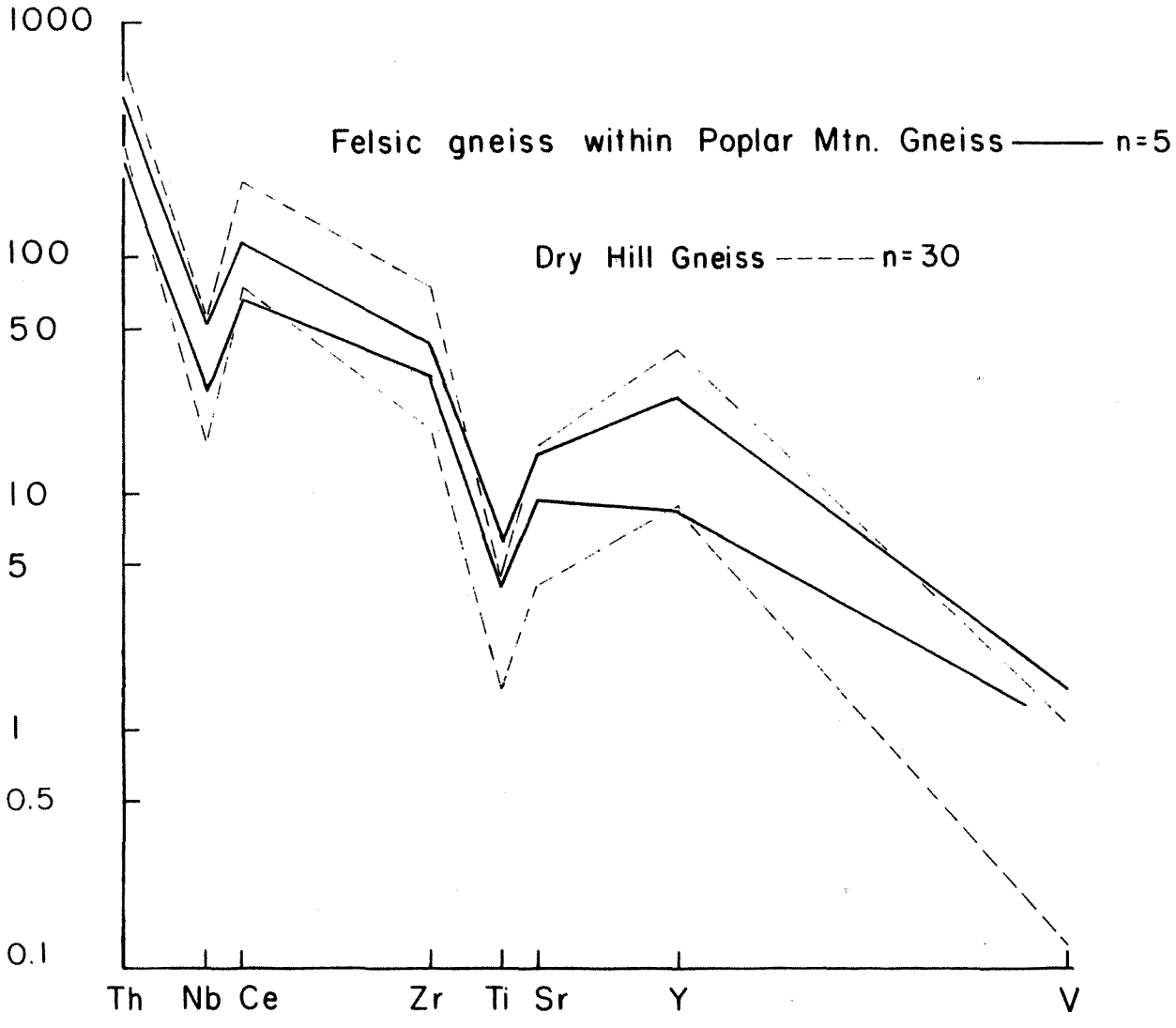

Figure 30. PMREE diagram of the felsic gneiss within the Poplar Mountain Gneiss (solid line) against the Dry Hill Gneiss (dashed lines).

Table 14. X-ray Fluorescence Analyses and CIPW Norms of Poplar Mountain Gneiss. Sr was determined using the molybdenum X-ray tube.

	TR21+07	TR25+86	TR26+01	TR26+40	TR26+60	TR26+95	TR27+92	TR30+18
SiO2	69.7	70.4	73.8	68.5	66.8	78.9	75.7	70.0
TiO2	0.51	0.44	0.23	0.35	0.69	0.42	0.44	0.64
Al2O3	12.9	14.3	14.0	15.0	15.5	9.5	10.1	12.8
FeO	7.1	4.0	2.1	3.9	4.8	2.6	2.7	4.4
Fe2O3	0.1	0.2	0.1	0.2	0.1	0.1	0.1	0.1
MnO	0.34	0.11	0.05	0.11	0.12	0.06	0.06	0.13
MgO	1.8	1.7	0.5	2.2	2.6	1.3	3.1	2.8
CaO	5.3	2.3	2.4	3.7	3.4	2.4	2.9	2.9
Na2O	1.3	2.5	3.3	3.2	3.1	2.0	1.8	2.5
K2O	1.4	3.4	3.1	2.4	2.9	2.4	2.6	3.0
P2O5	0.16	0.11	0.06	0.08	0.14	0.10	0.10	0.15
TOTAL	100.61	99.46	99.64	99.64	100.15	99.78	99.60	99.42
Rb	48	135	101	122	126	84	102	156
Pb	10	27	29	21	22	12	10	14
Sr	102	143	131	157	198	139	149	154
Ba	266	415	652	250	504	460	631	494
Ce	20	57	62	40	55	50	59	81
Y	33	20	20	20	21	22	19	28
Nb	3	16	13	14	14	16	16	26
Zr	90	112	89	65	153	197	200	168
Th	2	8	14	5	7	6	7	11
Ga	15	19	14	17	18	12	13	18
Zn	129	82	39	68	82	39	54	74
V	35	87	33	89	104	37	39	66
K/Rb	248	207	256	166	189	238	215	158
Rb/Sr	0.46	0.95	0.76	0.77	0.63	0.60	0.68	1.01
Ba/Sr	2.59	2.90	4.93	1.58	2.52	3.27	4.19	3.20
CIPW Norms								
Q	37.33	32.69	35.11	26.66	23.59	49.51	42.89	30.83
Or	8.45	19.92	18.44	14.42	16.96	14.24	15.66	17.49
Ab	11.00	21.16	28.66	26.91	26.06	17.09	15.49	21.16
An	25.17	10.66	11.36	18.03	16.09	9.79	11.60	13.26
C	0	2.65	1.00	0.56	1.41	0	0	0.67
Di								
En	0.03	0	0	0	0	0.31	0.52	0
Fs	0.08	0	0	0	0	0.39	0.29	0
Wo	0.10	0	0	0	0	0.70	0.86	0
Hy								
En	4.36	4.28	1.27	5.35	6.43	2.93	7.13	6.92
Fs	12.57	6.72	3.57	6.67	7.75	3.70	4.00	7.27
Mt	0.16	0.32	0.13	0.25	0.20	0.19	0.16	0.09
Il	0.97	0.84	0.44	0.66	1.31	0.80	0.84	1.22
Ap	0.35	0.24	0.13	0.17	0.31	0.22	0.22	0.33
TOTAL	100.55	99.47	99.70	99.69	100.11	99.86	99.64	99.22

plotted on several igneous diagrams (AFM, Streckeisen) for contrast with the igneous rocks of the Dry Hill Gneiss, and the felsic gneiss and granitic gneiss of more uncertain origin within the formation itself. The Poplar Mountain does not form any coherent trends on most diagrams.

A PMREE plot of Poplar Mountain Gneiss has more variety within the formation than the other rocks studied, in keeping with its probable sedimentary origin (Figure 31). The formation may be derived from the Dry Hill Gneiss because it has a similar slope, but it has much more titanium and vanadium than the Dry Hill Gneiss. It has slightly less thorium and cerium.

Both Ashenden (1973) and Robinson (1979) suggest that the Poplar Mountain Gneiss was derived by sedimentary process partly from the Dry Hill Gneiss. Perhaps it was derived from tuffs from the Dry Hill magma chamber, but the eruptions tapped a deeper, more primitive source.

Fourmile Gneiss

The SiO2 values of the Fourmile Gneiss range from 69.0 to 71.5 weight percent (Table 15). On a Harker diagram the four samples show a decrease in Al2O3, CaO, and TiO2 and an increase in K2O with increasing silica(Figure 15). There are no discernable trends for other elements.

The norms of the Fourmile Gneiss plot in a granodiorite (dacite) field of a modified Streckeisen diagram (Figure 16). The Fourmile Gneiss is subalkalic and plots in the calc-alkaline field of a calc-alkaline-tholeiite diagram (Figure 17). All samples plot in the calc-alkaline portion of an AFM diagram (Figure 18).

A PMREE plot of Fourmile Gneiss has a moderate amount LREE enrichment, and a slight negative Nb and Ti anomalies (Figure 32). The slight amount of Sr enrichment relative to the other PMREEs probably indicates some plagioclase accumulation. The pattern is a normal one for an andesite, although Th is somewhat high. The slope is not so steep as a typical trend for an ordinary granitic rock.

Fourmile Gneiss samples fit in the I-type classification of Chappell and White (1974), and plot on the I-side of an I/S diagram (White, et al., 1977). Although the classification scheme is not definitive, an origin from a melt derived from an igneous source is indicated. More on the origin of the Fourmile Gneiss will be discussed below.

Belchertown Tonalite

The Belchertown tonalite is only worthy of brief mention, because only two samples were collected after its serendipitous discovery in the Northfield Tunnel area (Table 15). A more detailed study of the

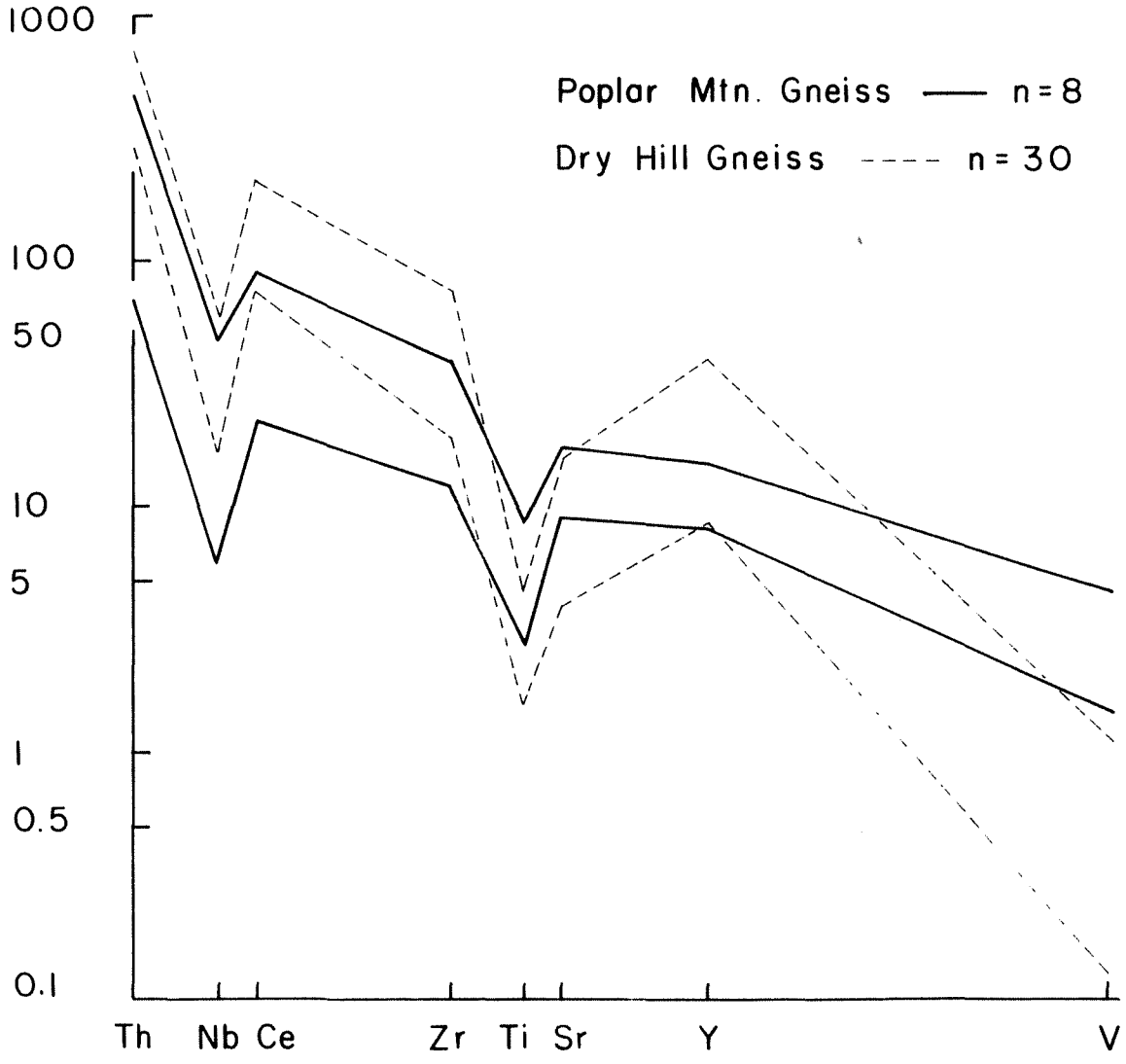

Figure 31. PMREE diagram of the Poplar Mountain Gneiss (heavy line) plotted against the Dry Hill Gneiss (dashed line).

Table 15. X-ray Fluorescence Analyses and CIPW Norms of Fourmile Gneiss and Belchertown Tonalite. Sr was determined using the molybdenum X-ray tube.

	Fourmile Gneiss				Belchertown	
	TR17+00	TR17+90	TR18+34	TR18+48	N164	TR25+06
SiO2	69.7	71.5	69.7	69.0	61.9	59.6
TiO2	0.29	0.23	0.28	0.36	0.62	0.77
Al2O3	15.7	15.1	15.3	16.2	15.5	15.2
FeO	2.7	1.7	2.8	2.4	3.8	4.2
Fe2O3	0.7	1.0	0.6	0.8	1.0	1.4
MnO	0.12	0.07	0.07	0.06	0.08	0.10
MgO	1.20	0.75	1.18	0.91	4.4	5.1
CaO	3.84	3.16	3.75	4.18	5.21	6.16
Na2O	3.30	3.36	3.27	4.01	3.8	3.3
K2O	2.44	2.98	2.51	1.92	2.5	3.0
P2O5	0.11	0.08	0.09	0.11	0.25	0.49
Total	100.10	99.93	99.55	99.95	99.06	99.32
Rb	111	94	90	61	72	78
Pb	30	29	18	13	32	38
Sr	306	271	274	336	951	1461
Ba	1146	1158	1173	1168	1242	2340
Ce	47	43	45	22	122	84
Y	14	13	13	9	14	20
Nb	9	8	8	6	6	6
Zr	102	118	108	166	115	144
Th	15	14	15	4	17	18
Ga	15	13	14	14	17	18
Zn	54	30	28	31	69	77
Ni	2	5	6	5	87	87
Cr	6	4	5	5	196	212
V	56	44	62	41	109	128
K/Rb	183	232	264	262	293	316
Rb/Sr	0.36	0.34	0.33	0.18	0.08	0.53
Ba/Sr	3.71	4.24	4.25	3.46	1.30	14.61
			CIPW Norms			
Q	29.55	31.96	29.52	26.74	11.91	9.27
Or	14.42	17.61	14.83	11.35	15.01	17.55
Ab	27.92	28.43	27.67	33.93	32.33	27.67
An	18.40	15.21	18.08	20.09	17.51	18.03
C	0.84	0.75	0.60	0.13	0	0
Di						
En	0	0	0	0	1.82	2.61
Fs	0	0	0	0	0.86	1.14
Wo	0	0	0	0	2.87	4.03
Hy						
En	2.99	1.87	2.94	2.27	9.21	9.99
Fs	4.20	2.08	4.24	3.35	4.35	4.36
Mt	1.01	1.39	0.88	1.15	1.46	1.97
Il	0.55	0.44	0.53	0.68	1.18	1.46
Ap	0.24	0.17	0.20	0.24	0.55	1.07
Total	100.12	99.91	99.57	99.92	99.06	99.16

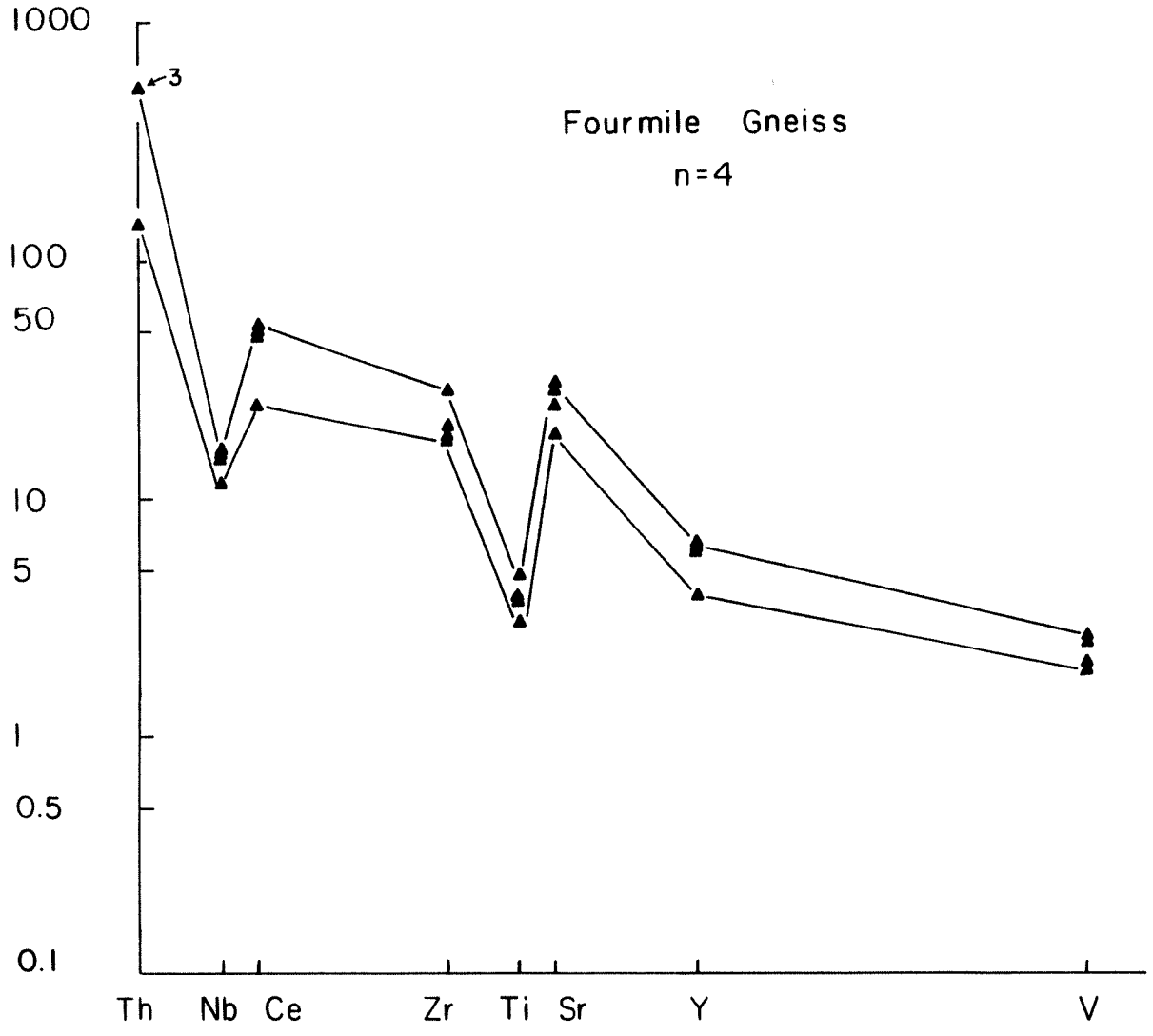

Figure 32. PMREE diagram of Fourmile Gneiss.

Belchertown Complex, south of the Pelham dome, can be found in Ashwal, et al., 1979.

The identification of the tunnel sill as Belchertown tonalite is based on three types of evidence. First, as mentioned above, the age of the sill is 370 my (G. W. Leo and R. E. Zartman, unpublished), which is close to the published age date of the Belchertown pluton of 380 ± 5 my (Ashwal, et al., 1979). Second, careful examination of thin sections of the sill rock compared to thin sections from the northern part of the Belchertown pluton prepared by Guthrie (1972) reveal strong similarities. Third, the two groups of rocks are chemically similar, although only major element analyses are available for the main pluton for comparison (Ashwal, et al., 1979).

The norms of the two samples plot in the field of quartz monzodiorite on a modified Streckeisen diagram, very close to samples from the study of Ashwal et al., 1979 (Figure 16). The modes of the samples of this study plot as tonalites and the difference between the modes and the norms may be due to modal biotite being calculated to normative orthoclase.

On a Harker diagram (not shown), one of the sill samples plots amidst the pluton samples, and one plots on the projections of the curves. With increasing silica, MgO, CaO, and P2O5 decrease in a linear manner. All other major elements remain approximately constant.

All Belchertown samples are subalkalic and calc-alkaline. The sill samples may be slightly more evolved, since the ratio of total Fe/Mg is 1.07 for the sill samples compared to 0.77 to 0.98 to the samples of Ashwal et al., 1979).

The PMREE of the Belchertown tonalite have a strong positive strontium anomaly, which may be the result of plagioclase feldspar enrichment (Figure 33). Niobium and titanium are slightly depleted, perhaps due to ilmenite fractionation. The formation is somewhat LREE enriched.

Robinson and Hall (1980) postulate a westward dipping subduction zone of Devonian age during the Acadian Orogeny. The Belchertown pluton cuts across early Devonian folds, but its metamorphism was completed by Middle Devonian about 361 ± 6 my (Ashwal, et al, 1979). It is likely that the Belchertown Quartz Monzodiorite formed by partial melting of subducted crustal rocks during the Acadian Orogeny.

STRATIGRAPHIC AND CHEMICAL COMPARISONS IN REGIONAL GEOLOGY

Introduction

The rocks of the Selden Neck and Lyme domes of southeastern Connecticut (Figure 1 on page 3) bear a stratigraphic and a lithic

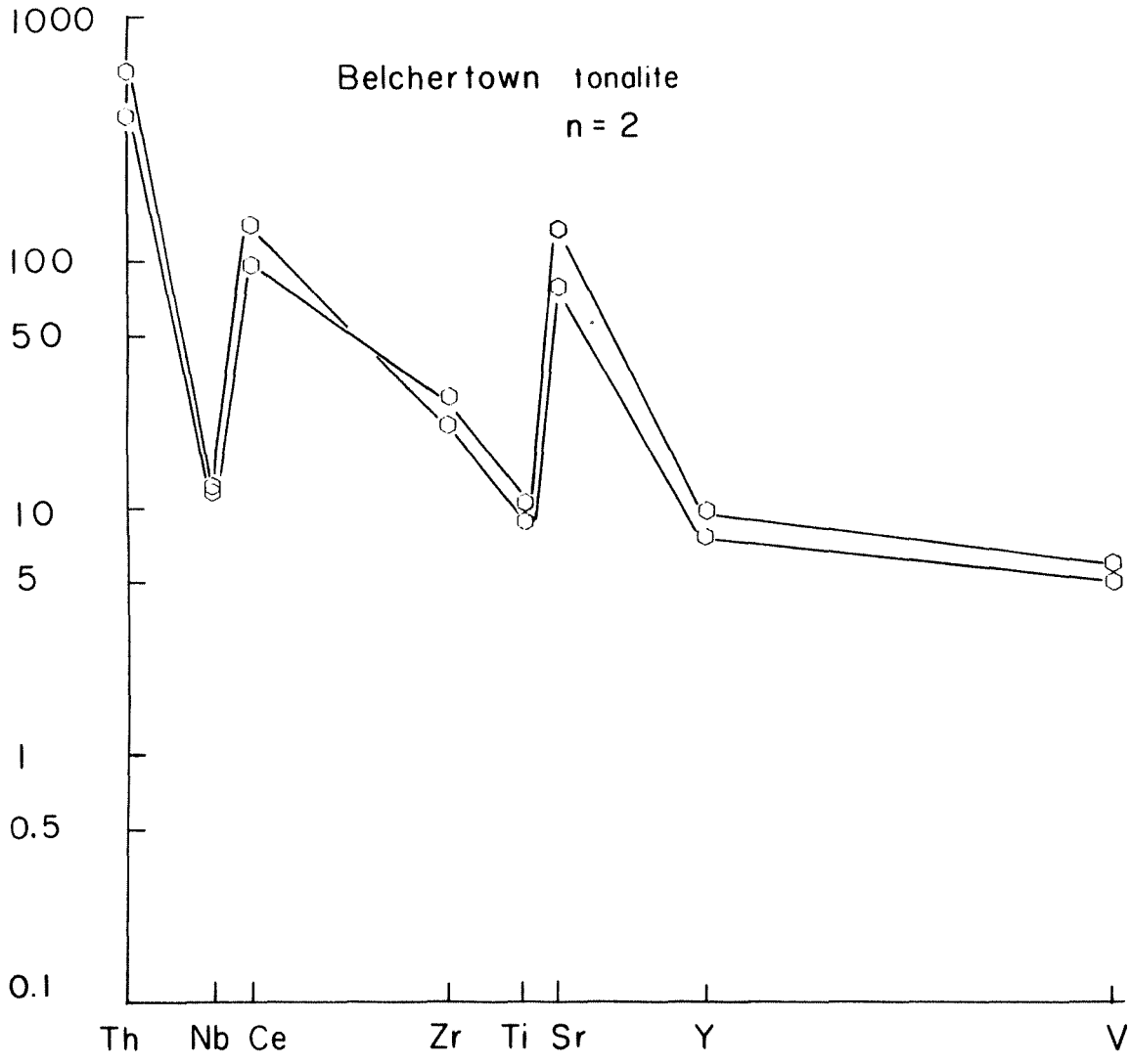

Figure 33. PMREE diagram of a tonalite sill correlated on lithic grounds with the Belchertown Complex.

resemblance to rocks of the Pelham dome (Hall and Robinson, 1982). Mapped by Lundgren (1963, 1964, 1966, 1967) and Goldsmith (1967a, b, c), the cores of the Connecticut domes contain the Sterling Plutonic Suite, a series of pink, granitic gneisses of late Proterozoic age. The Hope Valley Alaskite Gneiss of the Sterling Suite has an U-Th-Pb radiometric age on zircon of 601 ± 5 my (Hermes and Zartman, 1985). Ashenden (1973) suggested that the rocks of the Sterling Suite may correlate with the Dry Hill Gneiss. Discontinuous quartzites, calc-silicate bearing quartzites, schists and gneisses of the Precambrian Plainfield Formation outcrop in the central parts of the domes. Lundgren interprets the Sterling Plutonic Suite to be intrusive into the older Plainfield, so that the Plainfield forms discontinuous beds floating in the granite gneiss. However, some of the contacts between the two are concordant or semi-concordant and the Plainfield in the Selden Neck and Lyme domes may have a similar stratigraphic position and derivation to the Poplar Mountain Gneiss and Quartzite in the Pelham dome of Massachusetts.

Stratigraphically above the Plainfield is the Waterford Group, consisting of the Mamacoke Formation, the Joshua Rock Member of the New London Gneiss, the New London Gneiss, and the Rope Ferry Gneiss. The Mamacoke Formation, possibly of sedimentary origin, locally lies directly on the rocks of the Sterling Plutonic Suite and may represent an unconformity(Lundgren, 1966). The New London Gneiss consists of granodioritic gneisses and is of especial interest because it may correlate with the Fourmile Gneiss (Ashenden, 1973).

A correlation between the Monson Gneiss of Emerson (1898), and the Fourmile Gneiss has been suggested by several workers (c.f. Ashenden, 1973, Hall and Robinson, 1982). Several analyses of Monson, collected in the main body of the Monson Gneiss in south-central Massachusetts and north-central Connecticut, have been published by Leo, et al. (1984). Leo M. Hall, on the basis of unpublished work in the Shelburne Falls dome, suggests that the core rocks of that dome may be correlative with Fourmile Gneiss (Hall and Robinson, 1982). He has provided unpublished major element analyses and instrumental neutron activation analyses for three samples collected in the core of the dome. Unpublished Rb/Sr age dating by Douglas Mose establishes an isochron of 503 ± 26 million years for samples collected by Hall in the Shelburne Falls dome.

Recent geochemical work in the Killingworth dome by Webster and Wintsch (1984) suggests a correlation between rocks of the central part of the dome and Monson Gneiss and between rocks of the southern part of the dome and gneisses of the Waterford Group.

Recently, Richard Goldsmith made available unpublished major element analyses of the Hope Valley Alaskite and the Potter Hill Granite Gneiss, both of the Sterling Plutonic Suite; analyses of the lower and middle members of the Plainfield formation; and analyses of

all members of the Waterford Group. The samples were collected in the Selden Neck and Lyme domes in the Niantic, Uncasville, Montville, Ashway and New London quadrangles of Connecticut. Samples were analysed by a single-solution wet-chemical procedure.

The Stony Creek dome of Connecticut has a core of pink granitic gneiss which is similar in appearance to the Dry Hill Gneiss. Quartzites of the Plainfield Formation and gneiss of the Mamacoke Formation are crosscut by the Stony Creek Granite. Hills and Dasch (1972) describe the quartzites as xenoliths surrounded by Stony Creek Granite. Based on evidence of Rb mobility, they suggest a remobilization of granitic or rhyolitic rocks crystallized during the Precambrian Avalonian Orogeny. Their date on the core rocks is 616 $\pm$ 78 million years ago by Rb/Sr isotope dilution analyses. The age date is comparable to that of the Dry Hill Gneiss but unfortunately no published chemical data exists for the Stony Creek dome.

Eileen L. McLellan of the University of Maryland has recently undertaken a project of detailed mapping of the Stony Creek dome to characterize the dome rocks and to attempt to correlate them to other southern Connecticut domes, especially the Lyme dome (McLellan, 1984). The dome is composed of the lower, middle and upper members of the late Precambrian Plainfield Formation, and the Cambrian(?) Mamacoke Formation. It has a core of the older Stony Creek Granite I and the younger Stony Creek Granite II. McLellan has characterized both granites as intrusive. Stony Creek Granite I is about 600 million years old, although the age date needs to be refined. Both granites are sheared and the dominant mineral lineation dips radially outward from the core of the dome. McLellan attributes this to diapiric rise, not to cross folding. McLellan plans to do some geochemistry to compare the Stony Creek Granite to other members of the Sterling Plutonic Suite in southern Connecticut.

The Dry Hill Gneiss resembles the pink, granitic Yonkers Gneiss of southeastern New York. The Yonkers is 560 $\pm$ 30 million years old, which is nearly the same age as the Dry Hill Gneiss, so it is suitable to compare the two in an effort to understand whether the core rocks of the Pelham dome are correlative with the Yonkers Gneiss.

In 1978, Leo Hall and Madeline Goldstein collected samples of the Yonkers Gneiss to study major and trace element chemistry of the formation. They sampled a rock quarry in Yonkers, New York, in the Mount Vernon quadrangle, attempting to collect as wide a variety of textures as possible (Leo M. Hall, personal communication, 1983). The quarry is essentially the type locality of the formation. They collected other samples of Yonkers to the northeast in the White Plains and the Glenville quadrangles along strike from the type locality.

Goldstein prepared the samples in a similar manner to this study, and analysed them for major element chemistry and Y, Sr, Rb, Nb, Pb,

and Th by X-ray fluorescence spectroscopy on the X-ray fluorescence analyser at the University of Massachusetts (Goldstein, unpublished master's project).

Comparisons of Major Element Chemistry: Dry Hill Gneiss and Other Granitoid Gneisses

The Dry Hill Gneiss, the Hope Valley Alaskite Gneiss, the Potter Hill Granite Gneiss, and the Yonkers Gneiss all plot normatively in the granite field of a modified Streckeisen diagram in a remarkably tight cluster (Figure 34). Their chemistries overlap to a great extent, but there are some dissimilarities discussed below.

A plot of alkalies and calcium oxide versus SiO2 illustrates some differences in chemistry between the formations (Figure 35). The Potter Hill Gneiss has less silica and more CaO than the other formations, although it overlaps the field of Dry Hill Gneiss slightly. All the formations have similar amounts of K2O and Na2O, but both Hope Valley Gneiss and Yonkers Gneiss have very little CaO and less normative anorthite than the other two gneisses. All are high in K2O and K2O/Na2O and have low weight percent CaO, which points toward an anorogenic origin (Loiselle and Wones, 1979).

A diagram based on Shand's alumina saturation diagram illustrates that all of the formations plot near the peraluminous/metaluminous boundary (Figure 36). In the previous chapter, a similar diagram shows the fields of the Wolf River Batholith and the Rapakivi Granite of Finland, and they both straddle the boundary. The Hope Valley Alaskite and the Potter Hill Granite Gneiss both plot entirely in the peraluminous field, but close to the dividing line. The Potter Hill has an anomalous trend that looks slightly calc-alkaline, but that, once again, could be the result of insufficient sampling. In the metaluminous field, the Yonkers Gneiss exhibits a decided trend toward peralkaline compositions.

The four gneisses were plotted on a anorthite-albite-orthoclase ternary diagram (Figure 37). Hope Valley and Yonkers Gneiss contain less normative anorthite than the Dry Hill Gneiss, which is a reflection of their smaller amounts of CaO. Hope Valley has the most normative albite. Potter Hill defines a trend of variable orthoclase content. The two split samples of Dry Hill Gneiss plot nearer to the orthoclase apex of the diagram, because they contain a large amount of orthoclase.

In common with most anorogenic granites, the four gneisses exhibit a strong MgO-depletion trend coupled with a marked FeO-enrichment trend (Figure 38). Figure 38 especially illustrates the trend because the Yonkers has weight percents of MgO below X-ray spectroscopic detection limits, which can be treated as zero. Most of the Dry Hill is extremely low in MgO, also. Potter Hill Gneiss is the most MgO-rich of

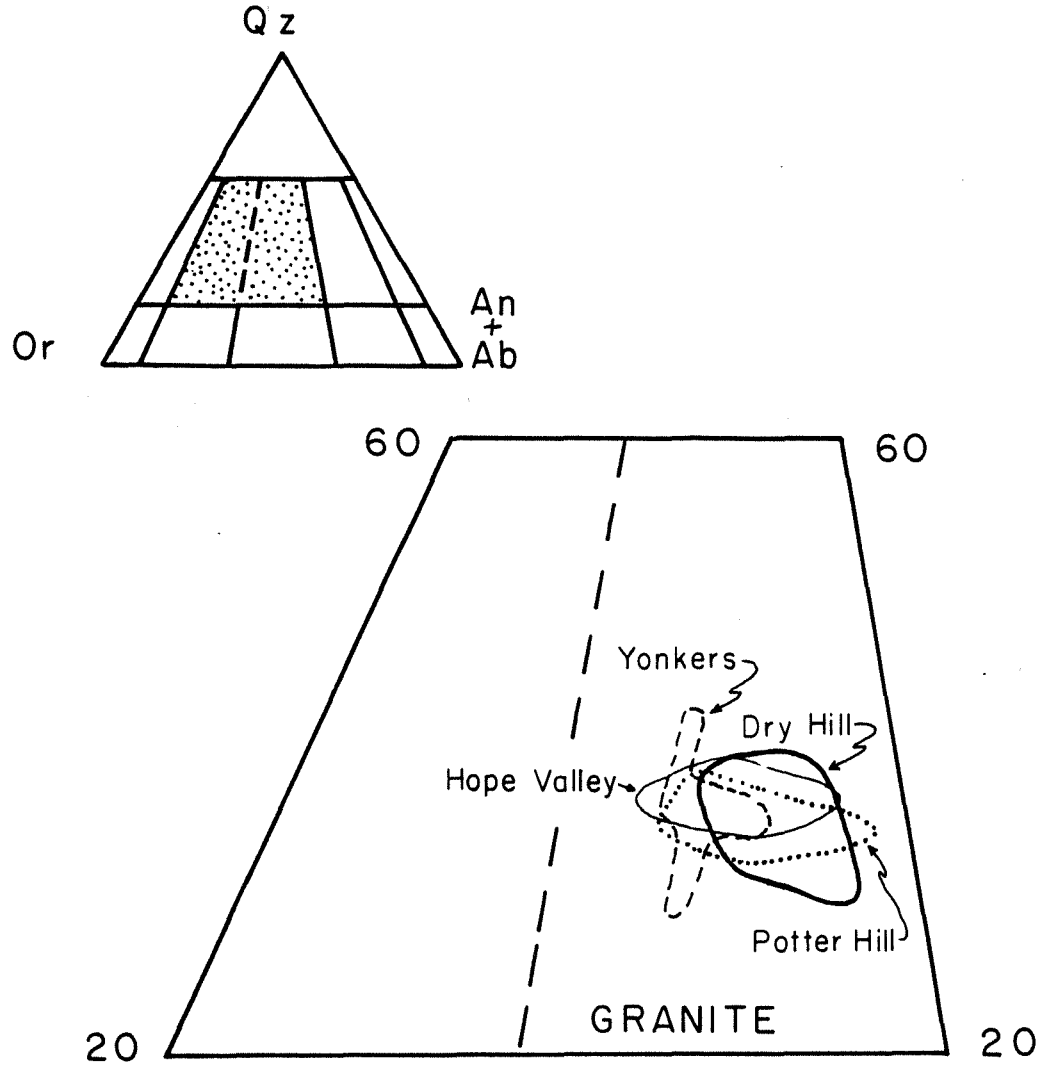

Figure 34. Clustering of norms of Dry Hill Gneiss, Yonkers Gneiss, Potter Hill Granite Gneiss and Hope Valley Alaskite Gneiss plotted on a modified Streckeisen diagram. Norms of quartz, orthoclase, anorthite, and albite were recalculated by density before plotting.

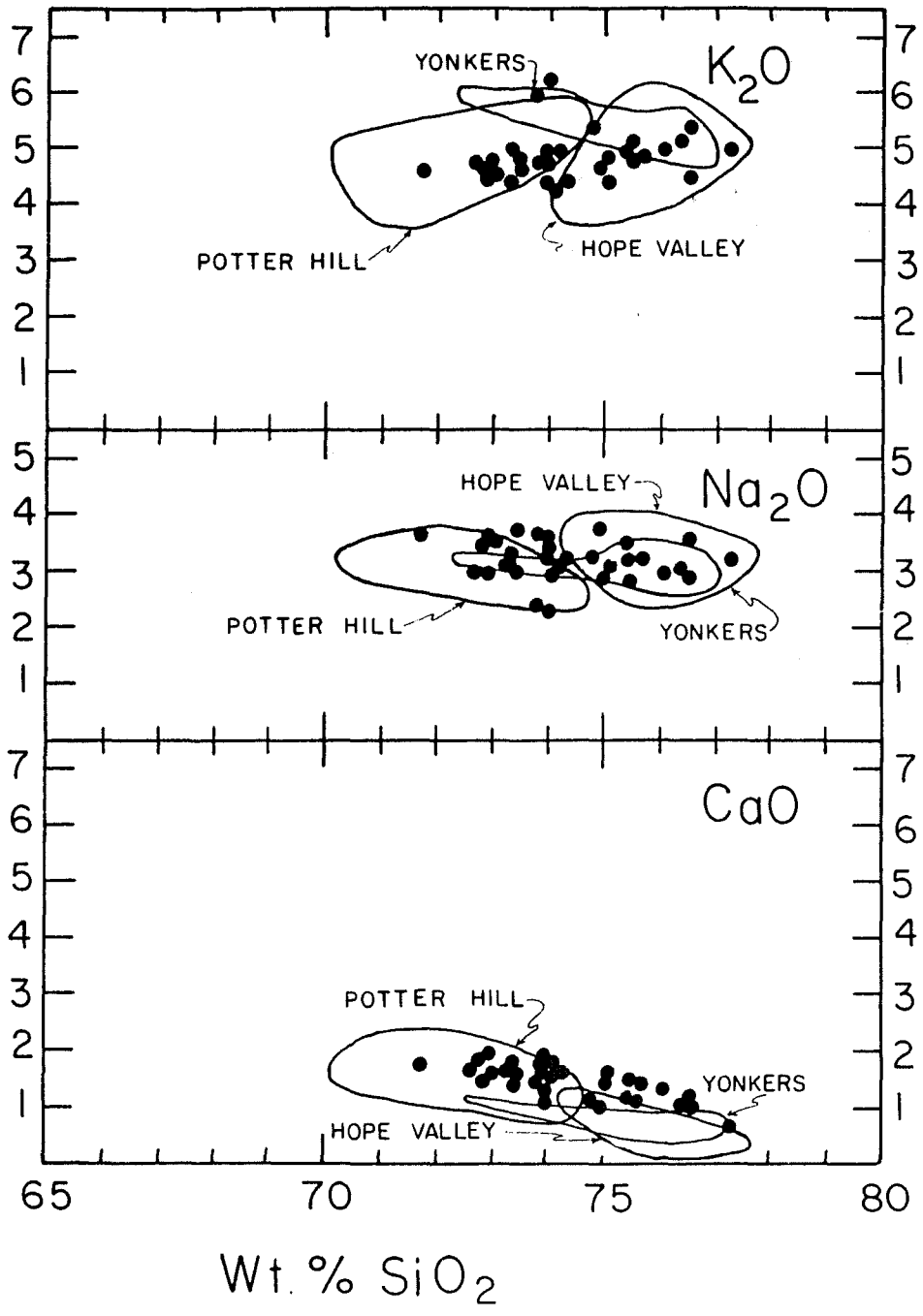

Figure 35. Harker diagram comparing Dry Hill Gneiss (solid circles) to Connecticut and New York gneisses.

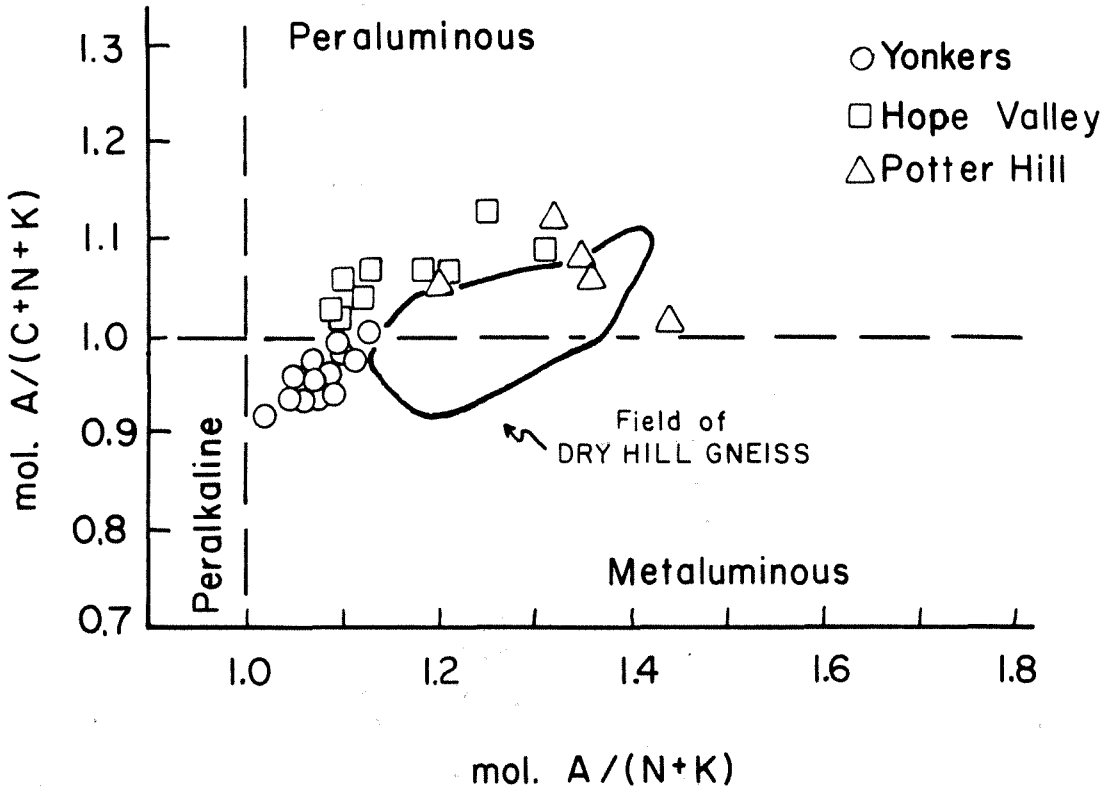

Figure 36. Peraluminous/metaluminous diagram adapted from Lidiak and Denison (1983), modified from Shand (1927). A/(C+N+K) is molecular Al2O3/(CaO+Na2O+K2O), and A/(N+K) is molecular Al2O3/(Na2O+K2O).

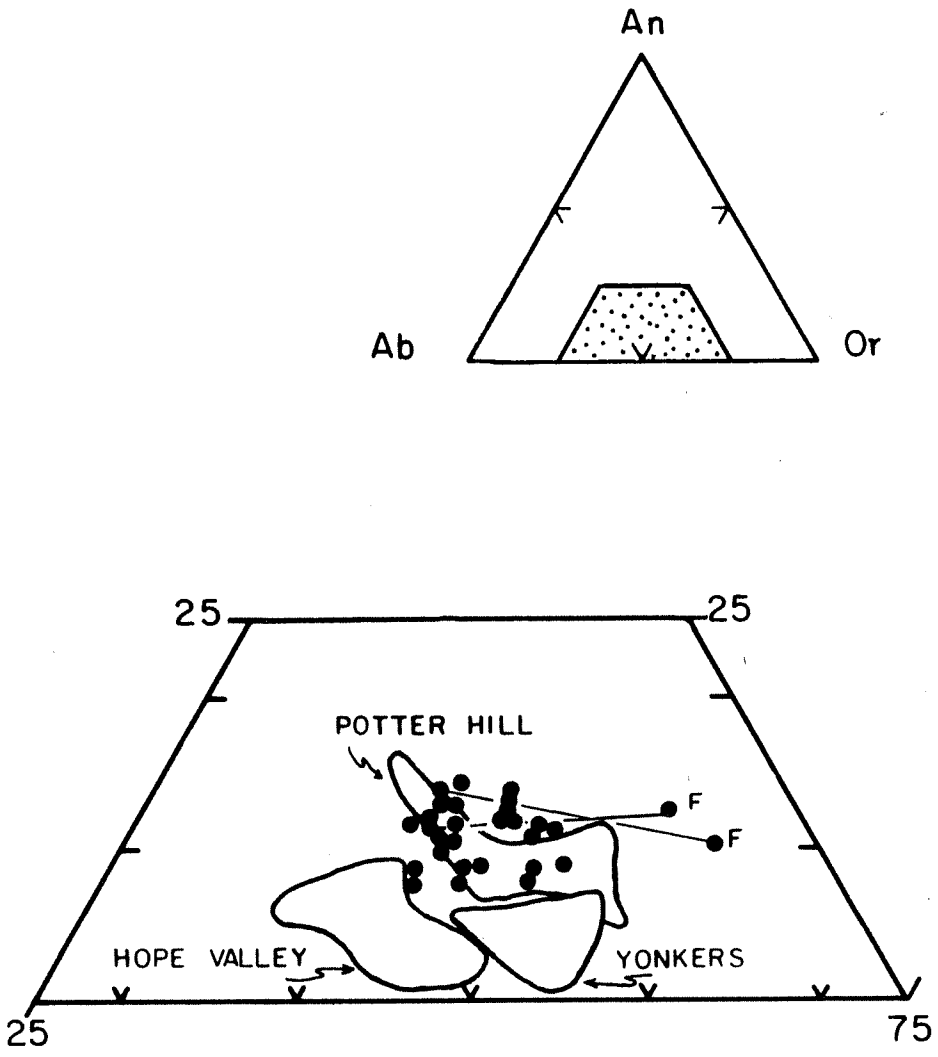

Figure 37. Plot of albite-anorthite-orthoclase for Dry Hill Gneiss (solid circles), Yonkers Gneiss, Hope Valley Alaskite Gneiss and Potter Hill Granite Gneiss.

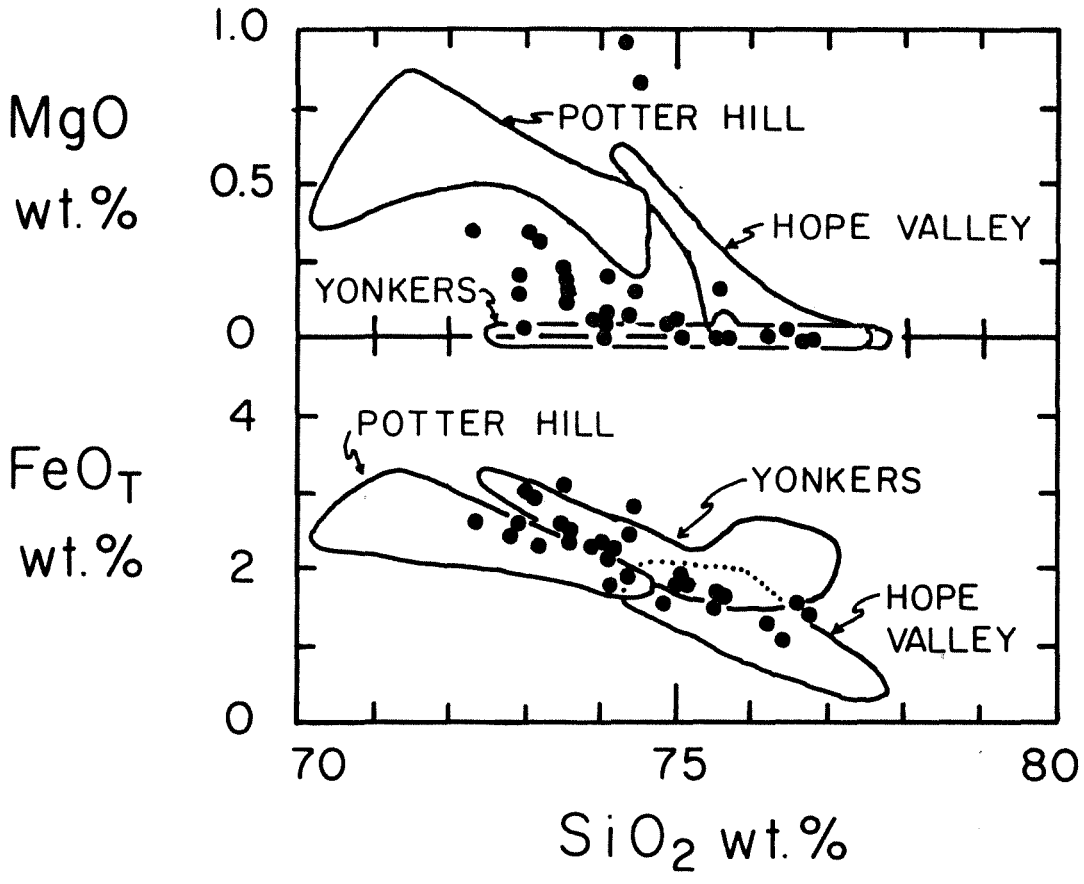

Figure 38. Harker diagram of mafics vs. silica for Dry Hill Gneiss, Yonkers Gneiss, Hope Valley Alaskite Gneiss and Potter Hill Gneiss.

the rocks in question. All three formations overlap the field of Dry Hill Gneiss.

The ratio of FeO/(FeO + MgO) is at or very close to one for the Yonkers Gneiss, the Dry Hill Gneiss and most of the Hope Valley Alaskite. These formations plot in the tholeiitic field of a calc-alkaline/tholeiite discriminant diagram (not shown). The Potter Hill analyses plot across the boundary, but mostly in the calc-alkaline field. In general, the Potter Hill is more MgO-rich than the other three gneisses, so it may be less evolved.

The question of the extent of igneous evolution of each of the formations is best examined by plotting mafic versus felsic components(Figure 39). Dry Hill and Yonkers Gneiss are enriched in iron relative to magnesium. This may be a result of fractionation and removal of mafic crystals from both protoliths, and it may mean that both crystallized from a very evolved magma. The leucogneiss layers (F) were probably accumulations of crystals, and composed mostly of quartz and orthoclase, so they may simply have had a low mafic content. Hope Valley Alaskite is more evolved with respect to felsic components. Potter Hill Gneiss is less evolved than any of the other formations.

The same trends are visible on a standard AFM diagram (Figure 40). The compositions of the gneisses appear to indicate an igneous history of extreme MgO depletion accompanied by FeO enrichment.

The Potter Hill Granite Gneiss and the Hope Valley Alaskite Gneiss of Connecticut and the Yonkers Gneiss of New York have marked anorogenic affinities and can be classified chemically as A-type granites as defined by Loiselle and Wones (1979). They are extremely evolved. A strong possibility exists that the igneous protoliths formed under similar conditions to the Dry Hill Gneiss, possibly in a tensional tectonic regime and furthermore, at about the same time. The similarities between the four groups of rocks may, however, be a result of anorogenic affinities rather than a true stratigraphic correlation. The question of their correlation and origin should be explored further using trace elements.

Trace Element Data

Data for Y, Sr, Rb, Th, Pb, and Ga are available in limited quantity for the Yonkers Gneiss (Goldstein, unpublished). The Th, Pb, and Ga abundances are all similar to those in the Dry Hill Gneiss, but the quantity of the other trace elements, particularly Y and Sr, differ markedly. Yonkers Gneiss has, on the average, slightly less Rb than the Dry Hill Gneiss. Yonkers Gneiss has approximately four times more Y than the Dry Hill Gneiss, but only one tenth the amount of Sr. A plot of Y/Ti vs. Sr illustrates this difference (Figure 41).

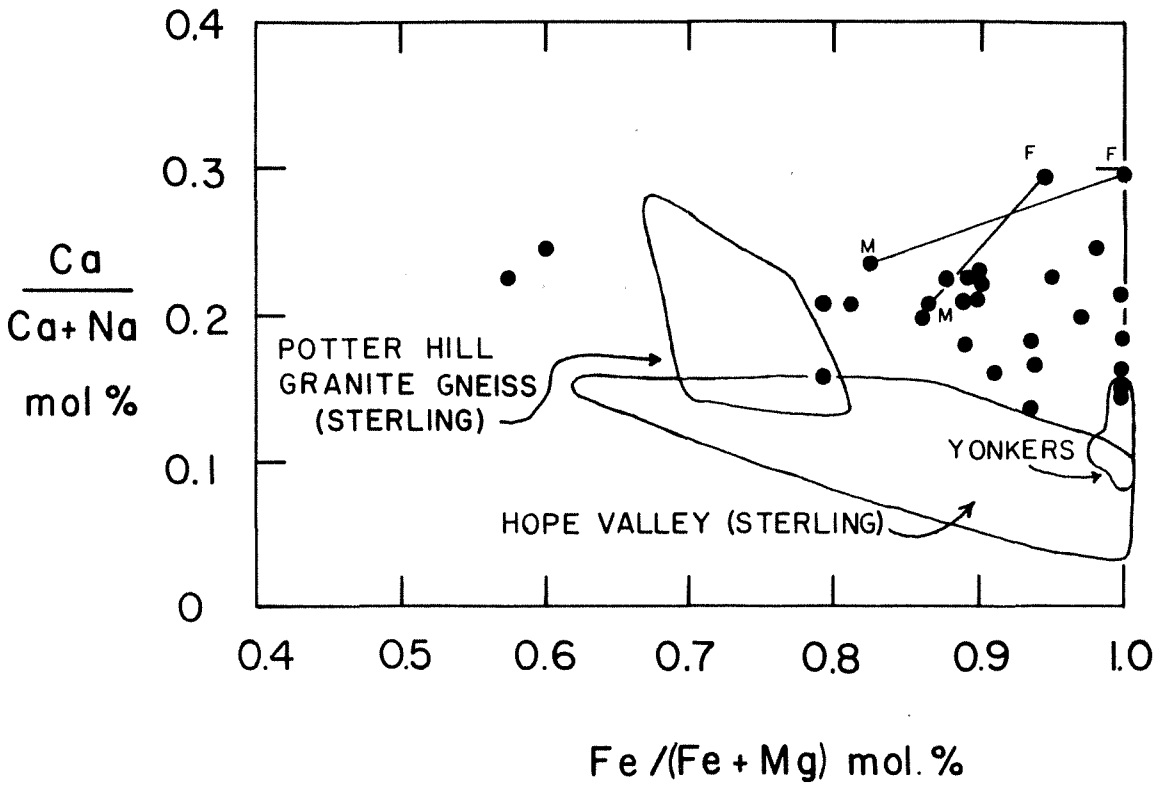

Figure 39. Felsic vs. mafic components of Dry Hill Gneiss vs. Yonkers Gneiss, Hope Valley Alaskite Gneiss and Potter Hill Gneiss.

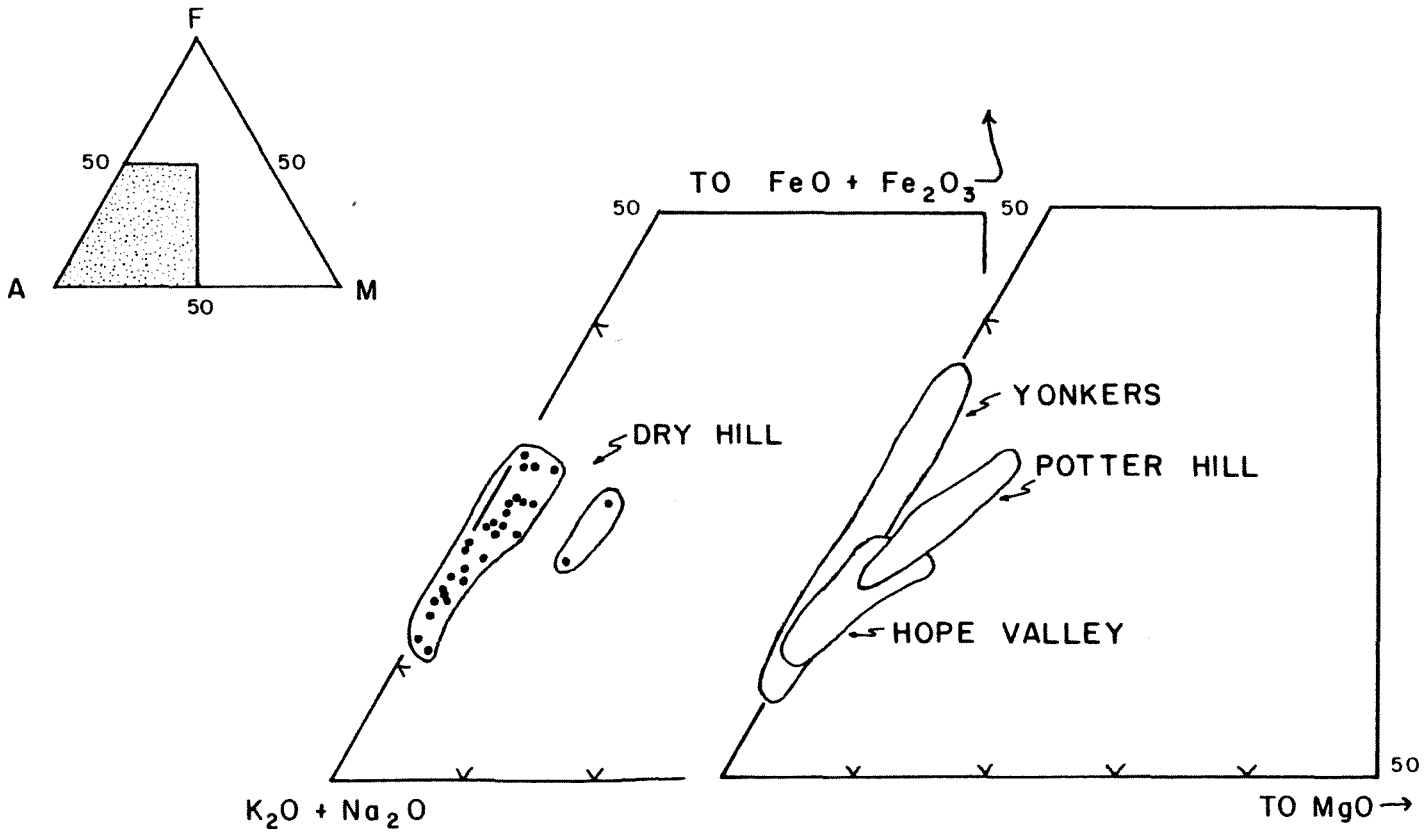

Figure 40. AFM diagram comparing Dry Hill Gneiss with Yonkers Gneiss, Hope Valley Alaskite Gneiss and Potter Hill Gneiss.

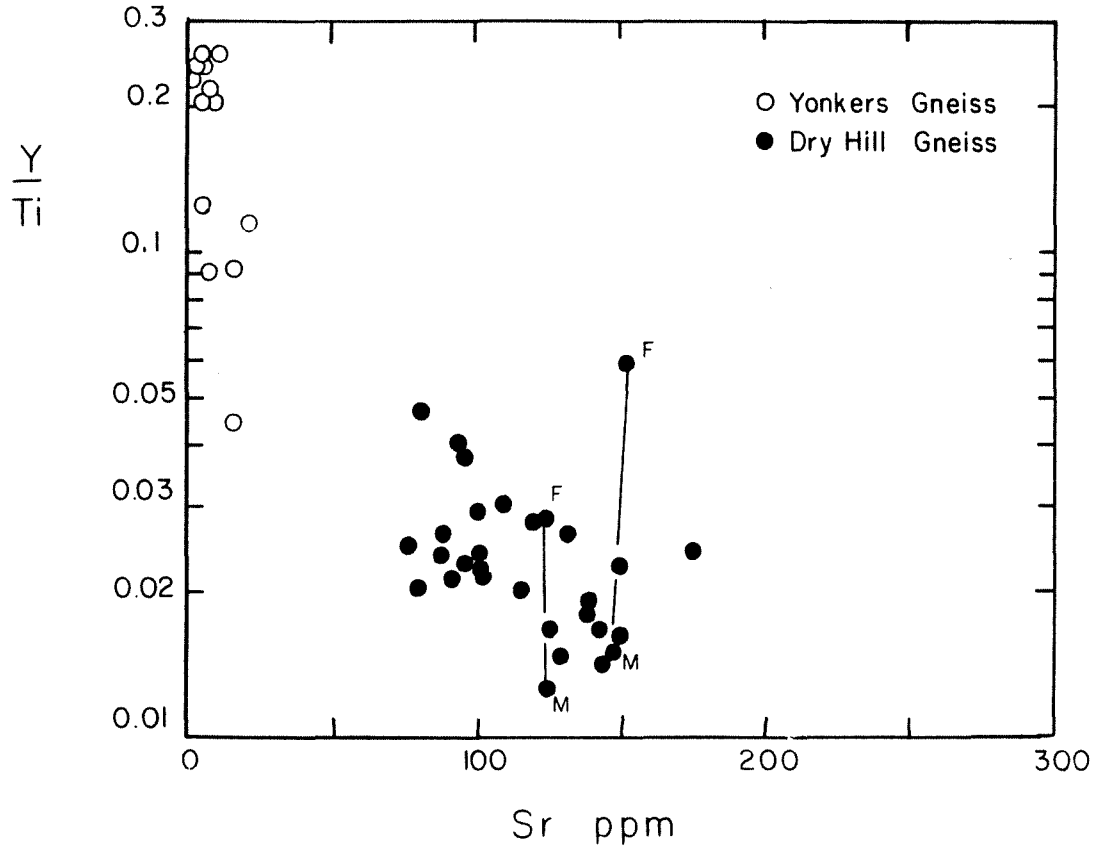

Figure 41. A comparison of selected trace element data for Dry Hill Gneiss and Yonkers Gneiss.

It is likely that the Yonkers Gneiss protolith melted from a different source than the Dry Hill Gneiss. The source of the Yonkers Gneiss must have been enriched in Y. An extraordinary amount of plagioclase fractionation would be required to deplete a melt in Sr to the extreme extent that Yonkers is depleted, so perhaps the source rock was itself depleted in Sr or plagioclase remained in the restite. Clastic sediments especially reworked clastic sediments, are normally depleted in Sr, with weathering of plagioclase (McCulloch and Wasserburg, 1978). A sedimentary source for the Yonkers should mean that the Yonkers would be peraluminous, but the Yonkers is metaluminous. The matter needs further study. What can be concluded is that a correlation between the rocks in the core of the Pelham dome and Yonkers Gneiss of New York is unlikely, despite their many similarities in major element chemistry.

Comparisons between Fourmile Gneiss and Local Plagioclase Gneisses

The norms of the Fourmile Gneiss plot in the granodiorite (dacite) field of a modified Streckeisen diagram as do most samples of the Waterford Group of Connecticut (Figure 42). The samples from the Shelburne Falls dome plot near the boundary of the granodiorite and the tonalite field, on either side of the boundary. Samples of Monson Gneiss plot in the granodiorite and tonalite fields, also. Norms of Joshua Rock Granite Gneiss proved difficult to calculate, due to the extremely low Al2O3 amounts, relative to the alkalies. The placement of the norms was based on the ratio of the alkalies. Perhaps the Al2O3 values are in error.

The number of samples of each formation is limited, so trends on a Harker diagram must be interpreted with caution (Figure 43). Each formation merits a detailed geochemical study in the future. The greatest amount of variation between the formations is displayed on a plot of alkalies and CaO versus SiO2 (Figure 51). Both New London Granodiorite and the Shelburne Falls dome rocks decrease in K2O with increasing SiO2, unlike any of the other gneisses. Monson has uniformly low K2O relative to the other New England gneisses. It also has a bimodal silica distribution. Joshua Rock Granite Gneiss has more SiO2 than any of the other formations, with the exception of some Monson samples and the Shelburne Falls dome rocks, but it has far less CaO and far more K2O than the latter two. Fourmile Gneiss overlaps the Mamacoke Formation and the Rope Ferry Formation of the Waterford Group, and has a similar slope with varying silica. The sample of "Monson" of Emerson falls on the extrapolation to the Fourmile trend at less SiO2 and is quite close to the modern analyses of Leo, et al. (1984). The mafic elements, phosphorous, and aluminum decrease with increasing silica for all formations, which is a typical granitic trend.

All of the gneisses, with the exception of some samples of Monson Gneiss and the possible exception of Joshua Rock Granite Gneiss, plot in the calc-alkaline field of a calc-alkaline vs. tholeiite diagram

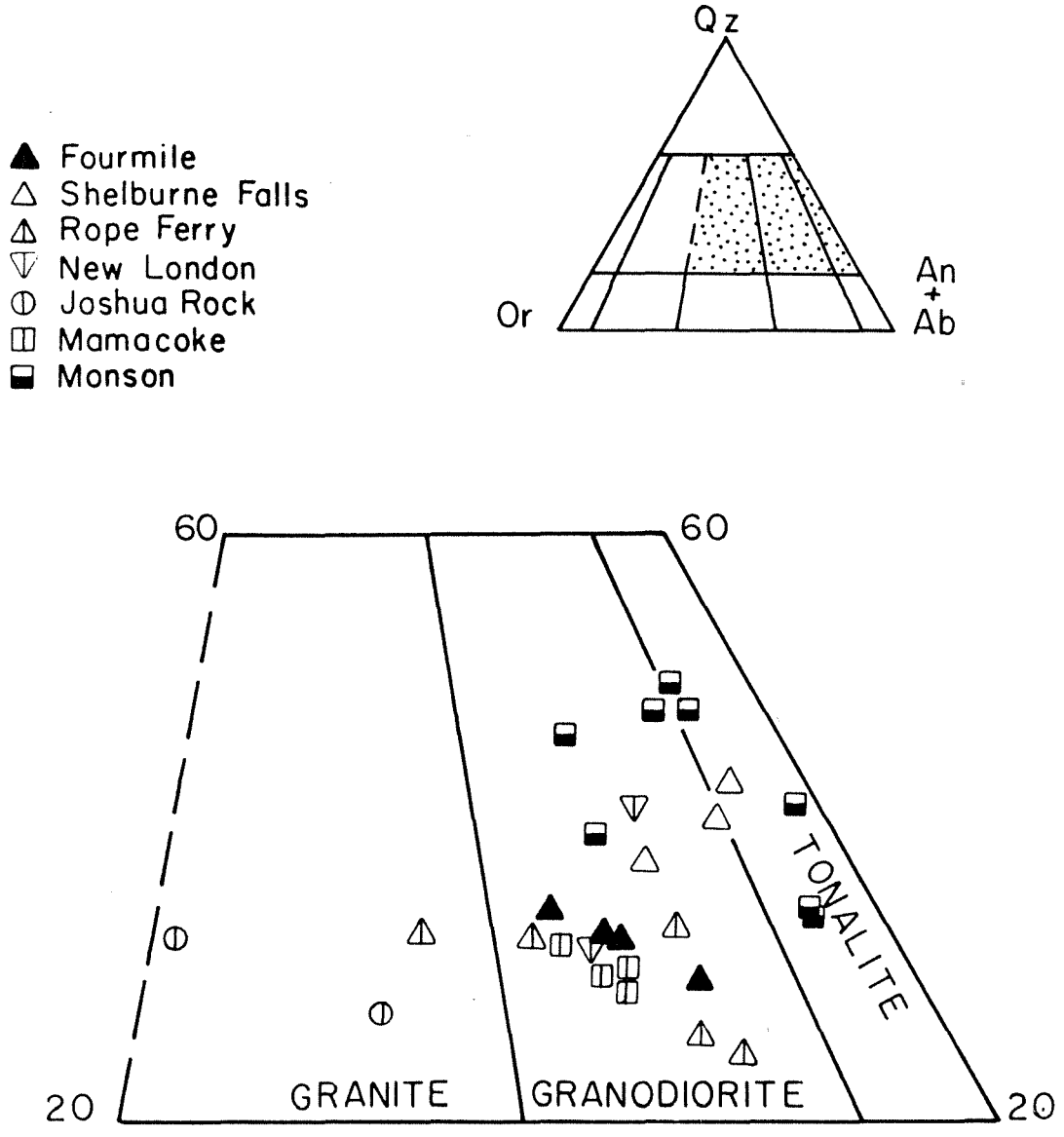

Figure 42. Norms of Fourmile Gneiss, the Waterford Group, Shelburne Falls dome gneiss, and Monson Gneiss plotted on a modified Streckeisen diagram.

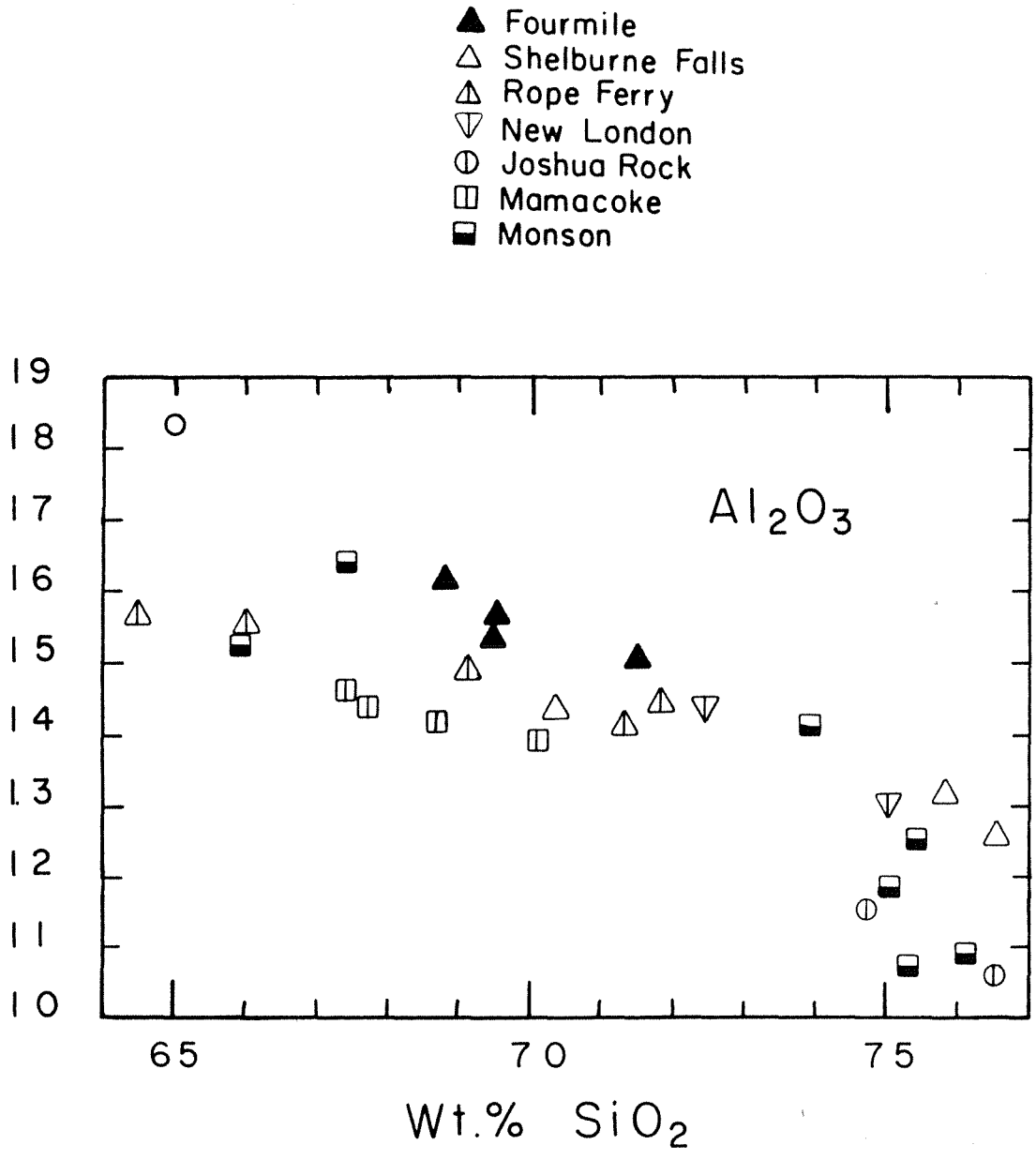

Figure 43. Harker diagram comparing Fourmile Gneiss to the Waterford Group, Shelburne Falls dome gneiss, Monson Gneiss (Leo, et al., 1984) and a sample of Monson Gneiss (open circle) from Emerson (1917). Analyses from the Shelburne Falls dome provided by Leo M. Hall.

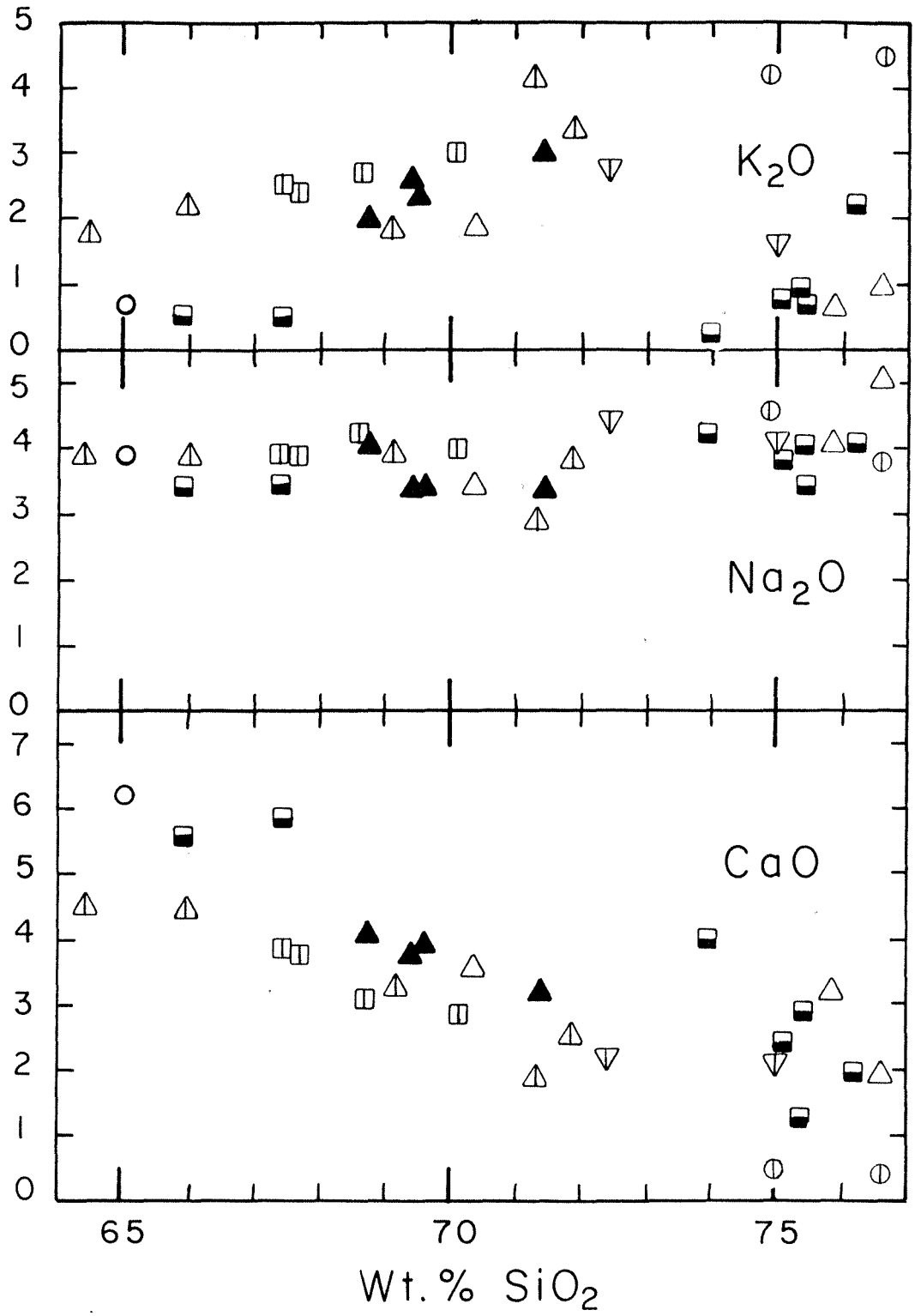

Figure 43, continued.

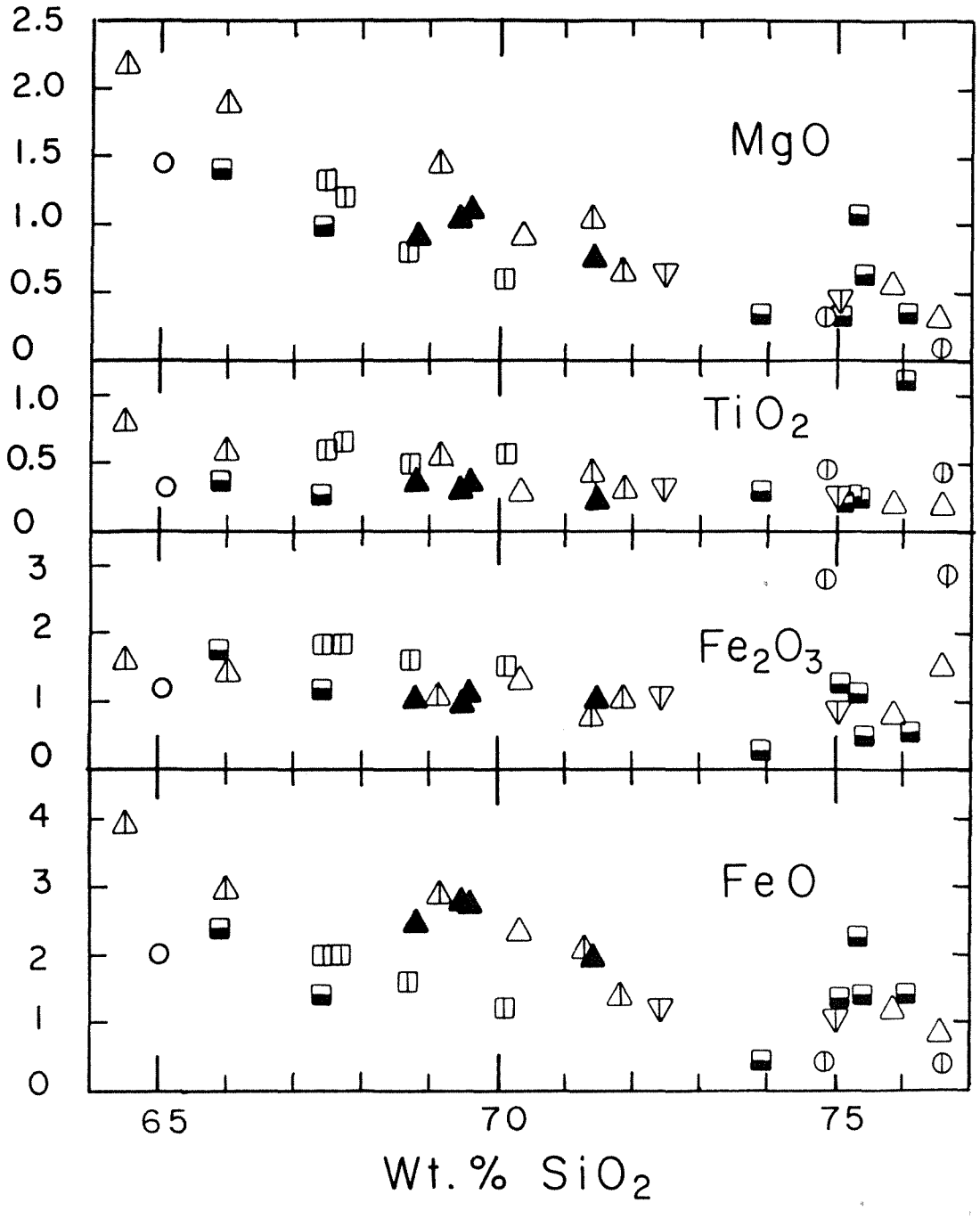

Figure 43, continued.

(Figure 44). This suggests that the rocks had an origin similar to that of a typical calc-alkaline rock series along a continental margin or island arc. The rocks probably had an orogenic rather than an anorogenic origin. Some of the Monson samples are fairly evolved with respect to mafics and are rich in quartz. Perhaps they fractionated longer than the protoliths of the other gneisses.

Robinson and Hall (1980) postulate that there were widespread volcanic eruptions and pluton emplacement during the early stages of the Taconian Orogeny on the Avalon microcontinent. The melting episode might have occurred as a result of subduction of oceanic crust beneath the Bronson Hill plate during events leading to the closing of an ocean that was between North America and Avalonia. The rocks so formed were the Monson Gneiss and related rocks. Robinson and Hall liken the volcanism to that which occurs today in the Andes as oceanic crust is subducted beneath the South American continent.

Twelve samples of orogenic andesite from northern Chile, mostly from the San Pedro and San Pablo volcanoes, are typical continental margin calc-alkaline andesites and representative of the regime (Gill, 1981; Thorpe, et al., 1976). The andesites plot in the calc-alkaline field of Figure 44, which compares FeOT/(FeOT + MgO) to silica. Some of the andesites have more silica than the 63 per cent maximum for orogenic andesites as defined by Gill (1981), so the Chilean rocks overlap the field of the Rope Ferry Gneiss.

A similar pattern emerges on an AFM diagram because the andesites and the New England gneisses all plot in the calc-alkaline field (Figure 45). The samples containing the most silica tend to plot towards the alkali corner of the triangle, indicating a history of MgO depletion and FeO enrichment. The fields of Chilean andesites and New England gneisses overlap. Joshua Rock Granite Gneiss may not fall into the calc-alkaline field per se, because it plots near the boundary with the tholeiitic trend. Monson Gneiss has a greater range than the other gneisses, because some of the Monson samples are quite evolved. It is likely that the protoliths of these plagioclase gneisses in New England, with the exception of Joshua Rock Granite Gneiss, represent an igneous suite of calc-alkaline, orogenic origin that may have been generated under conditions similar to those which occur today in the Andes of South America.

CONCLUSIONS

The Dry Hill Gneiss is of rhyolitic composition, and has the compositional characteristics of an anorogenic granite and related rhyolites (Loiselle and Wones, 1979). Based on mineralogical and chemical layering in the present rock, the protolith of the Dry Hill Gneiss is interpreted to have been a sequence of layered tuffs. The layering was formed by accumulations of crystals which settled out by density, as part of the glass was winnowed away and deposited nearby.

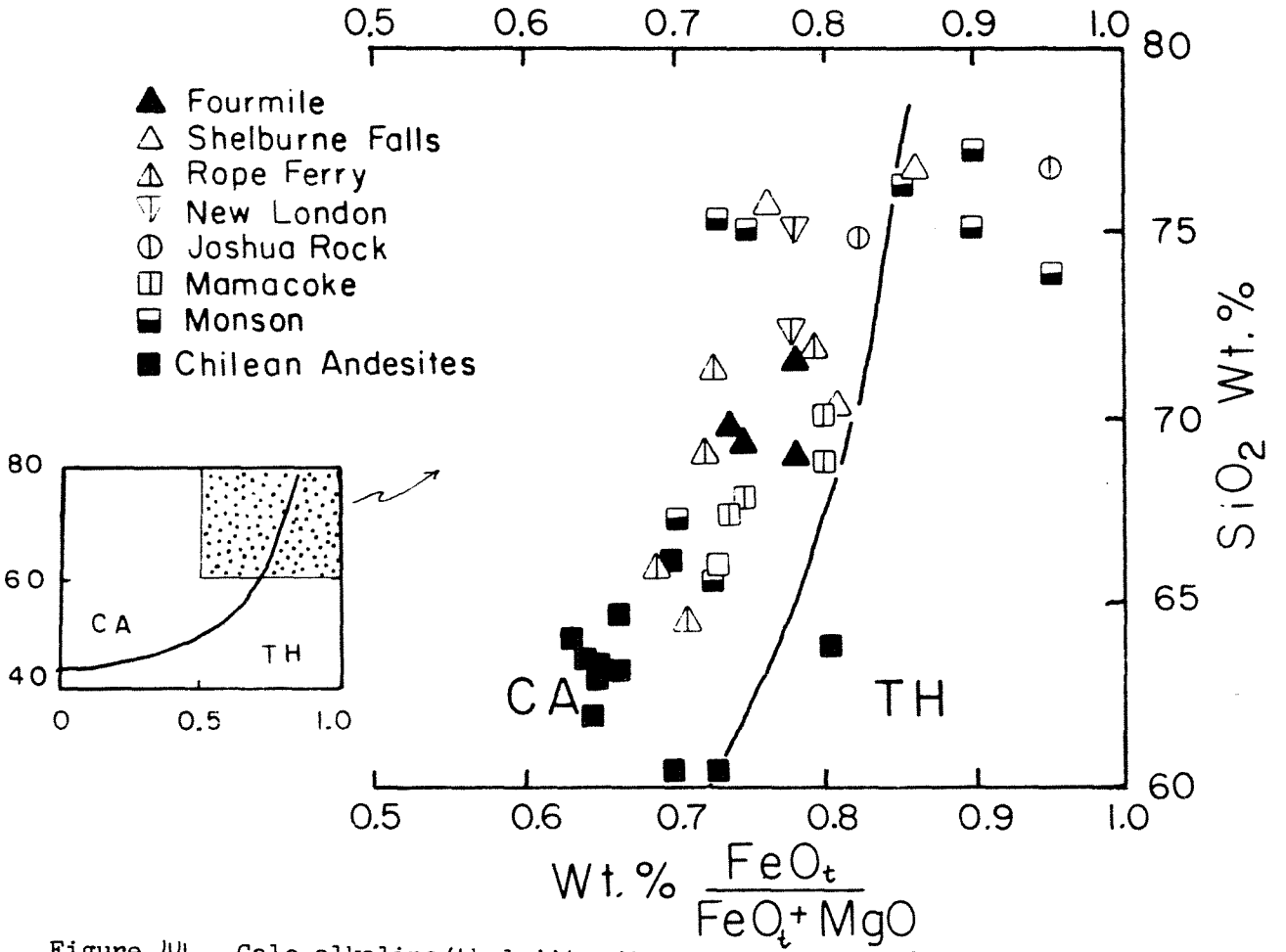

Figure 44. Calc-alkaline/tholeiite discrimination diagram. Adapted from Miyashiro (1974). Compared to andesites from northern Chile (Gill, 1981; Thorp, et al., 1976).

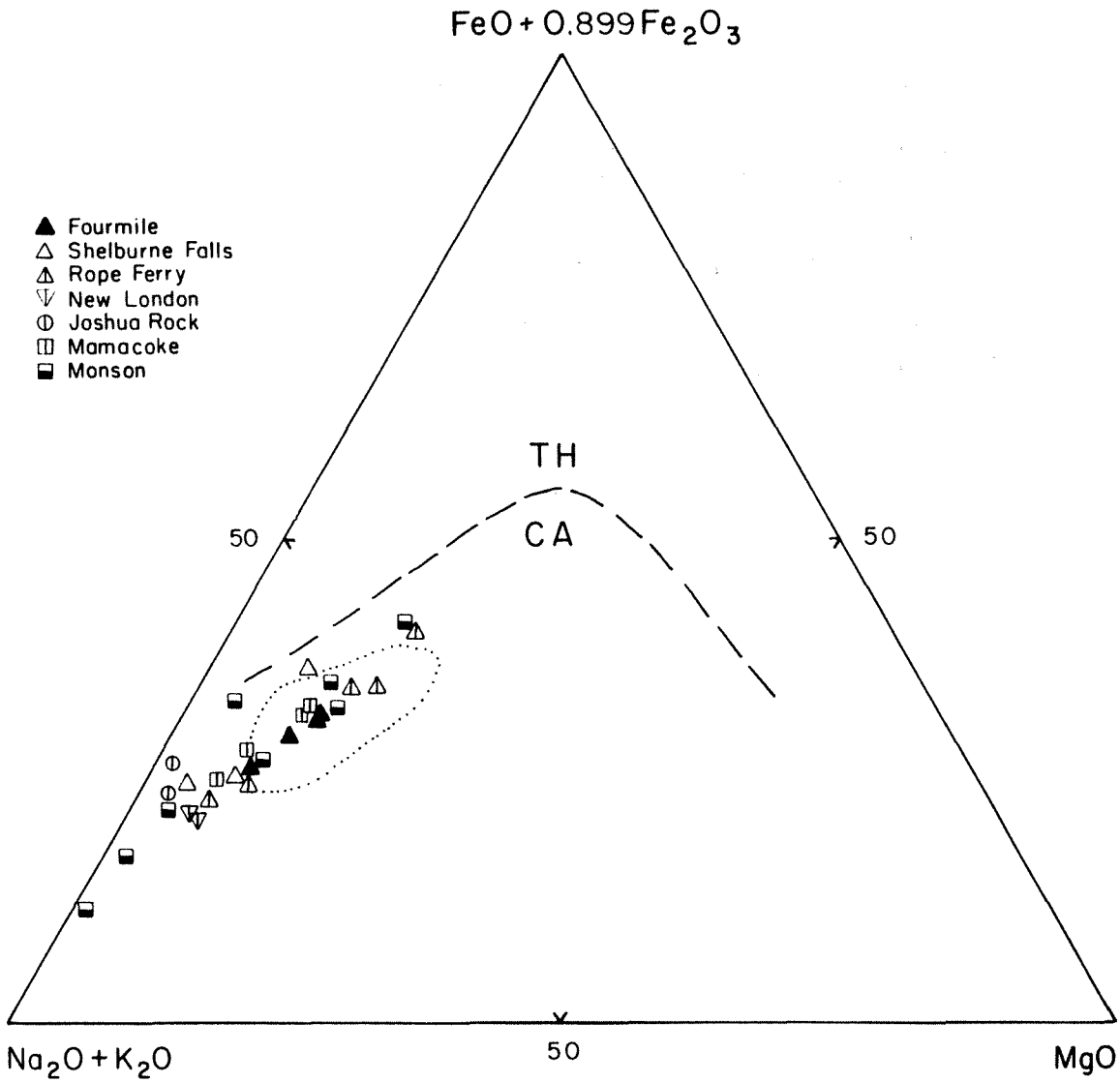

Figure 45. AFM diagram comparing the field of andesites from northern Chile (dotted line) to New England gneisses.

The granitic gneiss within the Poplar Mountain Quartzite is chemically similar to the Dry Hill Gneiss and probably had a similar origin. The felsic gneiss within the Poplar Mountain Gneiss may have been derived from a slightly more primitive layer in the Dry Hill protolith magma chamber. The Poplar Mountain Gneiss is a sedimentary formation probably derived from reworked tuffs with compositions slightly more primitive than the protoliths of the Dry Hill Gneiss. The four analysed samples of Fourmile Gneiss are chemically dacites, and their protolith may have evolved in an orogenic environment similar to that which exists today in the Andes of South America.

The Dry Hill Gneiss is similar in its major element chemistry to the Hope Valley Alaskite Gneiss and Potter Hill Granite Gneiss of Connecticut and the Yonkers Gneiss of New York. Trace element chemistry precludes a correlation with the Yonkers Gneiss. No trace element data are available for the Hope Valley and Potter Hill Gneisses in Connecticut, so a correlation between them and the Dry Hill Gneiss is still possible.

REFERENCES

Anderson, J. L., 1983, Proterozoic anorogenic granite plutonism of North America: Geological Society of America, Memoir 161, p. 133-154.

_____, 1980, Mineral equilibria and crystallization conditions in the late Precambrian Wolf River rapakivi massif, Wisconsin: American Journal of Science, v. 280, p. 289-332.

Anderson, J. L., and Cullers, R. L., 1978, Geochemistry and evolution of the Wolf River Batholith, a late Precambrian rapakivi massif in northern Wisconsin, U. S. A: Precambrian Research, v. 7, p. 287-324.

Anderson, J. L., Cullers, R. L., and Van Schmus, W. R., 1980, Anorogenic metaluminous and peraluminous granite plutonism in the Mid-Proterozoic of Wisconsin, U. S. A: Contributions to Mineralogy and Petrology, v. 74, p. 311-328.

Ashenden, D. D., 1973, Stratigraphy and structure of the northern portion of the Pelham dome, north-central Massachusetts: Contribution No. 16 (M. S. thesis), Department of Geology and Geography, University of Massachusetts, Amherst, 133 p.

Ashwal, L. D., Leo, G. W., Robinson, Peter, Zartman, R. E., and Hall, D. J., 1979, The Belchertown Quartz Monzodiorite pluton, west-central Massachusetts: a syntectonic Acadian intrusion: American Journal of Science, v. 279, p. 936-969.

Balk, Robert., 1956a, Bedrock geology of the Massachusetts portion of the Northfield quadrangle, Massachusetts, New Hampshire, and Vermont: United States Geological Survey, Geologic Quadrangle Map GQ-92.

_____, 1956b, Bedrock geology of the Millers Falls quadrangle, Massachusetts: United States Geological Survey, Geologic Quadrangle Map GQ-93.

Barker, Fred, Wones, D. R., Sharp, W. N. and Desborough, G. A., 1975, The Pikes Peak batholith, Colorado Front Range, and a model for the origin of the gabbro-anorthosite-syenite-potassic granite suite: Precambrian Research, v. 2, p. 97-160.

Bickford, M. E., Sides, J. R., and Cullers, R. L., 1981, Chemical evolution of magmas in the Proterozoic terrane of the St. Francois Mountains, southeastern Missouri: I. Field, petrographic, and major element data: Journal of Geophysical Research, v. 86, no. B11, p. 10365-10386.

Binns, R. A., 1965, The mineralogy of metamorphosed basic rocks from the Willyama Complex, Broken Hill district, New South Wales. Part I. Hornblendes: Mineralogical Magazine, v. 35, p. 306-326.

Bougault, Henri, 1980, Contribution des elements de transition a la comprehension de la genese des basalts oceaniques: Ph. D. thesis, Universite de Paris VII, 221 p.

Bougault, Henri, and Treuil, M., 1980, Mid-Atlantic Ridge: zero-age geochemical variations between Azores and 22o N: Nature, v. 286, p. 209-212.

Chappell, B. W. and White, A. J. R., 1974, Two contrasting granite types: Pacific Geology, v. 8, p. 173-174.

Clemens, J. D., 1984, Origin of A-type granites-experimental constraints: Geological Society of America Abstracts with Programs, v. 16, p. 473.

Cullers, R. L., Koch, R. L., Bickford, M. E., 1981, Chemical evolution of magmas in the Proterozoic terrane of the St. Francois Mountains, southeastern Missouri: II. Trace element data: Journal of Geophysical Research, v. 86, no. B11, p. 10388-10401.

Czamanske, G. K., Wones, D R., and Eichelberger, J. C., 1977, Mineralogy and petrology of the intrusive complex of the Pliny Range, New Hampshire: American Journal of Science, v. 277, p. 1073-1123.

Dodge, F. C. W., Papike, J. J., and Mays, R. E., 1968, Hornblendes from granitic rocks of the Central Sierra Nevada batholith, California: Journal of Petrology, v. 9, p. 378-410.

Emerson, B. K., 1898, Geology of old Hampshire county, Massachusetts: United States Geological Survey Monograph 29, 720 p.

_____, 1917, Geology of Massachusetts and Rhode Island: United States Geological Survey Bulletin 597, 289 p.

Emslie, R. F., 1978, Anorthosite massifs, rapakivi granites, and late Proterozoic rifting of North America: Precambrian Research, v. 7, p. 61-98.

Eskola, P. E., 1948, The problems of mantled gneiss domes: Geological Society of London Quarterly Journal, v. 104, p. 461-476.

Flanagan, F. J., 1976, 1972 values for international geochemical reference samples: Geochimica et Cosmochimica Acta, v. 37, p. 1189-1200.

Gill, J. B., 1981, Orogenic andesites and plate tectonics: Springer Verlag, Berlin, 390p.

Goldsmith, Richard, 1967a, Bedrock geology of the Montville Quadrangle, New London County, Connecticut: United States Geological Survey, Geologic Quadrangle Map GQ-609.

_____, 1967b, Bedrock geologic map of the New London Quadrangle, in Connecticut: United States Geological Survey, Geologic Quadrangle Map GQ-574.

_____, 1967c, Bedrock geologic map of the Uncasville quadrangle, New London County, Connecticut: United States Geological Survey, Geologic Quadrangle Map GQ-576.

Guidotti, C. V., 1984, Micas in metamorphic rocks, in Bailey, S. W., ed., Micas: Reviews in Mineralogy, v. 13, Mineralogical Society of America, Washington, 584 p.

Guthrie, J. O., 1972, Geology of the northern portion of the Belchertown intrusive complex, west-central Massachusetts: Contribution No. 8 (M. S. thesis), Department of Geology and Geography, University of Massachusetts, Amherst, 110 p.

Hall, L. M. and Robinson, Peter., 1982, Stratigraphic-tectonic subdivisions of southern New England, in St-Julien, P. and Beland, J., eds., Major structural zones and faults of the Northern Appalachians: Geological Association of Canada Special Paper 24.

Hanson, G. N., 1978, The application of trace elements to the petrogenesis of igneous rocks of granitic conposition: Earth and Planetary Science Letters, v. 38, p. 26-43.

Haskin, L. A., Haskin, M. A., Frey, F. A., 1968, Relative and absolute terrestrial abundances of the rare earths, in Origin and Distribution of the Elements: International Series of Monographs in Earth Sciences, v. 30, p. 889-912.

Hawthorne, F. C., 1981, Crystal chemistry of the amphiboles. in Veblen, D. R., ed., Amphiboles and other Hydrous Pyriboles-Mineralogy: Reviews in Mineralogy, v. 9A, Mineralogical Society of America, Washington, 372 p.

Hayama, Yoshikazu, 1959, Some considerations on the colour of biotite and its relation to metamorphism: Journal of the Geological Society of Japan, v. 65, p. 21-30.

Hedge, C. E., 1970, Whole-rock Rb-Sr age of the Pikes Peak batholith, Colorado: United States Geological Survey Professional Paper No. 700-B, p. 86-89.

Hermes, O. D., and Zartman, R. E., 1985, Late Proterozoic and Devonian plutonic terrane within the Avalon zone of Rhode Island: Geological Society of America Bulletin, v. 96, p. 272-282.

Hildreth, Wes, 1979, The Bishop Tuff: Evidence for the origin of compositional zonation in silicic magma chambers: Geological Society of America Special Paper 180, p. 43-75.

Hills, F. A., and Dasch, E. J., 1972, Rb/Sr study of the Stony Creek Granite, southern Connecticut: a case for limited remobilization: Geological Society of America Bulletin, v. 83, p. 3457-3464.

Irvine T. N. and Baragar, W. R. A., 1971, A guide to the chemical classification of the common volcanic rocks: Canadian Journal of Earth Science, v. 8, p. 523-548.

Jaffe, H. W., 1947, Reexamination of sphene (titanite): American Mineralogist, v. 32, p. 637-642.

_____, 1951, The role of yttrium and other minor elements in the garnet group: American Mineralogist, v. 36, p. 133-155.

James, R. S. and Hamilton, D. L., 1969, Phase relations in the system $NaAlSi_3O_8$-$KAlSi_3O_8$-$CaAl_2Si_2O_8$-SiO_2 at one kilobar water vapor pressure: Contributions to Mineralogy and Petrology, v. 21, p, 111-141.

Laird, H. S., 1974, Geology of the Pelham dome near Montague, west-central Massachusetts: Contribution No. 14 (M. S. thesis), Department of Geology and Geography, University of Massachusetts, Amherst, 84 p.

Lappin, A. R. and Hollister, L. S., 1980, Partial melting in the Central Gneiss Complex near Prince Rupert, British Columbia: American Journal of Science, v. 280, p. 518-545.

Leake, B. E., 1978, Nomenclature of amphiboles: Canadian Mineralogist, v. 16, p. 501-520.

Leo, G. W., Zartman, R. E., and Brookins, D. G., 1984, Glastonbury Gneiss and mantling rocks (a modified Oliverian dome) in south-central Massachusetts and north-central Connecticut:

geochemistry, petrogenesis, and isotopic age: United States Geological Survey Professional Paper, No. 1295, 45p.

Lidiak, E. G. and Denison, R. E., 1983, Petrology and physical properties of granites from the Illinois deep hole in Stephenson County: Journal of Geophysical Research, v. 88, no. B9, p. 7287-7299.

Loiselle, M. C., and Wones, D. R., 1979, Characteristics and origin of anorogenic granites: Geological Society of America Abstracts with Programs, v. 11, p. 468.

Long, L. E., 1969, Whole rock Rb-Sr age of the Yonkers Gneiss, Manhattan Prong: Geological Society of America Bulletin., v. 80, p. 2087-2090.

Lundgren, L., Jr., 1966, The bedrock geology of the Hamburg quadrangle: State Geological and Natural History Survey of Connecticut. Quadrangle Report No. 19, 41 p.

_____, 1967, The bedrock geology of the OLd Lyme quadrangle: State Geological and Natural History Survey of Connecticut. Quadrangle Report No. 21, 30 p.

Luth, W.C., Jahns, R. H., and Tuttle, O. F., 1964, The granite system at 4-10 kilobars: Journal of Geophysical Research, v. 69, p. 759-773.

Maczuga, D. E., 1981, The petrology and chemistry of the Fitchburg Plutonic Complex, central Massachusetts: Contribution No. 36 (M.S. Thesis), Department of Geology and Geography, University of Massachusetts, Amherst, 127p.

Maxwell, J. A., 1968, Rock and mineral analysis: Chemical Analysis. v. 27, Interscience Publishers, p. 419-421.

McCulloch, M. T., and Wasserburg, G. J., 1978, Sm-Nd and Rb-Sr chronology of continental crust formation: Science, v. 200, p. 1003-1011.

McLellan, E. L., 1984, Multiple intrusion in the Stony Creek area, eastern Connecticut: Geological Society of America Abstracts with Programs, v. 16, p. 49.

Michener, S. R., 1983, Bedrock geology of the Pelham-Shutesbury syncline, Pelham dome, west-central Massachusetts: Contribution No. 43 (M. S. Thesis), Department of Geology and Geography, University of Massachusetts, Amherst, 101p.

Miyashiro, A., 1974, Volcanic rock series in island arcs and active continental margins: American Journal of Science, v. 274, p. 321-355.

Moll, E. J., 1981, Geochemistry and petrology of mid-Tertiary ash flows from the Sierra el Virulento area, eastern Chihuahua, Mexico: Journal of Geophysical Research, v. 86, no. B11, p. 10321-10334.

Naylor, R. S., 1969, Age and origin of the Oliverian domes, central-western New Hampshire: Geological Society of America Bulletin, v. 80, p. 405-428.

Norrish, Kenneth, and Chappell, B. W., 1967, X-ray fluorescence spectrometry, p. 201-272, in Zussman, Jack, ed., Physical Methods in Determanitive Mineralogy: Academic Press, New York, 514p.

Norrish, Kenneth and Hutton, J. T., 1969, An accurate X-ray spectrographic method for the analysis of a wide range of geophysical samples: Geochimica et Cosmochimica Acta, v. 33, p. 431-453.

Onasch, C. M., 1973, Analysis of the minor structural features in the north-central portion of the Pelham dome: Contrbution No. 12 (M. S. thesis), Department of Geology and Geography, University of Massachusetts, Amherst, 87 p.

Robinson, Peter, 1963, Gneiss domes in the Orange area, Massachusetts and New Hampshire: Ph. D. thesis, Harvard University Cambridge, 253 p.

_____, 1967, Gneiss domes and recumbent folds of the Orange area, west-central Massachusetts, p. 12-47. in Robinson, Peter and Drake, D. P., Editors, Guidebook for Field Trips in the Connecticut Valley: New England Intercollegiate Geological Conference, 59th annual meeting, 194 p.

_____, July 1968 to March 1970, Unpublished field notes from excavations of Northfield Mountain Pumped Storage Hydroelectric Project.

_____, 1979, Bronson Hill anticlinorium and Merrimack synclinorium in central Massachusetts, p. 126-174. in Skehan, J. H. and Osberg, P. H., Editors, The Caledonides in the U. S. A., Contributions to the International Geological Correlation Program, Project 27: Weston Observatory Press, 250 p.

Robinson, Peter, and Hall, L. M., 1980, Tectonic synthesis of southern New England, p. 73-82, in Wones, D. R., ed., Proceedings: the Caledonides in the U. S. A.: I. G. C. P. Project 27: Caledonide Orogen: Department of Geological Sciences Memoir 2: Virginia Polytechnic Institute and State University, Blacksburg Virginia, 329 p.

Robinson, Peter and Jaffe, H. W., 1969, Chemographic exploration of amphibole assemblages form central Massachusetts and southwestern New Hampshire: Mineralogical Society of America, Special Paper No. 2, p. 251-274.

Robinson, Peter; Ross, Malcolm; and Jaffe, H. W., 1971, Compositions of the anthophyllite-gedrite series, comparisons of gedrite and hornblende, and the anthophyllite-gedrite solvus: The American Mineralogist, v. 56, p. 1005-1041.

Robinson, Peter, Thompson, J. B., Jr., Rosenfield, J. L., 1979, Nappes, gneiss domes and regional metamorphism in western New Hampshire and central Massachusetts, p. 93-116, in Skehan, J. W., and Osberg, P. H., eds., The Caledonides in the U. S. A.: Geological Excursions in the Northern Appalachians: Contributions to the International Geologic Correlation Program: Project 27: Caledonide Orogen: Weston Observatory Publishers, Weston, Massachusetts, 250 p.

Robinson, Peter, Tracy, R. J., and Ashwal, L. D., 1975, Relict sillimanite-orthoclase assemblage in kyanite-muscovite schist, Pelham dome, west-central Massachusetts (abstract): EOS (Transactions of the American Geophysical Union), v. 56, p. 4666.

Sahama, T. G., 1946, On the chemistry of the mineral titanite: Bulletin de la Commission geologique de Finlande, No. 138.

Savolahti, Antti, 1962, The Rapakivi problem and the rules of idiomorphism in minerals: Bulletin de la Commission geologique de Finlande, v. 34, p. 33-111.

Shand, S. J., 1947, Eruptive rocks: their genesis, composition, classification, and their relation to ore-deposits, with a chapter on meteorites: 3d ed., J. Wiley, New York, 488 p.

Sheridan, M. F., 1979, Emplacement of pyroclastic flows: a review: Geological Society of America Special Paper 180, p. 125-136.

Simonen, Ahti, 1960, Pre-Quaternary rocks in Finland: Bulletin de la Commission geologique de Finlande, No. 191, 49p.

Smith, E. I., 1978, Precambrian rhyolites and granites in south-central Wisconsin: field relations and geochemistry: Geological Society of America Bulletin, v. 89, p. 875-890.

Steiger, R. H. and Jäger, E., 1977, Subcommission on Geochronology: Convention on the use of decay constants in geo- and cosmo-chronology: Earth and Planetary Science Letters, v. 36, p. 359-362.

Stewart, D. B., 1957, Four-phase curve in the system $CaAl_2Si_2O_8$-SiO_2-H_2O between 1 and 10 kilobars: Schweizerische Mineralogische und Petrographische Mitteilungen, v. 47, p. 35-59.

Taylor, S. R. and McLennan, S. M., 1981, The composition and evolution of the continental crust: rare earth element evidence from sedimentary rocks: Philosophical Transactions of the Royal Society of London, Series A, v. 301, p. 381-399.

Thompson, J. B. Jr., Robinson, Peter, Clifford, T. N., and Trask, N. J., 1968, Nappes and gneiss domes in west-central New England, p. 203-213, in Zen, E-an, White, W. S., Hadley, J. B., Thompson, J. B. Jr., eds., Studies of Appalachian Geology: Northern and Maritime: John Wiley and Sons, New York, 475 p.

Thorpe, R. S., Potts, P. J., Francis, P. W., 1976, Rare earth data and petrogenesis of andesite from the north Chilean Andes: Contributions to Mineralogy and Petrology, v. 54, p. 65-78.

Tracy, R. J., Robinson, Peter, and Thompson, A. B., 1976, Garnet composition and zoning in the determination of temperature and pressure of metamorphism, central Massachusetts: American Mineralogist v. 61, p. 726-775.

Tuttle, O. F. and Bowen, N. L., 1958, Origin of granite in the light of experimental studies in the system $NaAlSi_3O_8$-$KAlSi_3O_8$-SiO_2-H_2O: Geological Society of America Memoir 74, 153p.

von Platen, Hilmar, 1965, Experimental anatexis and genesis of migmatites, in Pitcher, W. S. and Flinn, G. W., eds., Controls of Metamorphism: Oliver and Boyd, Edinburgh, p. 203-218.

von Platen, Hilmar and Höller, H., 1966, Experimentelle anatexis des stainzer plattengneisses von der Koralpe, Steiermark, bei 2, 4, 7, und 10 Kb H_2O druck: Neues Jahrbuch fur Mineralogie Abhand, v. 106, p. 106-130.

Watson, E. B., 1979, Zircon saturation in felsic liquids: experimental results and applications to trace element

geochemistry: Contributions to Mineralogy and Petrology, v. 70, p. 407-419.

Watson, E. B., and Harrison, T. M., 1983, Zircon saturation revisited: temperature and composition effects in a variety of crustal magma types: Earth and Planetary Science Letters, v. 64, p. 295-304.

Webster, J. R. and Wintsch, R. P., 1984, Major element geochemistry and possible division of the Killingsworth Dome, south-central Connecticut: Geological Society of America Abstracts with Programs, v. 16, p. 70.

White, A. J. R., and Chappell, B. W., 1977, Ultrametamorphism and granitiod gneiss: Tectonophysics, v. 43, p. 7-22.

Wilson, A. D., 1955, A new method for the determination of ferrous iron in rocks and minerals: Bulletin of the Geological Survey of Great Britain, v. 9, p. 56.

Winkler, H. G. F., 1976, Petrogenesis of metamorphic rocks: Springer-Verlag, New York, 334 p.

Winkler, H. G. F.; Boese, Manfred; Marcopoulos, Theodor, 1975, Low temperature granitic melts: Neues Jahrbuch fur Mineralogie Monatshefte, p. 245-268.

Winkler, H. G. F. and Ghose, N. C., 1973, Further data on the eutectics in the system Qz-Or-An-H2O: Neues Jahrbuch fur Mineralogie Monatshefte, p. 481-484.

Winkler, H. G. F. and Lindemann, Wolfgang, 1972, The system Qz-Or-An-H2O within the granite system, application to granite magma formation: Neues Jahrbuch fur Mineralogie Monatshefte, p. 49-61.

Wones, D. R., Fahey, J. J., and Ayuso, R. A., 1977, A search for "Annite": EOS (Transactions of the American Geophysical Union), v. 58, p. 525.

Zartman, R. E., and Naylor, R. S., 1984, Structural implications of some radiometric ages of igneous rocks in southeastern New England: Geological Society of America Bulletin, v. 95, p. 522-539.

APPENDIX A

Recently, it was possible to obtain rare earth element (REE) analyses of two rock samples from this study. This was an opportunity to compare true REE analyses to Bougault's "poor man's" rare earth element (PMREE) analyses. Accordingly, a typical sample of Dry Hill Gneiss, TR 44+50, and a typical sample of Fourmile Gneiss, TR 18+34, were selected and sent to NASA's Johnson Space Center, where they were analysed for REEs and other trace elements by instrumental neutron activation analysis, by P. D. Kempton (Table 16).

The slope of the REE line is shallower than the slope of the PMREE envelope (N=30) for the Dry Hill Gneiss (Figure 46). La and Ce averages, determined by INAA, are quite close to those determined by X-ray fluorescence analysis. Both are normalized by chondrite normalizing values of Haskin, et al., 1968. The heavy REEs (Yb and Lu) have a much shallower slope than the heavy PMREEs. Probably the negative V, Nb and Ti anomalies in the PMREEs are caused by fractionation of oxide phases, such as magnetite, or by such phases remaining in the restite. The whole slope of the REE curve is shallower than the PMREE curve, and the REE curve has a negative Eu anomaly. Either plagioclase fractionated from the original melt or plagioclase remained in the restite during melting. On this diagram Sr seems to be a good PMREE analog for Eu.

The substitution of Sr for Eu is not so successful for Fourmile Gneiss. The REE curve has a negative Eu anomaly, but the PMREE curve has a positive Sr anomaly (Figure 47). At this time, it is not possible to explain the discrepancy. The overall slope of the REE curve, with the exception of the negative Eu anomaly, is similar to the slope of the PMREE curve.

Table 16. Trace element data for Dry Hill Gneiss and Fourmile Gneiss. Rare earth element data normalized with chondrite normalizing values of Haskin, et al., 1968.

Dry Hill Gneiss

	Average	Std. Dev.	Norm. Values	Chondrite Normalized
La	82.05	0.92	La 0.33	248.64 ± 2.79
Ce	177.3	3.6	Ce 0.88	201.45 ± 4.09
Sm	13.200	0.051	Sm 0.181	72.93 ± 0.28
Eu	2.330	0.067	Eu 0.069	33.77 ± 0.97
Tb	1.84	0.36	Tb 0.047	39.15 ± 7.66
Yb	5.837	0.345	Yb 0.200	29.19 ± 1.73
Lu	0.984	0.060	Lu 0.034	28.9 ± 1.8
Sc	10.51	0.02		
Hf	13.33	0.219		

Fourmile Gneiss

	Average	Std. Dev.	Norm. Values	Chondrite Normalized
La	27.81	0.332	La 0.33	84.27 ± 1.01
Ce	51.72	0.61	Ce 0.88	58.77 ± 0.69
Sm	3.28	0.017	Sm 0.181	18.12 ± 0.09
Eu	0.683	0.065	Eu 0.069	9.89 ± 0.94
Tb	0.70	0.18	Tb 0.047	15.0 ± 3.8
Yb	1.624	0.083	Yb 0.200	8.12 ± 0.42
Lu	0.219	0.016	Lu 0.034	6.4 ± 0.5
Sc	9.41	0.025		
Hf	2.77	0.26		

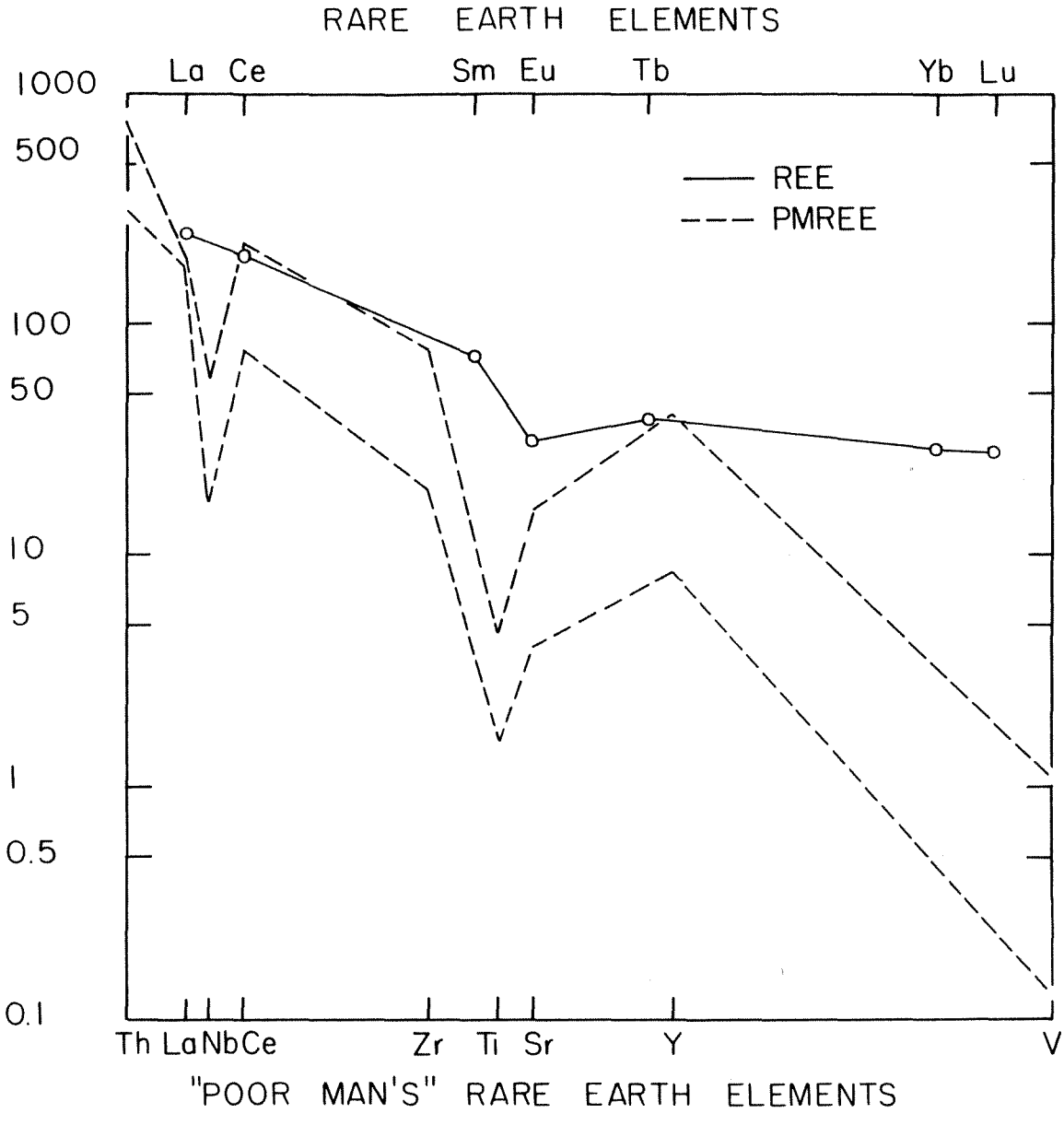

Figure 46. A plot of a rare earth element analysis of a typical Dry Hill Gneiss Hornblende Member sample TR 44+50 (solid line) vs. an envelope of thirty "Poor Man's" rare earth element analyses of Dry Hill Gneiss as a whole (dashed lines). REE normalized by chondrite values of Haskin et al., (1968) and PMREE normalized by normalizing factors of Bougault (1980).

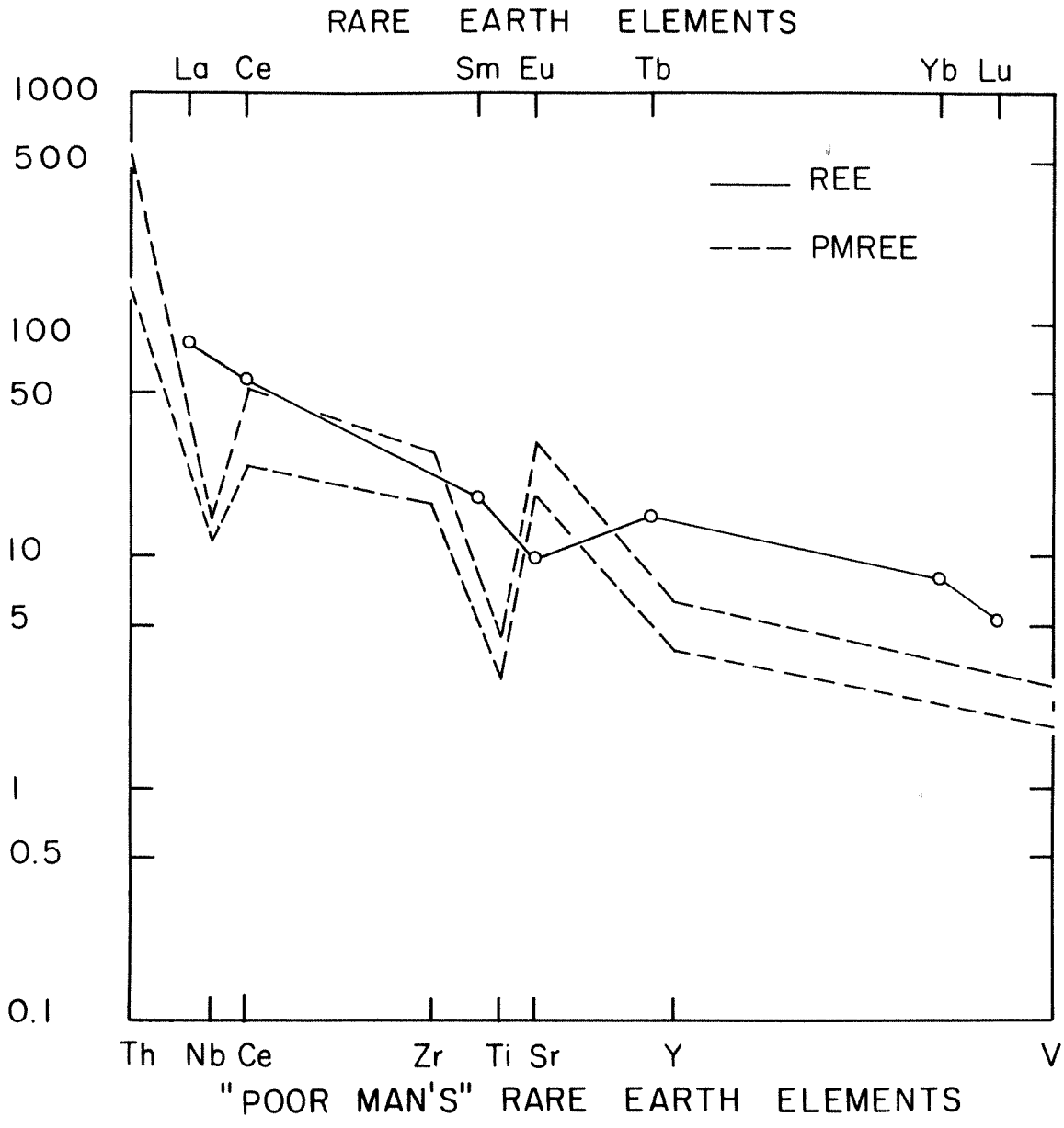

Figure 47. A plot of rare earth element analysis of a typical Fourmile Gneiss sample TR 18+38 (solid line) vs. envelope of four "Poor Man's" rare earth element analyses of Fourmile Gneiss (dashed lines). REE normalized by chondrite values of Haskin et al., (1968) and PMREE normalized by normalizing factors of Bougault (1980).